Title
SEMIANNUAL REPORT - BIOLOGY AND MEDICINE. Fall 1963

Author
Lawrence Berkeley National Laboratory

Publication Date
1964

LAWRENCE RADIATION LABORATORY · UNIVERSITY OF CALIFORNIA · BERKELEY

UCRL-11184
FALL 1963

SEMIANNUAL REPORT
BIOLOGY and MEDICINE

DONNER LABORATORY
and DONNER PAVILION

Research and Development

UCRL-11184
UC-48 Biology and Medicine
TID-4500 (24th Ed.)

DONNER LABORATORY AND DONNER PAVILION

LAWRENCE RADIATION LABORATORY — UNIVERSITY OF CALIFORNIA
BERKELEY, CALIFORNIA

SEMIANNUAL REPORT — BIOLOGY AND MEDICINE

FALL 1963

(January 1964)

John H. Lawrence, M.D., Editor

Tove Neville, Associate Editor

AEC Contract No. W-7405-eng-48

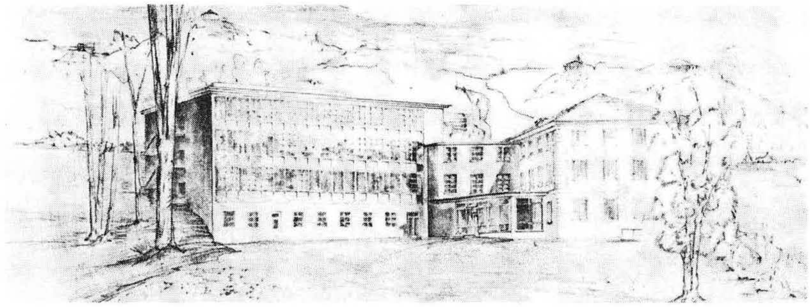

Foreword

This semiannual report reflects, as have previous ones, a cross section of our work in biology and medicine for a six-month period. The program--from its beginning in 1935 when the first tracer experiments with radioactive isotopes were carried out and the first studies on the biological effects of particle irradiation were initiated--has evolved in a broad fashion so that it continues to reflect basic research in biology and medicine, with much emphasis on biophysical and medical-physical research and the use of isotopes and nuclear radiations. The program has always embraced the philosophy that new knowledge is the goal and further that this knowledge should be applied where possible at once. Reflected in this issue are the continuing interests of the staff in the genetic and somatic effects of various types of radiation, the nature and control of erythropoiesis, the biochemistry and biophysics of fat metabolism, and other areas. The first article, by Manney and Mortimer, presents new work that is a milestone in the use of radiation for the study of genetic fine-structure. The continuing studies on erythropoietin and anti-erythropoietin reported in this issue are of special interest as is the investigation of continuous free-flow fractionation of protein solutions and bone-marrow cells. The refinement of techniques for detecting gamma rays in the body is also reported. Finally, the continuing interest of the laboratory in investigative therapy is exemplified by the report of Gottschalk _et al_. on the use of heavy particles in brain tumor therapy.

J.H.L.

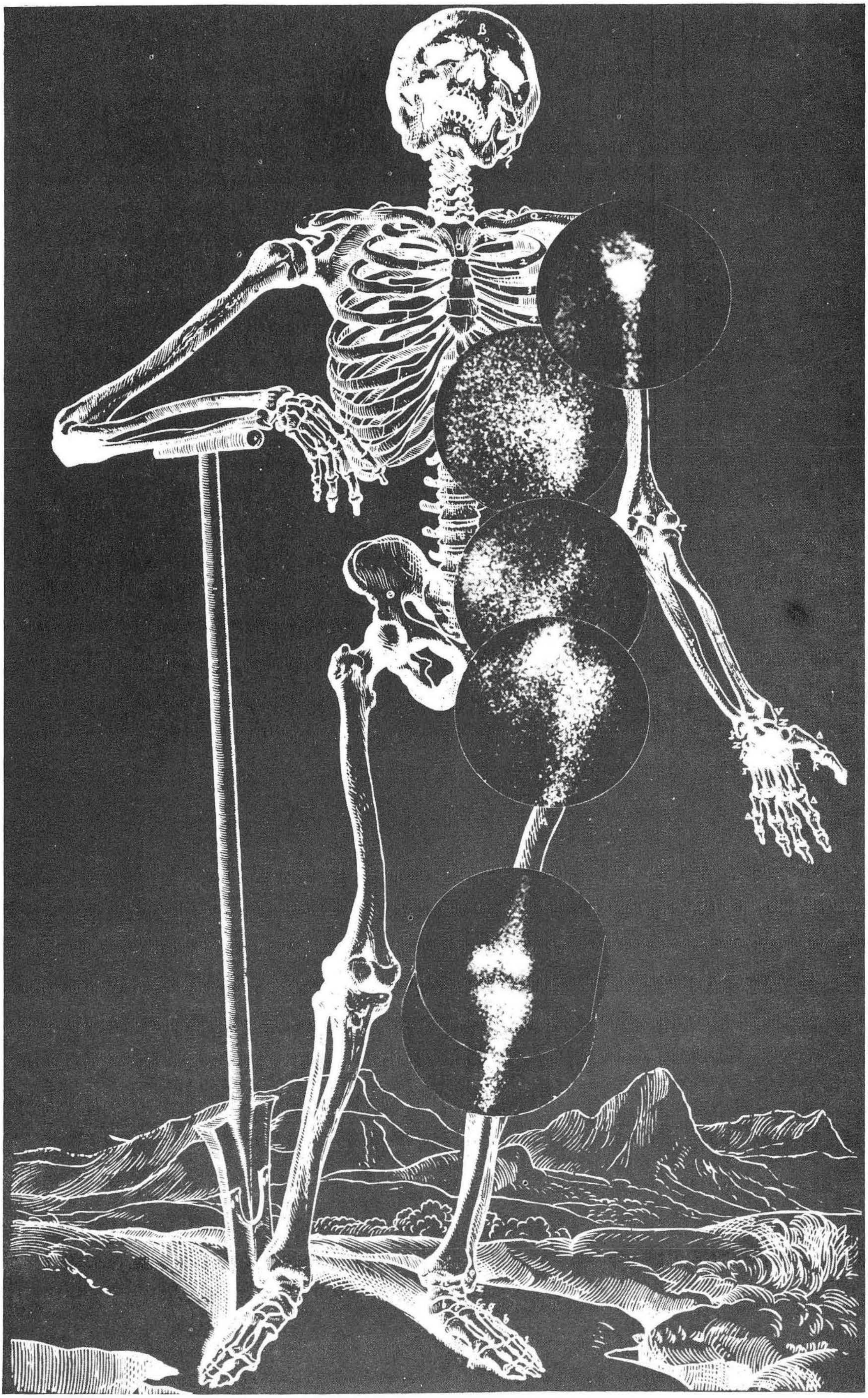

Distribution of erythropoietic bone marrow in patient with severe chronic blood loss shown in a composite picture taken with positron scintillation camera and superimposed on a copy of Vesalius' Fabrica of 1543. See p. 6

TABLE OF CONTENTS

Allelic Mapping in Yeast Using X-Ray-Induced Mitotic Reversion

Thomas R. Manney and Robert K. Mortimer

When two independently isolated mutant alleles of a given locus, a_1 and a_2, are placed in repulsion in the same diploid yeast cell (a_1/a_2) this heteroallelic diploid has a much higher frequency of reversion to wild type during mitotic division than either of the homoallelic combinations (a_1/a_1 or a_2/a_2). A process of allelic recombination in heteroallelic diploids has been suggested to account for this greater frequency (1). The effect can be stimulated both by ultraviolet light (2) and by X rays (3). Whereas the dose-effect relation with ultraviolet light is non-linear, with sub-lethal doses of X rays it is linear. We have found that the value of the slope of the X-ray curve depends on the pair of alleles involved. The nature of this dependence provides the basis for a new method for determining the sequence of alleles within a gene. We have tested this method at two nutritional loci in Saccharomyces cerevisiae: ar_4 (arginine biosynthesis) and tr_5 (tryptophan synthetase).

MATERIALS AND METHODS

The strains used in these experiments were cultured in rich liquid medium (two percent yeast extract, four percent peptone and four percent dextrose) to avoid preferential selection of revertants (prototrophs) which occur spontaneously during growth. Cultures were vigorously swirled in Erlenmeyer flasks for three days at 30°C. Between 10^6 and 10^8 washed cells, the number depending on the alleles and the dose, were plated on synthetic medium lacking either arginine or tryptophan. About 200 cells were plated on complete medium to assay viability. X rays from a beryllium-window tube (Machlett OEG 60) were delivered to the cells on the agar surface. The tube was operated at 50 kVp and 20 mA without additional filtration, giving a dose rate of about 200r/sec at the position of the cells. Visible colonies were counted after three to five days of incubation at 30°C. Less than one percent additional colonies appeared after five days incubation.

RESULTS

Dose-frequency curves for diploids with various allelic combinations at the ar_4 locus are shown in Fig. 1a. The slopes of these curves are highly reproducible from one culture of the same strain to another, although the intercept is extremely variable due to the clonal distribution of spontaneous revertants (4).

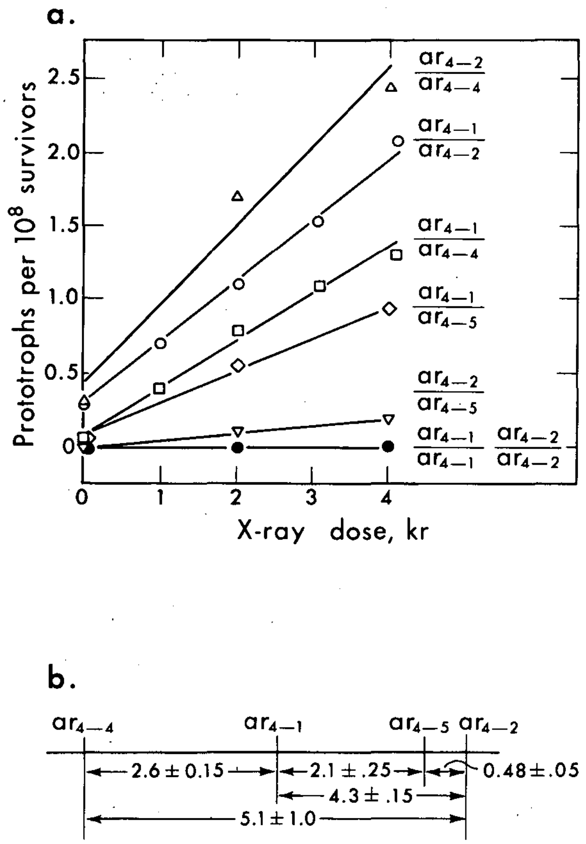

Figure 1. a) The frequency of arginine-independent revertants as a function of X-ray dose, for various heteroallelic and homoallelic diploid combinations at the ar_4 locus. b) Partial allelic map of ar_4 locus in Saccharomyces constructed from the slopes of the corresponding curves in Fig. 1a. Map intervals are in units of prototrophs/10^8 survivors/r. Standard deviations were calculated by the method of least squares.

MU-31855

The allelic map in Fig. 1b was constructed from the data in Fig. 1a by assuming that the slope of each curve is proportional to the distance between the two alleles involved. The map intervals so determined are consistently additive.

Figure 2 is a map of several alleles at the tr_5 locus constructed by this same method. Again, the intervals are consistently additive, permitting the sequence to be unambiguously determined.

The sequence assigned to the ar_4 alleles has also been confirmed by an entirely independent method. A cis double mutant $ar_{4-1}ar_{4-2}$ spore culture has been isolated by micromanipulation from asci of an ar_{4-1}/ar_{4-2} heteroallelic diploid, the double mutant strand evidently arising from reciprocal crossing-over between the two alleles. The diploid $ar_{4-1}ar_{4-2}/ar_{4-4}$ reverts to wild type spontaneously, at mitosis, with a high frequency, characteristic of heteroallelic strains, but the $ar_{4-1}ar_{4-2}/ar_{4-5}$ combination reverts at a

TABLE OF CONTENTS

Allelic Mapping in Yeast Using X-Ray-Induced Mitotic Reversion

Thomas R. Manney and Robert K. Mortimer

When two independently isolated mutant alleles of a given locus, a_1 and a_2, are placed in repulsion in the same diploid yeast cell (a_1/a_2) this heteroallelic diploid has a much higher frequency of reversion to wild type during mitotic division than either of the homoallelic combinations (a_1/a_1 or a_2/a_2). A process of allelic recombination in heteroallelic diploids has been suggested to account for this greater frequency (1). The effect can be stimulated both by ultraviolet light (2) and by X rays (3). Whereas the dose-effect relation with ultraviolet light is non-linear, with sub-lethal doses of X rays it is linear. We have found that the value of the slope of the X-ray curve depends on the pair of alleles involved. The nature of this dependence provides the basis for a new method for determining the sequence of alleles within a gene. We have tested this method at two nutritional loci in Saccharomyces cerevisiae: ar_4 (arginine biosynthesis) and tr_5 (tryptophan synthetase).

MATERIALS AND METHODS

The strains used in these experiments were cultured in rich liquid medium (two percent yeast extract, four percent peptone and four percent dextrose) to avoid preferential selection of revertants (prototrophs) which occur spontaneously during growth. Cultures were vigorously swirled in Erlenmeyer flasks for three days at 30°C. Between 10^6 and 10^8 washed cells, the number depending on the alleles and the dose, were plated on synthetic medium lacking either arginine or tryptophan. About 200 cells were plated on complete medium to assay viability. X rays from a beryllium-window tube (Machlett OEG 60) were delivered to the cells on the agar surface. The tube was operated at 50 kVp and 20 mA without additional filtration, giving a dose rate of about 200r/sec at the position of the cells. Visible colonies were counted after three to five days of incubation at 30°C. Less than one percent additional colonies appeared after five days incubation.

RESULTS

Dose-frequency curves for diploids with various allelic combinations at the ar_4 locus are shown in Fig. 1a. The slopes of these curves are highly reproducible from one culture of the same strain to another, although the intercept is extremely variable due to the clonal distribution of spontaneous revertants (4).

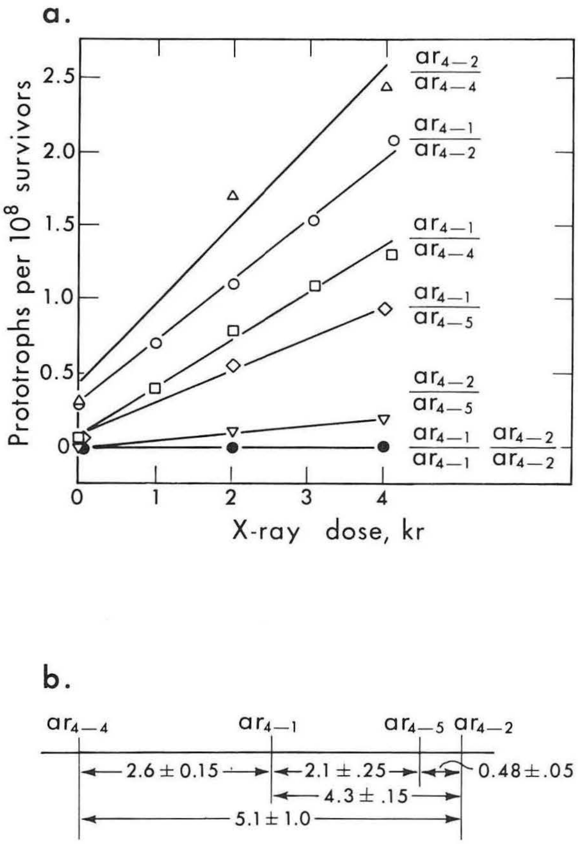

Figure 1. a) The frequency of arginine-independent revertants as a function of X-ray dose, for various heteroallelic and homoallelic diploid combinations at the ar_4 locus. b) Partial allelic map of ar_4 locus in Saccharomyces constructed from the slopes of the corresponding curves in Fig. 1a. Map intervals are in units of prototrophs/10^8 survivors/r. Standard deviations were calculated by the method of least squares.

MU-31855

The allelic map in Fig. 1b was constructed from the data in Fig. 1a by assuming that the slope of each curve is proportional to the distance between the two alleles involved. The map intervals so determined are consistently additive.

Figure 2 is a map of several alleles at the tr_5 locus constructed by this same method. Again, the intervals are consistently additive, permitting the sequence to be unambiguously determined.

The sequence assigned to the ar_4 alleles has also been confirmed by an entirely independent method. A cis double mutant $ar_{4-1}ar_{4-2}$ spore culture has been isolated by micromanipulation from asci of an ar_{4-1}/ar_{4-2} heteroallelic diploid, the double mutant strand evidently arising from reciprocal crossing-over between the two alleles. The diploid $ar_{4-1}ar_{4-2}/ar_{4-4}$ reverts to wild type spontaneously, at mitosis, with a high frequency, characteristic of heteroallelic strains, but the $ar_{4-1}ar_{4-2}/ar_{4-5}$ combination reverts at a

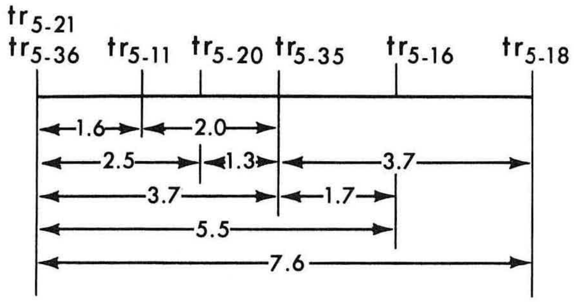

Figure 2. Partial allelic map of the tr_5 locus in *Saccharomyces* constructed by the X-ray mapping method illustrated in Fig. 1.

MU-32161

frequency that is more than an order of magnitude smaller. This is exactly the behavior predicted by the sequence deduced from X-ray data (Fig. 1b), since a double exchange would be required to produce a prototroph in the latter case, whereas a single event would suffice in the former.

The results of additional experiments at the tr_5 locus allow us to relate the map units of the X-ray method (1 unit = 1 prototroph/10^8 survivors/roentgen) to molecular dimensions. We have mapped more than 30 mutants at this locus. It is likely that the two alleles that are farthest apart are located near the ends of the gene, and we may consider the distance between them to be a minimum estimate of the length of the gene in X-ray mapping units. This distance, 10 prototrophs/10^8 survivors/roentgen, can then be compared with the size of the tryptophan synthetase molecule. Carsiotis *et al*. (5) found the molecular weight of *Neurospora* tryptophan synthetase to be about 122,000. Their studies of properties of the enzyme suggest a quaternary structure comprised of two or more subunits. An upper limit for the number of amino acid residues corresponding to the structural gene for the enzyme would therefore be of the order of 500. Assuming the same number for yeast, then, one map unit corresponds to approximately 50 amino acid residues or, assuming a triplet code, to 150 nucleotide pairs. On this basis, exchange between mutants in the same coding unit would occur with a frequency that would correspond to less than 10^{-2} units.

From the above relation, we can estimate the lower limit of resolution imposed by the background of homoallelic reversions; recombination between two alleles can be measured only if the frequency is significantly greater than this background. We have measured the X-ray-induced homoallelic reversion frequencies of four mutants, tr_{5-2}, tr_{5-4}, tr_{5-21} and tr_{5-36}, that appear to be repeat mutations at the same site. The mean value from nine determinations was 8×10^{-3} units with a standard deviation of 1.5×10^{-3}. This corresponds approximately to the length of one coding unit. Thus, if the relation between map units and molecular dimensions is constant down to this level we would expect to be able to resolve mutations in adjacent coding units. The closest pair of separable mutants we have encountered, however, are tr_{5-6} and tr_{5-18} at a distance of 0.30 units apart. This corresponds to about 15 amino acid residues.

DISCUSSION

The validity of the X-ray-mapping method for determining the sequence of mutational sites within a cistron is established by the internal consistency in our results. It is further supported by the agreement with the independently determined sequence of the ar_4 alleles. The method, in addition, has several advantages over previous approaches to allelic mapping. One alternative method is to measure spontaneous mitotic reversion frequencies. These, however, can be determined accurately only by the use of a method of the type devised by Luria and Delbrück (6). Such methods, however, are quite tedious and their precision is severely limited by the nature of clonal frequency distributions (4). The use of X rays circumvents these statistical limitations. Another alternative method is to measure prototroph frequencies among random spores. This, however, requires the technically difficult task, in yeast, of separating spores from unsporulated diploid cells. The X-ray method is much simpler than either of these alternatives and thereby makes extensive allelic mapping practical.

A simple hypothesis that is consistant with these experiments is that X rays produce lesions, distributed at random, in the genetic material, and a lesion of the appropriate type anywhere in the region between the two mutations leads to a recombination. This hypothesis is suggested, in part, by the results of Jacob and Wollman (7), who found that ultraviolet light greatly increases the frequency of recombination between different mutants in crosses of the temperate bacteriophage lambda. Their studies of the kinetics of recombination following irradiation of the parental phages support the conclusion that recombination occurs with high probability at the sites of radiation-induced lesions.

SUMMARY

A new method for determining the sequence of mutational sites is based on the linear dose-effect relation for X-ray induction of allelic recombination in Saccharomyces cerevisiae. Mutations at two loci have been mapped by this method. The use of X rays simplifies allelic mapping and greatly increases its sensitivity.

REFERENCES

1. Roman, H.; Cold Spring Harbor Symp. Quant. Biol. 21:175, 1956.
2. Roman, H., and Jacob, F.; Compt. rend. 245:1032, 1957.
3. Mortimer, R. K.; Radiation Res. Suppl. 1:394, 1959.
4. Lea, D. E., and Coulson, C. A.; J. Genet. 49:264, 1949.

5. Carsiotis, M., Appella, E., and Suskind, S. R.; Proc. XI Intern. Congr. Genet. 1:52, 1963.
6. Luria, S. E., and Delbrück, M.; Genetics 28:491, 1943.
7. Jacob, F., and Wollman, E. L.; Ann. Inst. Pasteur 88:724, 1955.

Received November 1963.

Effect of Erythropoietic Stimulation on Marrow Distribution in Man, Rabbit and Rat As Shown with Fe^{59} and Fe^{52}

Donald Van Dyke, Hal O. Anger and Myron Pollycove

In evaluating marrow one usually studies an aliquot of the marrow and from the findings draws conclusions regarding the entire marrow compartment. The aliquot consists of a sample from one bone, or in experimental animals, the entire marrow from a given bone. Conclusions are misleading if significant changes are occurring in the volume of the marrow or in distribution of marrow within the skeleton. Methods are needed to obtain information on the marrow as a whole.

This report presents three methods for obtaining information on the total marrow in the skeleton, making use of <u>in vivo</u> labeling of the marrow compartment with radioactive iron. The methods are (a) scanning large subjects such as human beings with a whole-body scanner, using Fe^{52} or Fe^{59}; (b) taking scintiphotos with the positron scintillation camera, using Fe^{52}; and (c) using a well counter and Fe^{59} for assaying individual bones of small animals.

In clinical investigation of human subjects, a whole-body scan at the time of maximum incorporation of iron in the marrow produces a good qualitative image of the marrow as well as of the liver and spleen. High-resolution pictures of smaller areas can be taken with the recently developed positron scintillation camera and the short-lived positron emitter Fe^{52}.

The resolution obtained with the positron scintillation camera and Fe^{52} is adequate to show the distribution of the isotope in the major bones of small animals and in selected parts of bones of human beings. After all major iron-containing compartments other than the marrow are removed from experimental animals by exsanguination, perfusion, and evisceration, scintiphotos show the distribution of radioiron in the erythropoietic marrow.

The third method utilizes a well-type scintillation counter to compare individual bones of a skeleton. The skeleton of a small animal is cleaned by a colony of carnivorous beetles (<u>Dermestes</u> <u>vulpinus</u>), as used by vertebrate zoologists (1). The Fe^{59} content of each bone is determed by γ-ray counting, and the fraction of the total marrow within each bone can be calculated.

INSTRUMENTATION

The whole-body scanner has been described in the literature (2,3). It has ten heavily shielded scintillation counters with single-bore collimators three-quarter of an inch in diameter by 3 in. long. Signals from the counters go through discriminator circuits to driver circuits that cause one of 10 glow lamps to flash with each count detected by a scintillation counter. Two images of each scan are recorded on Polaroid film. A telephoto lens and mirror arrangement allows recording an automatically superimposed optical image of the patient on one of the two γ-ray images. The other γ-ray image is recorded without the optical image.

The positron scintillation camera is a nonscanning electronic instrument that produces pictures of the distribution of positron-emitting isotopes in animal or human subjects. The instrument has been described (4) and is presently being used clinically to localize brain tumors in human subjects with Ga^{68} (5). Its image detector consists of a large solid sodium iodide scintillator, 11.5 in. in diameter by 0.5 in. thick, viewed by a bank of 19 multiplier phototubes and a focal detector. The subject is placed as close as possible to the image detector, and on the opposite side of the subject, about 24 in. away, is placed the focal detector, consisting of a bank of 19 scintillation counters. When positrons are emitted in the subject, two annihilation γ-rays are created which travel away in exactly opposite directions, producing coincident scintillations in the two detectors. Scintillations in the image detector that are coincident with scintillations in the focal detector are reproduced as flashes of light in their proper location on a cathode ray oscilloscope. There they are recorded by a time exposure on photographic film. Each gamma pair detected produces one dot on the film. The sensitivity of the instrument is such that a positron emitter with 100% abundance produces 1,500 dots per min/μC on the resulting picture.

MATERIALS AND METHODS

The Fe^{52} used in the present studies is produced by alpha bombardment of natural chromium in the Lawrence Radiation Laboratory 88-inch cyclotron. The radioactive iron is separated from the chromium by ether extraction. The half-life of Fe^{52} is 8.2 hr. It decays by positron emission 57% of the time into a radioactive daughter, Mn^{52m}, which in turn decays 100% of the time by positron emission into inactive Cr^{52}. The half-life of Mn^{52m} is 21 min. Fe^{52} has an effective positron abundance of 1.57, producing on the scintiphoto about 2,400 dots per min/μC of Fe^{52}. Although the daughter Mn^{52m} does not have the same distribution in the body as does iron, its half-life is short enough so that when it is photographed in a killed animal, most of it will have decayed before the picture is taken. The Mn^{52m} that is formed in the dead animal will have the same distribution as its parent iron. Information on the distribution of marrow in the skeleton of human subjects was obtained by scanning with the 10-channel whole-body scanner 24 hr after administration of Fe^{59}. The dose is usually 40 μC, given in connection with diagnostic ferrokinetic studies. Close-up views of the marrow concentration in various bones of human subjects were made with the scintillation camera at the same time whole-body scans were made.

Marrow distribution in severely anemic and normal New Zealand white rabbits was compared by means of the positron camera. Severe hemolytic anemia was produced by daily administration of 0.7 ml of a 2.5% solution of phenylhydrazine to a 6-pound female rabbit on days 1 through 7. By the 8th day, the reticulocyte count was 93% and the hemoglobin concentration was 4.7 g/100 ml. On day 9, 5 μC of Fe^{52} were given intravenously; five hours later the rabbit was exsanguinated, perfused, and eviscerated, and positron scintiphotos were taken to show the distribution of Fe^{52}.

Marrow distribution in severely bled and in normal rats of the Long-Evans strain was also studied with the positron camera. A 490-gram male rat was bled 8 cc, 7.5 cc, 8 cc, 2.5 cc, and 8 cc by cardiac puncture on days 1, 2, 3, 5, and 6 respectively. On day 7, 5 μC of Fe^{52} were given intravenously; five hours later the rat was exsanguinated, perfused, and eviscerated, and positron scintiphotos were taken. At the time of Fe^{52} administration, the hematocrit of the bled animal was 23.5% and reticulocyte count was 39.7%. The normals were subjected to the same procedure 5 hr after injection of Fe^{52}.

Because the field of view of the positron camera is about 9 in. in diameter, separate pictures were taken of the anterior and posterior parts of the rat. Three views were necessary for the rabbits, and many views for a man. Exposure times varied from 5 min to 4 hr. A standard roentgenogram of the skeleton was also taken for comparison with the positron picture.

When the Fe^{59} content of individual bones in the rat was to be determined, the following procedure was used: rats were given Fe^{59} intravenously, and 5 hr later [shown to be the time of maximum uptake of Fe^{59} by marrow in normal rats (6)] the rats were anesthetized with ether and a sample of blood was drawn from the inferior vena cava for determination of hematocrit and hemoglobin. A canula was inserted in the abdominal aorta, and the animal was thoroughly perfused (the inferior vena cava was lacerated to allow outflow of blood and perfusate) until the heart stopped beating.

The efficiency of the perfusion was demonstrated in a separate group of rats by giving a transfusion of Fe^{59}-labeled-erythrocytes prior to perfusion and subsequently counting one tibia. The amount of activity remaining in the bone as a result of contamination with blood following perfusion was shown to be insignificant, or less than 0.1%. After perfusion, the spleen and liver were weighed and counted for Fe^{59} content, and imprints were made for subsequent morphologic study. A well-type scintillation counter was used for determination of Fe^{59} content of all samples. Liver and spleen imprints were stained by LoBue's modification of Ralph's hemoglobin-staining technique (7,8).

The right tibia was cleaned of all soft tissue and counted for Fe^{59}; the ends were then perforated with a dental drill and the marrow was washed out by flushing 1 ml of serum through the shaft with a syringe. The washed-out bone was recounted to determine completeness of marrow collection. An even suspension of the marrow was made in a known volume of serum by gently drawing through a pipette. Duplicate cell counts of this suspension were made with a standard Levy hemacytometer. The suspension was then gently centrifuged, and the packed marrow cells were smeared and stained as above. The left tibia was cleaned of all soft tissue, counted for Fe^{59} content, and opened, and a portion of the marrow was removed, weighed, and counted to determine radioactivity per mg marrow.

The carcass was then eviscerated, skinned, rapidly and thoroughly desiccated in hot, dry air to avoid loss of marrow from the bones through liquefaction. It was then placed in a colony of carnivorous beetles. When the larvae had completely cleaned the skeleton externally, the larvae not being able to penetrate the nutritive foramina of the rat, the Fe^{59} content of the individual bones was determined by counting in a well-type scintillation counter.

For these studies specific-pathogen-free male rats, either untreated or erythropoietin-stimulated, and of the same age and strain, were used. Two rats of the Long Evans strain were given 13 standard A units of erythropoietin daily for 14 days prior to Fe^{59} administration. The erythropoietin was obtained by collodion adsorption from the urine of a patient with aplastic anemia. It had been assayed by a variety of methods (9) and standardized against a sample of standard A, provided by the Bureau of Biological Standards, Medical Research Council of Great Britain. Diet #1 was fed ad libitum. This diet, obtained from Simonsen Laboratories, Gilroy, California, consisted of 59.0% wheat, 11.7% skim milk, 11.2% casein, 11.2% rice bran, 3.3% vegetable oil, 1.3% $CaCO_3$, 0.7% NaCl, and vitamin and mineral mixtures to 100%.

RESULTS

HUMAN BEINGS. Whole-body scans of the distribution of Fe^{59} at the time of maximum marrow incorporation in a normal human being, a severe chronic bleeder and a person with relatively acute hemolytic anemia are shown in Fig. 1. The ribs are visible in all three subjects, the liver is seen in 1a and 1c, and the spleen in 1b and 1c. In the normal subject, 1a, the iron (excepting that in the liver) is concentrated in a cross-shaped area corresponding to spine and shoulders, a diffuse thoracic area corresponding to the ribs and a rectangular area corresponding to the pelvis. There is no significant amount of radioiron

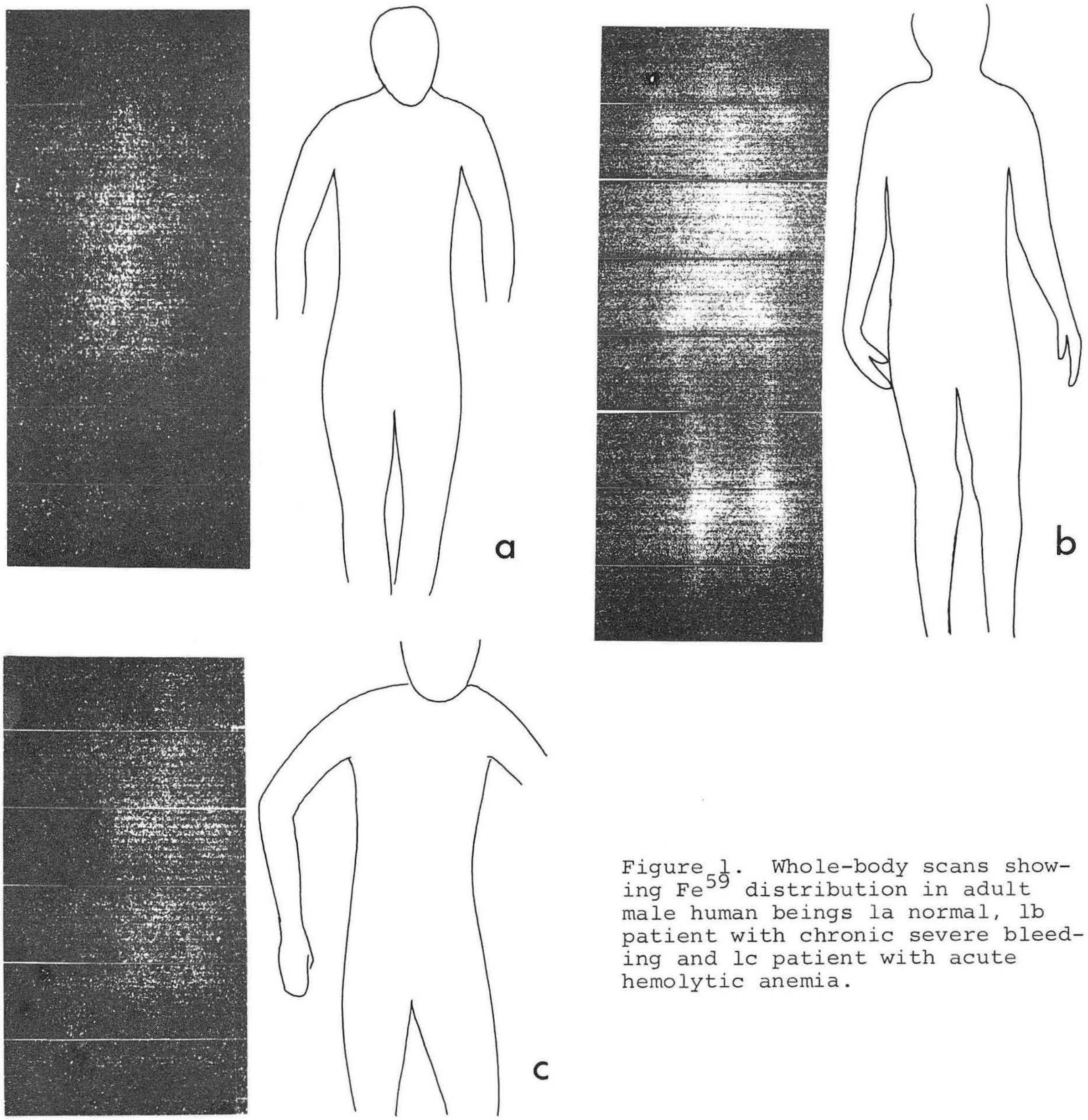

Figure 1. Whole-body scans showing Fe^{59} distribution in adult male human beings 1a normal, 1b patient with chronic severe bleeding and 1c patient with acute hemolytic anemia.

in the extremities, except for the heads of the humeri and femora. The iron distribution for the patient with severe bleeding of many years' duration, 1b, is clearly different from the normal, with extension of erythropoietic marrow into the lower limbs, particularly the knee. (This patient had aching pain and tenderness in this region.) The distribution of iron in the patient with subacute severe hemolytic anemia, of one to two months' duration, and erythropoiesis increased to 13 times normal, 1c, is indistinguishable from that of the normal control. The distribution patterns shown are illustrative of those seen in congenital anemia or anemia of long duration, 1b, and in acquired anemia of relatively short duration, 1c.

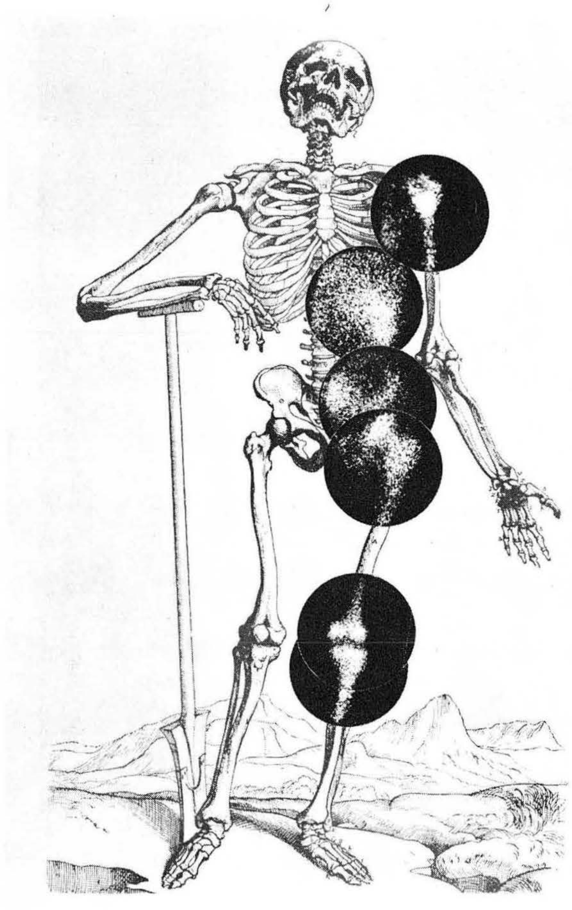

Figure 2. Positron scintillation camera closeups of Fe^{52} distribution in selected areas of patient 1b of Fig. 1. The exposure time for each area viewed was 10 min. (For enlarged view see frontispiece.)

Figure 2 is a composite of positron-camera pictures of the patient (chronic blood loss) whose whole-body scan is shown in Fig. 1b. In order to provide orientation, the positron pictures are superimposed on a copy of plate 21 of Vesalius' Fabrica of 1543. A comparison of the two figures illustrates how much greater resolution is obtained with the positron camera than with the whole-body scanner.

A summary of the case history of this patient has been published previously, ((10) Case K, Table 1). The patient has severe anemia of 20 years' duration, an elevated erythropoietin titer, and a markedly accelerated rate of red-cell production due to chronic blood loss. At the time the whole-body scan was made, the rate of hemoglobin synthesis, calculated from the rate of loss of erythrocyte radioiron as measured with a whole-body counter, was nine times normal. In order to prevent iron deficiency 1,500 mg iron (Inferon) per week were administered intravenously.

The second case (Fig. 1c) is that of a 32-year-old male of American Indian extraction with an 18-month history of mild fatigue and dyspnea on exertion, and severe symptoms associated with pallor and dizziness for several

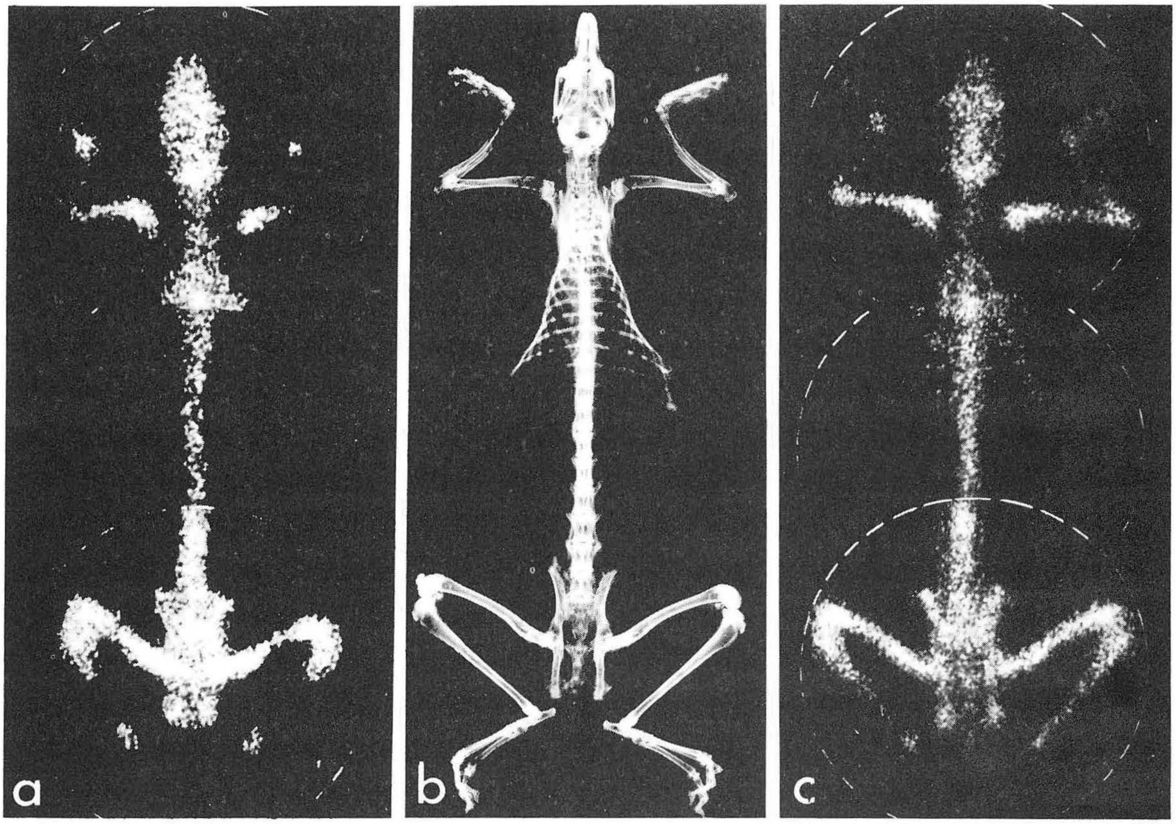

Figure 3. Positron scintiphotos of the marrow of 3a normal rabbit and 3c rabbit with phenylhydrazine-induced hemolytic anemia of eight days duration. The 3b roentgenogram of the normal rabbit is shown for orientation of the scintiphotos.

weeks prior to this study. At the time the scan was taken, his hemoglobin was 6.6 g %, hematocrit 20%. Leucocyte and platelet counts were normal. The reticulocyte count was 9% and the spleen was palpable two fingerbreadths below the costal margin. Serum bilirubin was 1.2 mg %. A direct Coombs test was positive at 32°C and 20°C. The indirect Coombs was negative. The marrow was markedly cellular, with tremendous erythroid hyperplasia and no evidence of maturation block. White-cell elements and megakaryocytes appeared normal.

Analysis of plasma radioiron for two weeks demonstrated marked increase of hemoglobin synthesis to 70.43 g/day, 16.6 g/liter/day (normal, 1.0-1.6). A mean erythron life span of only 2.7 days was obtained. In vivo measurements demonstrated rapid initial accumulation of radioiron in sacral marrow, with almost none in liver or spleen. There was rapid but incomplete net release of radioiron from sacral marrow, which attained virtual equilibrium by the 8th day. There was an associated marked secondary accumulation of radioiron in liver and spleen, slightly more in liver, reaching a maximum on the 6th day. There was some decrease but still distinctly positive accumulation of radioiron in liver and spleen at the end of two weeks.

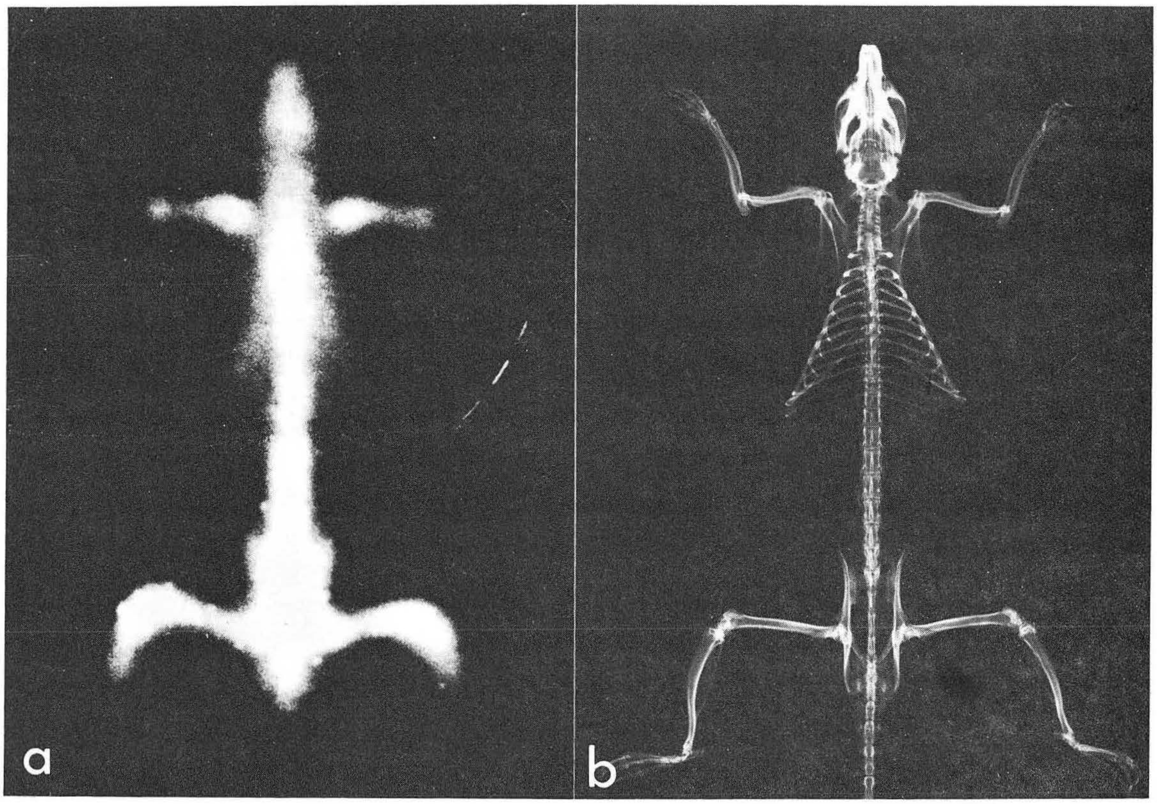

Figure 4. Positron scintiphoto of the marrow of a normal adult rat with a roentgenogram for comparison

The iron kinetic study demonstrated marked destruction of circulating erythrocytes, with sequestration and destruction of red cells in both liver and spleen. There was slightly more destruction in liver than in spleen; this abnormal finding suggested marked agglutination of circulating red cells. Partially compensatory erythropoiesis was increased approximately thirteenfold. This however, was distinctly inadequate to compensate for the marked destruction of red cells, which reduced their mean life span to approximately one-forty-fifth of normal. The diagnosis was idiopathic autoimmune hemolytic anemia.

RABBITS. A typical positron scintiphoto of the marrow compartment of an adult white New Zealand rabbit is shown in Fig. 3a. The blood, spleen and liver have been removed. A comparison of the intensity in different areas of the positron scintiphoto with a roentgenogram of the skeleton, 3b, shows qualitatively the distribution of erythropoietic marrow within the skeleton as a whole, and also the distribution in the large individual bones. One can conclude that the rabbit normally has marrow distributed throughout the skeleton, since the picture of the marrow distribution closely resembles the roentgenogram of the skeleton. Figure 3c shows a positron scintiphoto of the distribution of iron

Table 1. Proportion of the marrow Fe^{59} contained in the major bones and groups of bones in the rat

Bone	Proportion of total marrow (%)				
	Normal			Erythropoietin[a]	
	Sprague-Dawley 214 g	Long-Evans 430 g	Long-Evans 404 g	Long-Evans 386 g	Long-Evans 427 g
Femur (one)	7.66	8.99	8.69	7.89	10.75
Tibia (one)	4.80	5.61	6.56	8.17	7.29
Tibial epiphysis (one)	b	1.02	1.20	1.53	1.38
Fibula (one)	b	0.08	0.13	0.12	0.10
Innominate (one)	5.31	3.22	3.98	5.39	3.24
Skull	6.31	3.26	2.65	2.61	7.38
Mandible	3.05	2.35	2.34	2.36	1.68
Humerus (one)	3.38	3.88	3.18	4.25	3.24
Sternum (entire)	2.99	5.43	3.95	4.17	2.83
Scapula (one)	0.92	0.66	0.73	0.74	0.72
Cervical vertebrae (7)	2.89	1.69	2.65	1.19	1.32
Thoracic vertebrae (13)	7.78	11.58	10.27	5.89	7.56
Lumbar vertebrae (4)	6.39	8.41	8.01	7.38	8.84
Sacral vertebrae (5)	8.82	9.53	11.06	9.78	7.88
Caudal vertebrae (30)	9.30	4.24	3.70	6.21	3.50
Ribs (26)	5.70	6.40	6.57	4.44	5.57
Ulna (one)	0.509	0.445	0.580	0.610	0.594
Radius (one)	0.212	0.140	0.245	0.313	0.236
Clavicle (one)	0.143	0.078	0.094	0.171	0.098
Front foot (one)	0.188	0.064	0.063	0.073	0.068
Hind foot (one)	0.273	0.130	0.145	0.119	0.186

a. 13 Standard A units per day for 14 days prior to Fe^{59} administration.
b. Not counted.

in the skeleton of a rabbit made severely anemic with phenylhydrazine. A small but distinct difference exists between the distribution here and that obtained in several normal controls. The severely anemic rabbit shows an even distribution of radioiron through the bones of the foreleg and along the shaft of the tibia, whereas in normal rabbits little activity is seen in the distal third of the bones of the foreleg and in the distal third of the tibia.

RATS. Positron scintiphotos of the marrow compartment of a severely bled rat, were indistinguishable from those of normal controls, Fig. 4. However, at the time chosen (5 hr after Fe^{52} administration) a 17%-longer exposure was required for the bled rat than for the normal control in order to obtain an equal number of dots in the positron picture. The marrow of the bled rat, therefore, must have contained approximately 17% less Fe^{52} five hours after administration than the normal.

Table 2. Effect of erythropoietin on organ and body weights, hematological values, and marrow volume of adult rats

Group	Body wt. (g)	Liver wt. (g)	Spleen wt. (g)	Hct. (%)	Hgb. (g/100 ml)	Total marrow (g)	Marrow fraction of body weight (%)
Erythropoietin-treated	427	9.5	0.79	60.0	16.4	1.95	0.46
	386	9.8	0.96	56.1	14.7	1.52	0.39
Saline control	430	11.5	0.66	46.1	11.9	1.94	0.46
	404	9.9	0.55	47.1	12.8	1.68	0.42

An exact quantitation of the amount of marrow in the various bones was possible using a well counter and Fe^{59} following cleaning of the rat skeleton by the beetles. Table 1 lists the part of the total marrow volume (Fe^{59}) contained in each of the major bones and groups of bones (bones were arbitrarily grouped in order to shorten the list). The Fe^{59} activity per mg of marrow was determined using marrow from one tibia prior to placing the carcass with the beetles. Having determined the Fe^{59} activity per mg of marrow and having determined the Fe^{59} activity of the individual bones, one can calculate the mg of marrow per bone. The sum of these values gives the total amount of marrow in the entire skeleton, assuming that the myeloid-erythroid ratio and the proportion of storage iron in the tibia is representative of all bones. Total marrow volume in two normal adult control rats was found to be 0.46 and 0.42% of body weight, as shown in Table 2. This value is considerably smaller than estimates by previous investigators.

Counts of total nucleated cells and differential counts done on marrow from the tibia showed no significant difference between erythropoietin-treated and untreated rats. Morphologic examination of the smears from liver and spleen revealed no recognizable normoblasts in the liver and an average of 3.1% in the spleens of the erythropoietin-treated rats as compared with an average of 2.2% in the spleens of untreated rats. A subsequent study of nine erythropoietin-treated and nine untreated rats confirmed the observation that at the dose used no significant change occurred in marrow-nucleated-cell count or marrow differential count. A detailed analysis of iron kinetics and marrow morphology of erythropoietin-treated rats is presented in another report (11).

DISCUSSION

It is apparent from the whole-body scans of the three human subjects presented that the human being is capable of considerable peripheral extension of his bone marrow. However, significant extension occurs only after prolonged, massive stimulation. Increases in red-cell production up to 13 times normal can be achieved without any great marrow extension. It is well known (12) that in the human being blood loss or any other demand for increased erythropoiesis is followed by rapidly increasing density of erythroid elements in the marrow. It is apparent that a patient, such as the one illustrated in Fig. 1c, can increase the concentration of erythroid elements and thereby increase erythropoiesis 13-fold without evidence of significant peripheral extension of the marrow.

In severely anemic rabbits and rats, positron pictures also indicate that no considerable redistribution of marrow within the skeleton occurs during the initial erythropoietic response. Whereas the rabbit normally has marrow distributed throughout the skeleton (Fig. 3), and therefore can have little peripheral expansion, the normal rat is intermediate between man and rabbit in that the marrow is concentrated in the pelvis and proximal portion of the legs, with relatively little in the distal portion of the legs or the tail (Fig. 4).

Correlation of Fig. 4a with the Fe^{59} assay of the individual bones for the mature rat (Table 1) shows comparable distribution. The values obtained in this study for the fraction of marrow contained in one femur in normal rats (7.6 to 8.9%) are in agreement with the 8% obtained by Lamerton for young growing rats of the August strain (13). The values obtained by Lamerton for distribution of Fe^{59} within the skeleton are similar to those obtained in this study, with the exception that he observed considerably less activity in the tail. Neither Lamerton's findings for marrow distribution nor the results of this study agree with those of Kindred (14), obtained by cell counts in serial sections.

From Fig. 4 it can be seen that the femur of the rat contains marrow along its entire length, with concentrations at the proximal and distal ends. This is in agreement with the finding by LoBue _et al_. (7) that in the rat femur 55% to 65% of the marrow is located in the diaphysis, the remainder being in the epiphyseal region. In the positron picture the tibia, which contains approximately 6% of the marrow, is clearly visible only at its proximal end. When counted after separation at the proximal epiphyseal plate, the proximal epiphysis of the tibia was found to contain only 15% of the activity (Table 1). The dense spot in the positron picture represents the concentration of marrow in the proximal end of the tibial shaft.

A comparison of the individual bones of the 200-g Sprague-Dawley rat with those of the 400-g Long-Evans rats in Table 1 shows the two strains to be generally similar except for a greater proportion of the activity in the caudal vertebrae, and possibly also in the feet, of the smaller (younger) Sprague-Dawley rat. It is not known whether this difference is due to difference in age or in strain.

The values obtained for total marrow volume in normal rats were 0.42% and 0.46% of body weight, or less than half the value usually quoted in the literature. Kindred (14) estimated 1.176% of body weight, and Huff, et al. (15) estimated 1% of body weight. It must be remembered that the small figures obtained for marrow volume in this study apply to relatively old rats, whereas the values obtained by Kindred were from studies of relatively young rats (80 days of age). Because of the changing demands on the marrow during growth and aging (6), it is quite possible that the dissimilar values obtained by different investigators are correct for the specific age of rat studied. Using Fe^{59} marrow incorporation, Garcia (6) estimated marrow volume to be 0.8% of body weight in 150- and 250-day-old rats and 1.2% in 50-day-old rats of the Long-Evans strain.

The dose of erythropoietin (13 standard A units) was arbitrarily chosen as that which would triple or quadruple the rate of red-cell formation and produce an increase of approximately 60% in total circulating red cells in 14 days (9). The effectiveness of this dose of erythropoietin in increasing hematocrit and hemoglobin is shown in Table 2. Comparison of the Fe^{59} content of the individual bones (Table 1) and of the total marrow (Table 2) in erythropoietin-treated and in control rats revealed only slight difference in the size or distribution of marrow in the skeleton. The results indicate that erythropoiesis was markedly stimulated for two weeks by the administration of erythropoietin, but do not indicate considerable expansion of marrow volume. The fact that no difference was demonstrated in the distribution of marrow within the skeleton between severely bled and normal rats is in agreement with the results of Hudson (16), who studied the effect of hypoxia on the marrow volume of the guinea pig. Hudson concluded that the bone-marrow volume of the hypoxic guinea pig showed no increase over that of the controls, and that this finding applied both to total bone-marrow volume and to haemopoietic (red) bone-marrow volume. Dallwig et al. (17) found in rabbits exposed to reduced barometric pressure for one week that the bone marrow showed macroscopically a disappearance of fat and an extension of the marrow, and microscopically a marked hyperplasia of the erythrocyte-forming centers.

In the rat, failure to demonstrate an increase in erythropoietic marrow volume in the presence of a red-cell-production rate approximately three to four times normal raises the question: By what mechanism is the increased production achieved? One concludes that at least with this degree of stimulation and during the time period studied (14 days) red-cell production in the rat must be increased by mechanisms other than increased marrow mass. Other mechanisms by which erythropoietin may have its effect have recently been discussed by Borsook et al. (18), Hodgson and Eskuche (19), and Fischer (20). That one effect of erythropoietin is to stimulate conversion of stem cells into the erythron has been conclusively demonstrated by Gurney et al. (21). Our report does not deny such a mechanism but points out the possibility of other sites of action of erythropoietin, a more detailed analysis of which is presented in another report (11).

CONCLUSIONS

Distribution of marrow within the skeleton has been determined in man, rabbits, and rats by in vivo labeling of the marrow compartment with radioiron and, depending on the resolution required, either assaying each bone separately for radioactivity or obtaining a gamma-ray image of the distribution of the marrow by whole-body scanner or with the positron scintillation camera. In man, extension of marrow into unusual sites was demonstrated only in cases with prolonged and severe stimulation, excessive blood loss, or hemolysis for a long period. A rabbit made severely anemic by administration of phenylhydrazine for seven days showed extension of marrow into the distal portion of the humeri and femora. In rats in which erythropoiesis was stimulated by erythropoietin administration, no significant increase in total marrow volume and no change in distribution of marrow within the skeleton were found. The positron scintillation camera provides an excellent method for qualitative evaluation of the marrow distribution. The camera has sufficient resolving power to give a good picture of the distribution of marrow with Fe^{52} in a skeleton as small as that of the rat. The distribution apparent from the positron pictures has been confirmed by complete skeletal analysis of individual bones.

ACKNOWLEDGEMENTS

The Fe^{52} used in these studies was prepared by Mr. Yukio Yano. The phenylhydrazine-treated rabbit was kindly supplied by Dr. Geoffrey Keighley, California Institute of Technology, Pasadena, California.

This work was supported in part by the United States Atomic Energy Commission.

REFERENCES

1. Russell, W. D.; J. Mammalogy 28:284, 1947.
2. Anger, H. O.; Am. J. Roentgenol. Rad. Therapy Nucl. Med. 70:605, 1953.
3. Anger, H. O., and Tisjlar-Lentulis, G. M.; J. Nucl. Med. 2:99, 1961.
4. Anger, H. O.; Nucleonics 21:56, 1963.
5. Anger, H. O., and Gottschalk, A.; J. Nucl. Med. 4:326, 1963.
6. Garcia, J. F.; Am. J. Physiol. 190:31, 1957.
7. LoBue, J.; Dornfest, B. S.; Gordon, A. S.; Hurst, J., and Quastler, H.; Proc. Soc. Expertl. Biol. Med. 112:1058, 1963.
8. Ralph, P. H.; Stain Technol. 16:105, 1941.
9. Van Dyke, D., and Pollycove, M.; in Erythropoiesis, New York, Grune and Stratton, Inc., 1962, p. 340.
10. Van Dyke, D. C.; Layrisse, M.; Lawrence, J. H.; Garcia, J. F., and Pollycove, M.; Blood 18:187, 1961.
11. Van Dyke, D., and Parker, H.: Mechanism by which Erythropoietin Increases Red-Cell Production in the Rat. In preparation.
12. Custer, R. P.: An Atlas of the Blood and Bone Marrow, Philadelphia,

W. B. Saunders Co., 1949, p. 29.

13. Lamerton, L. F.; Belcher, E. H., and Harriss, E. B.; Proc. Roy. Soc. Med. 49:863, 1956.
14. Kindred, J. E.; Am. J. Anat. 71:207, 1942.
15. Huff, R. L.; Bethard, W. F.; Garcia, J. F.; Roberts, B. M.; Jacobson, L. O., and Lawrence, J. H.; J. Lab. Clin. Med. 36:40, 1950.
16. Hudson, G.; Brit. J. Haematol. 4:239, 1958.
17. Dallwig, H. C.; Kolls, A. C., and Loevenhart, A. S.; Am. J. Physiol. 39:77, 1915.
18. Borsook, H.; Lingrel, J. B.; Scaro, J. L., and Millette, R. L.; Nature 196:347, 1962.
19. Hodgson, G. S., and Eskuche, I.; in Erythropoiesis, New York, Grune and Stratton, Inc., 1962, p. 222.
20. Fischer, S.; in Erythropoiesis, New York, Grune and Stratton, Inc., 1962, p. 204.
21. Gurney, C. W.; Wackman, N., and Filmanowicz, E.; Blood 17:531, 1961.

Received December, 1963.

Some Properties of Serum from Rabbits Immunized with Human Urinary Erythropoietin

John C. Schooley and Joseph F. Garcia

Sera obtained from rabbits immunized with human urinary erythropoietin can neutralize the biological effects of human erythropoietin (1) and erythropoietin obtained from mice, rats, sheep, and rabbits (2). Injection of such immune sera into normal mice results in a selective erythroid aplasia of the bone marrow (3). Evidence has been presented that this neutralization is not the result of a cytotoxic action of the sera on erythroid cells (3), and it has been concluded that the neutralization of the biological activity of erythropoietin is the result of an antigen-antibody reaction.

The present investigations were undertaken to (a) characterize the components of the immune serum responsible for the neutralization of erythropoietic activity; (b) study the effects of absorptions, with various tissues and plasma proteins, on the neutralizing ability of such sera; and (c) compare the neutralizing ability of such sera with antisera obtained from rabbits immunized with various serum proteins and hormones.

MATERIALS AND METHODS

HUMAN URINARY ERYTHROPOIETIN (ESF) was obtained from the urine of patients with aplastic anemia. An extract of the urine was prepared by positive pressure ultrafiltration through collodion membranes as described by Van Dyke, Garcia, and Lawrence (4). Direct comparison of this preparation with Armour sheep erythropoietin, Lot No. K103-124, indicated that the urinary erythropoietin contained 23 cobalt units/mg dry wt.

IMMUNIZATION. Adult rabbits were immunized using either an alum-precipitate of the urinary erythropoietin or a mixture of urinary erythropoietin and Freund's adjuvant. The schedule for immunization with alum-precipitated ESF was essentially that given by Kabat and Mayer (5). The rabbits were given an intravenous injection three times a week following an initial intraperitoneal injection. The alum-precipitate contained 1.5 mg of extract per milliliter. The volume of the alum-precipitated suspension varied as follows: three injections of 1 ml, three injections of 1.5 ml, four injections of 2 ml, four injections of 3 ml, and two injections of 5 ml. In rabbits immunized with Freund's adjuvant, 16.6 mg of urinary erythropoietin were dissolved in 1 ml of saline, which was then completely emulsified with 1 ml of complete Freund's adjuvant. This mixture was injected subcutaneously. At monthly intervals a total of three booster injections of 16.6 mg of urinary erythropoietin in saline was given intravenously. Blood was collected from the central artery of the ear on the 5th to 7th day after the final immunizing injection. The serum was collected and stored frozen until used. The serum is termed "anti-ESF". Serum obtained from rabbits immunized with normal urinary protein is termed "anti-N". Rabbits were immunized against bovine growth hormone and ovine thyrotropic hormone using Freund's adjuvant and an injection schedule similar to that used above.

Precipitating rabbit immune sera against human transferrin, human ceruloplasmin and human orosomucoid were obtained from the Mann Research Laboratories, Inc. Precipitating rabbit serum against sheep interstitial cell-stimulating hormone was obtained from Dr. T. Hayashida,* and dog plasma having a high anti-hog renin activity (10 anti-renin units/ml) was obtained from Dr. W. F. Ganong.*

DETECTION OF ERYTHROPOIETIC NEUTRALIZING ABILITY. Method 1: 0.25 ml of the serum obtained from immunized rabbits was injected subcutaneously into normal mice, weighing approximately 28 g, on 4 successive days. On the 5th day 0.5 μC of Fe^{59} as iron citrate (specific activity approximately 10 μC/μg) was injected intraperitoneally, and 24 hr later a sample of blood was taken by cardiac puncture. The radioactivity in 0.5 ml of blood was determined, and the percent of the injected Fe^{59} in the total red-blood-cell (RBC) volume was calculated. It was assumed that the blood volume of the mice was five percent of the total body weight.

Method 2: Known amounts of human urinary erythropoietin or, in some cases, sheep plasma erythropoietin were dissolved in a small amount of saline, and aliquots were placed in test tubes. To each tube was added known amounts of the immune serum to be tested for neutralizing ability. Normal serum was added to a tube as a control. The contents of the tubes were mixed, incubated at 37°C or room temperature for 1 hr and placed in the refrigerator overnight. The tubes were then centrifuged, the supernatant removed if a precipitate formed, and the tubes diluted to a known volume so that each milliliter of the supernatant would contain the same amount of erythropoietin (generally, each 1 ml contained 1 cobalt unit of erythropoietin). The erythropoietic activity of the supernatants was then assayed in transfusion-induced polycythemic mice. The dilutions were made with normal rabbit serum in experiments designed to study the effects of serial dilution of the immune serum.

---

*University of California Medical Center, San Francisco, Calif.

ASSAY OF ERYTHROPOIETIC ACTIVITY. Erythropoietic activity was assayed in transfusion-induced polycythemic mice using the procedures of DeGowin et al. (6). Groups of from six to ten female Swiss mice, weighing 19 to 23 g, were given 1 ml of washed red blood cells intraperitoneally on 2 successive days. On the 5th day following the last transfusion, the test material was given subcutaneously. About 56 hr later, approximately 0.5 μC of Fe^{59} as iron citrate was given intraperitoneally. The mice were bled 3 days later, and the radioiron in 0.5 ml blood was determined. In some experiments the animals were bled 24 hr after Fe^{59} injection. Values from any animal losing weight or whose hematocrit was less than 55% at the time of sacrifice were discarded. Results are expressed as percent of the injected dose of Fe^{59} in the calculated RBC volume. The red-blood-cell volume of the hypertransfused mice was assumed to be seven percent of the total body weight.

ABSORPTIONS OF THE IMMUNE SERUM. Aqueous tissue homogenates were made using the kidneys, spleen, and liver of normal mice, mice injected with phenylhydrazine, mice injected with cobalt, and transfusion-induced polycythemic mice. The phenylhydrazine-treated mouse tissues were obtained from animals the day after the subcutaneous injection, given every other day, of three doses of 1.5 mg phenylhydrazine hydrochloride. The cobalt-treated mice received subcutaneously 5 μ<u>M</u> of cobaltous chloride 9 hr before collection of the tissues. The tissue homogenates, normal mouse serum, and normal urinary proteins were lyophylized. Of these lyophylized powders, 0.5 g was added to test tubes containing 0.6 ml of anti-ESF rabbit immune serum or 0.6 ml of normal rabbit serum. The tubes were mixed frequently and allowed to stand at room temperature for 1 hr and then centrifuged. A 5-ml aliquot from each tube containing either anti-ESF or normal rabbit serum was added to a known aliquot of ESF (calculated to be just neutralized by the added anti-ESF). The effect of the absorptions on the erythropoietin neutralizing ability of the anti-ESF was then determined in polycythemic mice by Method 2. The erythropoietic activity of saline extracts of the powders and of homogenates of some of the powders was assayed in polycythemic mice.

ABSORPTION OF ANTI-ESF WITH ACID HYDROLYZED ERYTHROPOIETIN. A known amount of erythropoietin was dissolved in distilled water and equal aliquots were added to each of two test tubes. Five milliliters of 0.01N H_2SO_4 were added to one tube, and 5 ml of distilled water to the other. The tubes were placed in a water bath at 80°C for 1 hr. The tubes were then cooled and the acid neutralized with NaOH. The contents of each tube were then dialyzed against distilled water overnight in the refrigerator. NaCl was added to each tube to a concentration of 0.9%. Equal aliquots of each dialyzate were then placed in two test tubes. Enough anti-ESF was added to the hydrolyzed and control ESF for the biological activity to be just neutralized. The same amount of normal rabbit serum was added to the other tubes. The content of each tube was mixed and allowed to stand at room temperature for 1 hr. Equal additional amounts of untreated ESF were then added to each tube. Each tube was mixed, allowed to stand at room temperature for an hour and was then placed in the refrigerator overnight. The tubes were then centrifuged, and the erythropoietic activity remaining in the supernatant was assayed in polycythemic mice (Method 2).

FRACTIONATION OF SERUM γ GLOBULIN. γ globulin was separated from anti-ESF immune serum and from normal rabbit serum both with the ammonium sulfate precipitation procedure of Kendall (7) and on a diethyl amino ethyl (DEAE) cellulose column using the procedure of Riggs et al. (8). The DEAE fractionations were performed by Antibodies, Inc., Davis, California. The ammonium sulfate precipitate was reprecipitated three times, dialyzed at 0°C against saline until free from sulfate, and diluted. The diluted precipitates were then assayed for their ability to neutralize erythropoietic activity by Method 1. Identical dilutions of untreated sera were used for comparisons. The fractions from the DEAE column were collected; the first fraction of 42 ml of eluate (primarily γ globulin) and the second fraction of 48 ml of eluate were concentrated by pervaporation, and the protein content was determined. Two milligrams of protein from these two fractions of anti-ESF and the same two fractions of serum obtained from rabbits immunized with normal human urinary proteins were added to tubes containing known amounts of ESF. The contents of the tubes were then assayed for erythropoietic activity by Method 2.

RESULTS AND DISCUSSION

The ability of serum obtained from rabbits immunized with human urinary erythropoietin to modify the erythropoietic response of normal mice after subcutaneous injections is shown in Fig. 1. The serum obtained from 31% of the immunized rabbits markedly decreased the 24-hr Fe^{59} uptake into the red blood cells of normal mice. The 24-hr Fe^{59} uptake was decreased to less than five percent by the serum of seven percent of the immunized rabbits. The serum obtained from 40% of the immunized animals showed no neutralizing ability. Interestingly, 29% of the immunized rabbits yielded serum which increased the Fe^{59} uptake above that found when normal rabbit serum was injected. This may be due to the presence of human urinary erythropoietin remaining in the rabbit after the last immunizing injection, or it may result from an increased endogenous erythropoietin production by the rabbit to compensate for the neutralization of endogenous erythropoietin.

A correlation exists between the hematocrit and the erythropoietic neutralizing ability of the serum of individual rabbits immunized according to this schedule, i.e., rabbits having good neutralizing titers have low hematocrits. This fact, and the observation that the immune serum can neutralize rabbit erythropoietin, suggest that an auto-immune state has been produced,

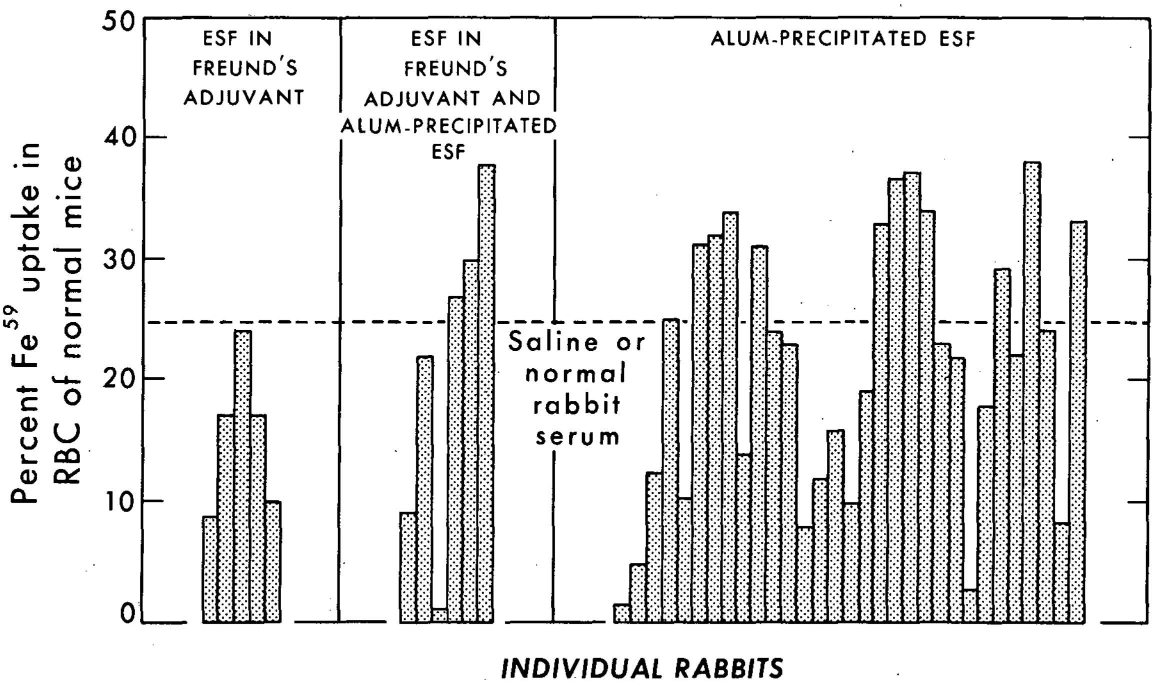

Figure 1. The 24-hr uptake of Fe^{59} into the red blood cells of normal mice following the injection of sera obtained from rabbits immunized with human urinary erythropoietin. Each bar represents the average Fe^{59} uptake found in 10 mice after the injection of serum obtained from an individual rabbit.

MU-32924

as we have stated before (2). The changes in the neutralizing ability of sera from individual rabbits during the course of immunization are being investigated, and preliminary results (Garcia, unpublished observations) indicate that, although in most instances a correlation does exist between the hematocrit and neutralizing ability, at least one rabbit had a high neutralizing titer and a normal hematocrit.

The effect of injecting dilutions of a pooled sample of anti-ESF on the erythropoietic activity of normal mice is shown in Table 1. The 24-hr uptake of Fe^{59} into the red blood cells of hypertransfused mice on the 5th day after transfusion is indicated for comparison. No corrections have been made for

Table 1. Effect of various dilutions of anti-ESF on the erythropoiesis of normal mice

	Percent Fe^{59} in blood of normal mice in 24 hr
Anti-ESF	1.5 ± 0.1*
Anti-ESF diluted 1:2	2.7 ± 0.4
Anti-ESF diluted 1:4	9.0 ± 1.2
Anti-ESF diluted 1:8	12.3 ± 1.5
Anti-ESF diluted 1:16	15.8 ± 1.7
Anti-ESF diluted 1:32	17.9 ± 1.6
Normal rabbit serum	21.8 ± 1.0
Hypertransfused mice	2.2 ± 0.4

*Standard error of the mean, 8 mice per group. All dilutions made with normal rabbit serum.

plasma Fe^{59}. In this assay system the Fe^{59} uptake after injections of a 1:2 dilution of anti-ESF was about the same as that found in hypertransfused mice. Greater dilutions of anti-ESF only partially decreased the Fe^{59} uptakes. The injection of about 0.5 ml (1:2 dilution) of anti-ESF and the production of polycythemia by hypertransfusion both decrease erythropoiesis after 5 days to the same extent.

The effect of in vitro additions of various dilutions of the same pool of anti-ESF on the erythropoietic activity (of 2.3 cobalt units) of exogenous human urinary ESF is shown in Table 2. Dilutions greater than 1:100 had no effect on the erythropoietic response to 2.3 cobalt units of ESF, but dilutions of 1:10 partially decreased the response. Reference to a previously published dose response curve for this particular polycythemic mouse assay (1) indicates that the erythropoietic response observed at a 1:10 dilution of anti-ESF is equivalent to that of 0.59 cobalt units of ESF. Since an equivalent of 2.3 cobalt units was injected into each mouse, the anti-ESF, at this dilution, neutralized 2.3-0.59 or about 1.7 cobalt units of erythropoietic activity. It can be calculated from the amounts of anti-ESF present at this dilution that 0.04 ml of this particular anti-ESF can neutralize 1.7 cobalt units of erythropoietin.

Assuming that: 1. the neutralization of ESF by anti-ESF is the result of an antigen-antibody reaction, 2. the combining proportions of ESF and anti-ESF in these in vitro and in vivo conditions are similar, 3. the anti-ESF reacts with human urinary ESF and endogenous mouse ESF with equal avidity and 4. the

Table 2. Neutralization of human urinary ESF by various dilutions of anti-ESF

	Percent Fe^{59} in blood of hypertransfused mice in 24 hr
ESF + anti-ESF	1.1 ± 0.08*
ESF + anti-ESF diluted 1:1	1.7 ± 0.18
ESF + anti-ESF diluted 1:10	11.7 ± 1.2
ESF + anti-ESF diluted 1:100	21.6 ± 0.82
ESF + anti-ESF diluted 1:1,000	21.2 ± 0.82
ESF + anti-ESF diluted 1:10,000	22.7 ± 0.60
ESF + normal rabbit serum	21.8 ± 0.60

*Standard error of the mean, 10 mice per group. All dilutions made with normal rabbit serum.

neutralization of the endogenous mouse ESF does not result in an increased production of ESF during the test period, an estimation of the maximum amount of ESF produced in the mouse during the 5-day test period can be made. Thus, since 0.5 ml of anti-ESF decreases erythropoiesis to that observed following hypertransfusion, the equivalent of $\frac{0.5}{0.04} \times 1.7$ or a maximum of 21.25 cobalt units is produced in 5 days or 4.25 cobalt units/day.

It is of interest to calculate further, from what is known of the plasma clearance rate of ESF, the amount of ESF in a normal mouse. The $T_{1/2}$ for the plasma clearance of ESF in mice has not been determined, but Stohlman and Howard (9) and Keighley (10) have made such measurements in rats, and obtain values of from 3 to 5 hr and 1 hr respectively. Utilizing these values for the mouse, and assuming that the plasma clearance of endogenous ESF in the mouse is exponential, the total amount of ESF in a mouse can be calculated to be less than 0.77 cobalt units if the $T_{1/2}$ is 3 hr, or less than 0.25 cobalt units if the $T_{1/2}$ is 1 hr. Keighley (10) finds that the amount of ESF in lymph is roughly proportional to the amount in plasma, which suggests that ESF is distributed in the total extracellular fluid. Thus, in the 28-gram mice used in these experiments, a maximum of from 0.14 to 0.04 cobalt units of ESF should be found in 1 ml of plasma, assuming that the extracellular fluid is 20% of the body weight. These maximal values are not unreasonable and are at the borderline of detection in the polycythemic mouse assay. We have occasionally found detectable titers in plasma obtained from normal mice using this assay, i.e., the Fe^{59} uptakes are significantly higher than saline-injected controls.

Table 3. Effect of γ globulin prepared by ammonium sulfate precipitation on the erythropoiesis of normal mice

	Percent Fe^{59} in blood of normal mice in 24 hr	
	Anti-ESF	Normal rabbit serum
Whole serum	12.2 ± 1.6*	26.9 ± 2.1
Ammonium sulfate precipitate	13.6 ± 1.5	23.5 ± 1.0

*Standard error of the mean, 9-10 mice per group.

Table 4. Effect of DEAE column separation of anti-ESF on the neutralization of ESF activity

	Percent Fe^{59} uptake in RBC of hypertransfused mice	
	Fraction 1	Fraction 2
Human urinary ESF + anti-ESF	0.15 ± 0.02*	3.96 ± 0.85
Human urinary ESF + anti-N	7.99 ± 0.58	8.93 ± 1.2

*Standard error of the mean, 9-10 mice per group.

The results shown in Tables 3 and 4 indicate that the neutralizing ability of anti-ESF sera is associated with γ globulin fractions prepared either by ammonium sulfate precipitation or by separation on a DEAE column. The presence of precipitins in the sera obtained from the rabbits immunized with human urinary ESF has not been systematically studied. Some sera that have high ESF neutralizing titers do not show any evidence, either in the test tube or in double diffusion studies in agar, of precipitin formation. This suggests that the neutralization of ESF, at least in these sera, is by means of a nonprecipitating antibody. Conversely, some immune sera give good precipitin formation against human urinary ESF but give no neutralization of ESF. Presumably these precipitates are the result of interactions of antibodies in the immune sera with various plasma protein contaminants, which are normally present in the concentrates of

Table 5. Effect of mild acid hydrolysis on the erythropoietic activity of human urinary ESF

	Treatment	Percent Fe^{59} uptake in RBC of hypertransfused mice
Human urinary ESF (hydrolyzed)	1 hr in $0.01NH_2SO_4$ at 80°C	0.13 ± 0.02*
Human urinary ESF (control)	1 hr in distilled water at 80°C	6.2 ± 0.93

*Standard error of the mean, 8-10 mice per group.

erythropoietically active human urine (1). Goldwasser, et al. (11) have prepared precipitating antisera against highly purified preparations of sheep plasma ESF (Steps III and IV fractions), but such antisera did not neutralize the biological activity of these preparations. Goldwasser (personal communication) finds that our antiserum, which does neutralize human urinary ESF and sheep plasma ESF, does not form precipitin bands against Steps III and IV fractions of sheep plasma ESF.

A preliminary attempt to tag the γ globulin obtained by DEAE chromatography with fluorescein isothiocyanate was found to decrease the ESF neutralizing ability of the γ globulin by 70%. In spite of this, the possibility that immunofluorescent techniques can be used to identify ESF in tissues is being actively pursued.

Heating anti-ESF for 30 min at 56°C did not alter the ability of anti-ESF to neutralize human urinary ESF, which suggests that complement is not involved in the neutralization reaction. However, since the evidence for neutralization, after the addition of anti-ESF to ESF *in vitro*, must be obtained by the biological assay, the participation of complement contributed by the assay animal cannot be excluded.

Data presented in Table 5 indicate that mild acid hydrolysis of human urinary ESF completely destroys the biological activity when compared to a control sample of urinary ESF heated in distilled water. Mild acid hydrolysis of guinea-pig plasma α_1-glycoprotein selectively removed sialic acid (12). Rambach *et al*. (13) have reported that similar hydrolytic treatment of rabbit plasma ESF destroys the biological activity with the release of sialic acid and small amounts of fucose and hexoses. Removal of sialic acid from rabbit plasma ESF by the enzyme, neuramimidase, has been found by Lowy *et al*. (14) to destroy the biological activity of the ESF molecule. These findings suggest that bound sialic acid is probably an essential part of the biologically active ESF

Table 6. Effect of mild acid hydrolysis of human urinary ESF on the reaction between ESF and anti-ESF

	Percent Fe^{59} uptake in RBC of hypertransfused mice
Human urinary ESF (hydrolyzed) + anti-ESF[1] + Human urinary ESF (untreated)	2.9 ± 0.53*
Human urinary ESF (control) + anti-ESF[1] + Human urinary ESF (untreated)	6.4 ± 0.67
anti-ESF[2] + Human urinary ESF (untreated)	0.10 ± 0.01
Human urinary ESF	7.7 ± 1.15
Saline	0.13 ± 0.02

*Standard error of the mean, 8-10 mice per group.

[1] 0.015 ml of anti-ESF per cobalt unit.

[2] 0.03 ml of anti-ESF per cobalt unit.

molecule. This group might therefore be expected to be an important determinant of immunological specificity. The results, presented in Table 6, indicate that the ability of anti-ESF to combine with ESF is decreased after hydrolysis. Thus, the addition of anti-ESF to a mixture containing the equivalent amount of biologically active ESF and hydrolyzed ESF decreases the erythropoietic response to 2.9%, whereas, the addition of the same amount of anti-ESF to a mixture containing equivalent amounts of ESF, heated at 80°C for 1 hr, and untreated ESF (both biologically active) gives an erythropoietic response of 6.4%. These differences are significant, the P value being < 0.001. This evidence suggests that antigenic determinants of importance in the immunological reaction between ESF and anti-ESF have been removed by hydrolysis. These results tempt us to suggest that bound sialic acid is a major antigenic determinant; however, the possibility that other bonds, affecting other antigenic determinants, were also disrupted by the mild acid hydrolysis cannot be excluded. Indeed, Athineos _et al_. (15) have recently presented evidence that sialic acid is not an important antigenic group in precipitin reactions involving the α_1-glycoprotein, orosomucoid. Further work involving the more specific enzymatic removal of sialic acid from ESF may help resolve the question of the importance of this group in the neutralization reaction.

The question of the specificity of the neutralization of ESF by anti-ESF was further studied by investigating the effects of absorptions of anti-ESF on the neutralizing ability. An amount of anti-ESF just sufficient to neutralize a known amount of ESF was added to the ESF after absorption with various powders.

Table 7. The ability of anti-ESF to neutralize a standard amount of human urinary ESF after absorption with various powders

	Percent Fe^{59} uptake in RBC of hypertransfused mice
Human urinary ESF + anti-ESF absorbed with the following powders:	
Normal mouse spleen	0.10 ± 0.00*
" " kidney	0.11 ± 0.01
" " liver	0.13 ± 0.02
Polycythemic mouse spleen	0.18 ± 0.09
" " " kidney	0.11 ± 0.01
" " " liver	0.13 ± 0.02
Cobalt-injected mouse spleen	0.18 ± 0.05
" " " kidney	0.12 ± 0.01
" " " liver	0.07 ± 0.01
Phenylhydrazine-injected mouse kidney	0.21 ± 0.07
Normal mouse serum	0.14 ± 0.04
Normal human urinary proteins	0.09 ± 0.01
Human urinary ESF + unabsorbed anti-ESF	0.20 ± 0.05
Human urinary ESF	9.02 ± 0.67
Saline-injected	0.13 ± 0.01

*Standard error of the mean, 8-10 mice per group.
0.03 ml of anti-ESF per cobalt unit.
833 mg of the various powders per 1 ml of anti-ESF.

The results are shown in Table 7. None of these absorptions decreased the ability of anti-ESF to neutralize ESF. If the anti-ESF antibodies involved in the neutralization were simply directed against antigenic determinants common to the class of proteins to which ESF belongs, a reduction in the neutralizing ability after absorption might be expected, since large amounts of glycoproteins similar to ESF must certainly be present in these powders. Indeed, in the case of absorptions with kidney powders obtained from mice injected with phenylhydrazine or cobalt, such a reduction might be expected simply because of the presence of ESF in these kidneys. Rambach _et_ _al_. (16) have recently shown that the injection of homogenates of a variety of normal tissues increased the 24-hr Fe^{59} uptake and reticulocyte count of dehydrated rats. Saline extracts of such homogenates demonstrated little activity. Injection of saline extracts of the different kidney powders used in the absorptions of anti-ESF did not stimulate erythropoiesis in the polycythemic mouse. Injection of homogenates, equivalent to

0.2 g of dry powder of normal mouse liver and spleen, likewise did not stimulate erythropoiesis, but injections of homogenates of normal mouse kidney elevated the Fe^{59} uptake to 1.20 ± 0.31% compared to saline-injected control values of 0.18 ± 0.06% ($P < 0.01$). The failure of absorptions with kidney powders to decrease the neutralizing ability of anti-ESF suggests that the factor present in the kidney homogenate which stimulates erythropoiesis as measured by Fe^{59} uptake in polycythemic mice is either a) not present in sufficient amounts, b) not identical to plasma or urinary ESF, or c) if it is identical to plasma or urinary ESF, the antigenic determinants necessary for the immunological reaction with anti-ESF are masked. Injections of anti-ESF, after absorption with Cohn Fraction IV-4 of human plasma, decreased erythropoiesis in the normal mouse to the same extent as nonabsorbed anti-ESF. Kuratowska et al. (17) have shown that erythropoietic activity is associated with this plasma fraction when prepared from the plasma of permanent blood donors. Considerable amounts of transferrin are normally present in this fraction. Thus, in these experiments, of all the various proteins that have been used to block the neutralizing activity of anti-ESF sera, only one--biologically active ESF--completely prevented neutralization.

Injections into normal mice of rabbit serum containing precipitins against normal human urinary proteins, bovine serum albumin, or Cohn fraction VI of human plasma (α_1-acid glycoproteins), did not decrease erythropoiesis as measured by the 24-hr Fe^{59} uptake.

The effect of antisera against various plasma proteins on the ability of sheep or human ESF to stimulate erythropoiesis in polycythemic mice is shown in Table 8. The finding that antisera against ceruloplasmin do not neutralize ESF is of particular interest because Hatta et al. (18) have presented evidence that apoceruloplasmin stimulates erythropoiesis in the rat. The production of apoceruloplasmin, by the removal of copper, destroys the copper oxidase activity of ceruloplasmin (19), and it has been demonstrated that removal of the groups responsible for the enzymatic activity are not blocked by an antigen-antibody combination (20). This suggests that anti-ceruloplasmin can combine with both ceruloplasmin and apoceruloplasmin. The failure of such antisera to neutralize the biological activity of sheep ESF indicates that sheep ESF does not have antigenic determinants in common with ceruloplasmin. The failure of anti-orosomucoid to neutralize ESF indicates that very few, if any, of the antigenic determinants of the α_1-glycoprotein, orosomucoid, and ESF are similar.

Considerable numbers of erythroid cells are observed in the marrow of polycythemic mice 24 hr after the injection of exogenous ESF. We have previously shown that injections of anti-ESF, at this time, have very little effect on the subsequent development of the erythropoietic response (3). It is well known that copper, as well as iron, is necessary for normal erythropoiesis.

Table 8. Effect of anti-sera against various plasma proteins on the erythropoietic activity of sheep or human urinary ESF

	Percent Fe^{59} uptake in RBC of hypertransfused mice
Sheep ESF + normal rabbit serum	22.0 ± 1.1*
Sheep ESF + anti-ESF	0.98 ± 0.23
Sheep ESF + anti-human ceruloplasmin	29.2 ± 2.7
Sheep ESF + anti-human ceruloplasmin injected 24 hr after ESF	20.9 ± 2.9
Sheep ESF + anti-human transferrin	24.3 ± 3.2
Sheep ESF + anti-human transferrin injected 24 hr after ESF	27.4 ± 3.6
Human urinary ESF + anti-human orosomucoid	22.4 ± 3.0
Human urinary ESF + normal rabbit serum	22.2 ± 2.0
Saline injected	0.22 ± 0.02

*Standard error of the mean, 6 mice per group.

0.04 ml of anti-sera per cobalt unit of ESF.

All anti-sera obtained from rabbits except anti-human orosomucoid which was obtained from goats.

Transferrin and presumably ceruloplasmin are involved in the transport of these metals to the erythroid cells. Injection of antisera combining with these transport proteins at a time of active erythropoiesis might be expected to decrease the erythropoietic response; however, such a decrease was not observed. This may be related to differences in the human and mouse proteins, or injections of antisera against these proteins into the mouse may not sufficiently reduce the plasma levels of these metal-binding proteins to interfere significantly with their transport functions.

Numerous hormones have been shown to stimulate erythropoiesis in the normal or hypophysectomized animal (21). The data presented in Table 9 indicate that thyroxin, hydrocortisone, and ACTH do not stimulate erythropoiesis in the polycythemic mouse, i.e., these hormones cannot stimulate the stem cells to differentiate into erythroid cells. The role such hormones may have in regulating the maturation of erythroid cells is not known. The effects of antisera against various hormones on the ability of sheep or human urinary ESF to stimulate erythropoiesis in the polycythemic mouse are shown in Tables 10 and 11.

The addition of rabbit anti-ovine thyrotropin partially neutralized the erythropoietic response of sheep ESF ($P < 0.01$). None of the other antisera

Table 9. Effect of thyroxin, hydrocortisone and ACTH on the erythropoiesis of hypertransfused mice

	Percent Fe^{59} uptake in RBC of hypertransfused mice
Throxine 10 γ	0.19 ± 0.06*
Hydrocortisone 1 mg	0.12 ± 0.01
Corticotropin (ACTH) 1 unit	0.16 ± 0.03

*Standard error of the mean, 6 mice per group.

were effective. The anti-ovine thyrotropin could have decreased the erythropoietic response either by a direct combination with sheep ESF, which would alter the differentiation of stem cells, or by a combination with mouse thyrotropin, which might influence the maturation of erythroid cells.

The failure of anti-renin to neutralize human urinary ESF is of interest because of current speculations regarding the relationship between the juxtaglomerular cells, their granules and erythropoietin (22,23). The juxtaglomerular cells and the macula densa are thought to be the source of the pressor enzyme, renin. Renin interacts with hypertensinogen to produce angiotensin. It has been shown that injection of angiotensin into hypophysectomized-adrenalectomized rats stimulates erythropoiesis (24). The presence of antibodies against renin does not affect the ability of exogenous ESF to stimulate erythropoiesis; however, the possibility that renin is involved, in some unknown manner, in the production of endogenous ESF cannot be excluded.

SUMMARY

Sera obtained from rabbits after immunization with human urinary ESF can neutralize the biological activity of human urinary, sheep, rat, and rabbit plasma ESF. Such sera can depress erythropoiesis in normal mice. The neutralizing ability of such sera is found in the γ globulins. The finding that absorptions of the immune sera with a wide variety of proteins did not alter the neutralizing ability suggests that considerable immunological specificity is involved in the neutralization reaction. This suggestion is further supported by the finding that immune sera against a variety of proteins do not effect the erythropoietic response elicited by the injection of exogenous erythropoietin. The injection or addition of antisera against proteins or protein hormones known to be of importance in normal erythropoiesis has little or no effect on the ability of exogenous ESF to stimulate erythropoiesis in polycythemic mice.

Table 10. Effect of anti-sera against various hormones on the erythropoietic activity of sheep ESF

	Percent Fe^{59} uptake in RBC of hypertransfused mice
Sheep ESF + normal rabbit serum	12.0 ± 1.7*
Sheep ESF + anti-bovine growth hormone	16.4 ± 1.7
Sheep ESF + anti-ovine thyrotropin	8.89 ± 1.6
Sheep ESF + anti-ESF	0.11 ± 0.01
Saline injected	0.18 ± 0.02

*Standard error of the mean 8-10 mice per group.

0.08 ml of anti-sera per cobalt unit of sheep ESF.

Table 11. Effect of anti-sera against various hormones on the erythropoietic activity of human urinary ESF

	Percent Fe^{59} uptake in RBC of hypertransfused mice
Human urinary ESF + normal rabbit serum	7.65 ± 1.5*
Human urinary ESF + anti-hog renin	6.07 ± 1.3
Human urinary ESF + anti-sheep interstitial cell stimulating hormone	9.57 ± 1.1
Human urinary ESF + anti-ESF	0.28 ± 0.04
Saline injected	0.30 ± 0.08

*Standard error of the mean, 8-10 mice per group.

0.17 ml of anti-sera per cobalt unit of human urinary ESF.

Anti-hog renin anti-sera obtained from a dog; all other anti-sera from rabbits.

One exception is anti-ovine thyrotropin, which significantly decreased the erythropoietic response seen in polycythemic mice after the injection of sheep ESF. The finding that mild acid hydrolysis destroyed the biological activity of human urinary ESF and altered antigenic determinants on the ESF molecule suggests that the groups necessary for biological activity may be specific antigenic determinants.

These properties of the immune sera are consistent with the concept, which we previously proposed, that the neutralization of the biological activity of ESF by anti-ESF is the result of an immunological reaction. The availability of such immune sera offers a potent tool for investigating many of the current problems on the role of ESF in the regulation of erythropoiesis.

REFERENCES

1. Schooley, J. C., and Garcia, J. F.; Proc. Soc. Exptl. Biol. Med. 109:325, 1962.
2. Garcia, J. F., and Schooley, J. C.; Proc. Soc. Exptl. Biol. Med. 112:712, 1963.
3. Schooley, J. C., and Garcia, J. F.; Proc. Soc. Exptl. Biol. Med. 110:636, 1962.
4. Van Dyke, D. C.; Garcia, J. F., and Lawrence, J. H.; Proc. Soc. Exptl. Biol. Med. 96:541, 1957.
5. Kabat, E. A., and Mayer, M. M.: Experimental Immunochemistry, Springfield, Ill., Charles C. Thomas, 2nd edition, 1961, p. 871.
6. DeGowin, R. L.; Hofstra, D., and Gurney, C. W.; Proc. Soc. Exptl. Biol. Med. 110:48, 1962.
7. Kendall, F. E.; J. Clin. Invest. 16:921, 1937.
8. Riggs, J. L.; Loh, P. C., and Eveland, W. C.; Proc. Soc. Exptl. Biol. Med. 105:655, 1960.
9. Stohlman, F. Jr., and Howard, D.; in Erythropoiesis, edited by L. O. Jacobson and M. Doyle, New York, Grune & Stratton, 1962, p. 120.
10. Keighley, G.; in Erythropoiesis, edited by L. O. Jacobson and M. Doyle, New York, Grune & Stratton, 1962, p. 106.
11. Goldwasser, E.; White, W. F., and Taylor, K. B.; Biochim. Biophys. Acta 64:487, 1962.
12. Bostrom, H.; Roden, L., and Yamashina, I.; J. Biol. Chem. 230:381, 1958.
13. Rambach, W. A.; Shaw, R. A.; Cooper, J. A. D., and Alt, H. L.; Proc. Soc. Exptl. Biol. Med. 99:482, 1958.
14. Lowy, P. H.; Keighley, G., and Borsook, H.; Nature 185:102, 1960.
15. Athineos, E.; Thornton, M., and Winzler, R. J.; Proc. Soc. Exptl. Biol. Med. 111:353, 1962.
16. Rambach, W. A.; Alt, H. A., and Cooper, J. A. D.; Proc. Soc. Exptl. Biol. Med. 108:793, 1961.

17. Kuratowska, Z.; Kowalski, E.; Lipinski, B., and Michalak, E.; in Erythropoiesis, edited by L. O. Jacobson and M. Doyle, New York, Grune & Stratton, 1962, p. 58.
18. Hatta, Y.; Maruyama, Y.; Tsuruoka, N.; Yamaguchi, A.; Ando, M.; Ueno, T., and Shimizu, M.; Acta Haematol. Japan. 26:174, 1963.
19. Morell, A. G., and Scheinberg, I. H.; Science 127:588, 1958.
20. Uriel, J.; Nature 181:999, 1958.
21. Grant, W. C., and Root, W. S.; Physiol. Rev. 32:449, 1952.
22. Hirashima, K., and Takaku, F.; Blood 20:1, 1962.
23. Goldfarb, B., and Tobian, L.; Proc. Soc. Exptl. Biol. Med. 112:65, 1962.
24. Fisher, J. W., and Crook, J. J.; Blood 19:557, 1962.

Received December, 1963.

Electrophoretic Behavior of OsO_4-Fixed and $KMnO_4$-Fixed Rat Erythrocytes

Robert M. Glaeser and Howard C. Mel

Irreversible alteration of the electrophoretic mobility of intact erythrocytes (RBC) is a topic of current discussion in the literature. Prolonged exposure to low pH or to low salt concentration has been shown to reduce permanently the (negative) mobility of guinea pig RBC (1) as well as human RBC (2). The mobility of RBC from many species can also be reduced by incubation with various proteolytic enzymes as well as with the receptor destroying enzyme (RDE) (3,4,5), a glycosidase specific for the release of terminal sialic acid (6). A certain amount of information regarding the surface structure of the RBC membrane has already been obtained from these experimental observations.

While performing such experiments on rat RBC, it was felt that electron microscopy of the treated cell surfaces would be a valuable additional technique for studying the changes produced in the surface architecture. Preparation of samples for electron microscopy usually starts with fixation of the specimen. It is entirely possible that the method of fixation itself produces irreversible changes in the mobility. If this were true, electron microscopy of such fixed specimens might tell very little about the initial changes produced by the action of low pH, low salt concentration, or enzymes. Therefore the first step in the parallel microelectrophoresis and electron microscope study has been to compare the surfaces of OsO_4-fixed, $KMnO_4$-fixed and unfixed normal rat RBC according to electrophoretic criteria.

Some previous work has been reported on the effects of fixation upon the electrophoretic behavior of RBC. Heard and Seaman (7) describe a method of treatment with formaldehyde and acetaldehyde, which stabilizes human RBC against the usual irreversible mobility changes occurring in solutions of low pH or low salt concentration. Their method requires a period of approximately three weeks for completion in contrast to the very rapid fixation afforded by OsO_4 and $KMnO_4$. For this reason, it was thought that OsO_4 or $KMnO_4$ would be more suitable fixatives for electron microscopy, provided that they caused no changes in the cell surface, as judged by electrophoresis. The results and possible implications of this electrophoretic study are the subject of this communication.

MATERIALS AND METHODS

APPARATUS. The microelectrophoresis chamber was of the rectangular Northrup-Kunitz type (Arthur H. Thomas Co., Philadelphia) oriented in the lateral (8) position and connected by three way stopcocks either to the reversible Zn-$ZnSO_4$ electrodes or to the specimen exchange system. Special precautions were taken to keep heavy-metal ions out of the electrophoresis chamber by isolating each stopcock from its electrode with the following sequence of barriers: a glass tube 11 in. long and filled with Standard Buffer (see composition below), with glucose added to prevent convective exchange of sample and buffer at the stopcock; a fine sintered glass disk; a glass tube five inches long and filled with saturated Na_2SO_4; a sintered glass disk; a Zn-$ZnSO_4$ electrode chamber. The entire apparatus was placed on a shock-mounted table. A 325-volt (maximum) voltage-regulated power supply (Lambda Electronics, College Point, N. Y.) was used. The current was measured with an ammeter having 0 - 10 mA, 0 - 1 mA, and 0 - 50 µA scales (Supreme Instrument Corp., Philadelphia). The pH of solutions was measured with a Beckman, Model G, pH meter with a standard glass electrode and a calomel reference electrode. Specific conductivities were measured with a Model 4960 bridge and cell supplied by Leeds and Northrup (Philadelphia).

MATERIALS. All materials employed were of reagent grade. The following stock solutions were made as needed in the course of these experiments: (I) Standard Buffer: 3×10^{-4} $\underline{M}$ $NaHCO_3$ in 0.145 $\underline{M}$ NaCl; (II) 0.145 $\underline{M}$ HCl; (III) 0.145 $\underline{M}$ NaOH; (IV) 3×10^{-4} $\underline{M}$ $NaHCO_3$ with and without 4.5% glucose. Solutions of the desired pH (at constant ionic strength) were obtained by mixing appropriate volumes of (II) or (III) with Standard Buffer. Solutions of the desired ionic strength were obtained by mixing appropriate volumes of the $NaHCO_3$ solution (IV) with Standard Buffer (I).

PREPARATION OF RBC. Blood was taken from the vena cava of ether-anesthetized rats. Disposable plastic syringes were used without anticoagulants. The blood was immediately delivered into 10 to 20 volumes of buffer and centrifuged 10 min at approximately 250 g in a refrigerated centrifuge. The supernatant was removed by vacuum suction, the cells were washed once more in 10 volumes of Standard Buffer, and the final pellet was made into a 10% vol/vol cell suspension. The cells were stored at room temperature in this solution for the duration of the experiment (generally 4 to 5 hr and never more than 12 hr).

FIXATION. For OsO_4 fixation, the following stock solutions were used: (a) 0.143 $\underline{M}$ sodium barbital in 0.143 $\underline{M}$ sodium acetate; (b) 0.10 $\underline{M}$ HCl; (c) 2% wt/vol OsO_4 in Standard Buffer. One volume of the 10% cell suspension was added to a solution of two volumes (a), two volumes (b), and five volumes (c). After 1 min the cells were centrifuged (at room temperature) for 2 min at approximately 500 g. The supernatant was discarded, the fixed cells were washed twice with 100 volumes of Standard Buffer, and the final pellet was resuspended in 10 volumes of Standard Buffer. Because of the volatility and extreme toxicity of OsO_4, all work was carried out in a ventilated hood.

For permanganate fixation, the following additional stock solution was used: (d) 1.2% wt/vol $KMnO_4$ in Standard Buffer. One to two volumes of the 10% cell suspension were added (in an ice bath) to a solution of 2.5 volumes (a), 2.5 volumes (b), and 5.0 volumes (d). After 2 min the fixed cells were centrifuged, washed, and resuspended as described above.

In certain experiments (as indicated in the figures) the fixed cells were dehydrated in a manner similar to that employed with fixed tissues prepared for electron microscopy: 1 min in chilled 25% ethanol, 1 min in chilled 50% ethanol, 1 min in chilled 75% ethanol, 1 min in 95% ethanol at room temperature, and finally 15 min in 100% ethanol at room temperature. Between each step the cells were centrifuged, the supernatant discarded, and the cells resuspended in the new solvent solution. After the exposure to absolute ethanol, the cells were again washed with Standard Buffer and made into a 10% vol/vol cell suspension.

MEASUREMENTS. The 10% RBC suspensions described above were diluted 1:100 with salt solutions of the desired pH or ionic strength immediately before measurement of the mobility. The pH and specific conductivity of these samples were always recorded <u>after</u> the addition of the cells. When measuring the pH, it was found necessary to rinse the electrodes several times with the cell suspension before a constant reading could be obtained. In the pH range from 3.0 to 7.0, the value of the pH increased considerably after the addition of the cells. In computing the ionic strength, it was necessary to take into account the contribution made by the NaCl ions in the 10% cell suspension.

In order to insure that the apparatus was working properly, a complete velocity profile (9) was measured whenever the specimen was stable for a sufficiently long period of time. Between 10 and 20 experimental points were obtained for each velocity profile. This amount of data can be obtained in about 15 to 20 min. The observed velocities, obtained first with the electric field in one direction and then with the field reversed, were averaged in order to cancel out the effect of any possible fluid drift. A parabola was then fitted to the experimental data, and the mobility was computed from the velocity at the stationary level.

Under certain extreme conditions, the mobility of the cells was not constant for a long enough period to obtain a complete parabola. In these instances all measurements were made at a single stationary level. Again data were alternately recorded with the field first in one direction and then with the field reversed, and the velocities averaged. All velocity measurements were made at room temperature ($23^{\circ}C$ to $26^{\circ}C$). The electrophoretic <u>velocity</u> at constant

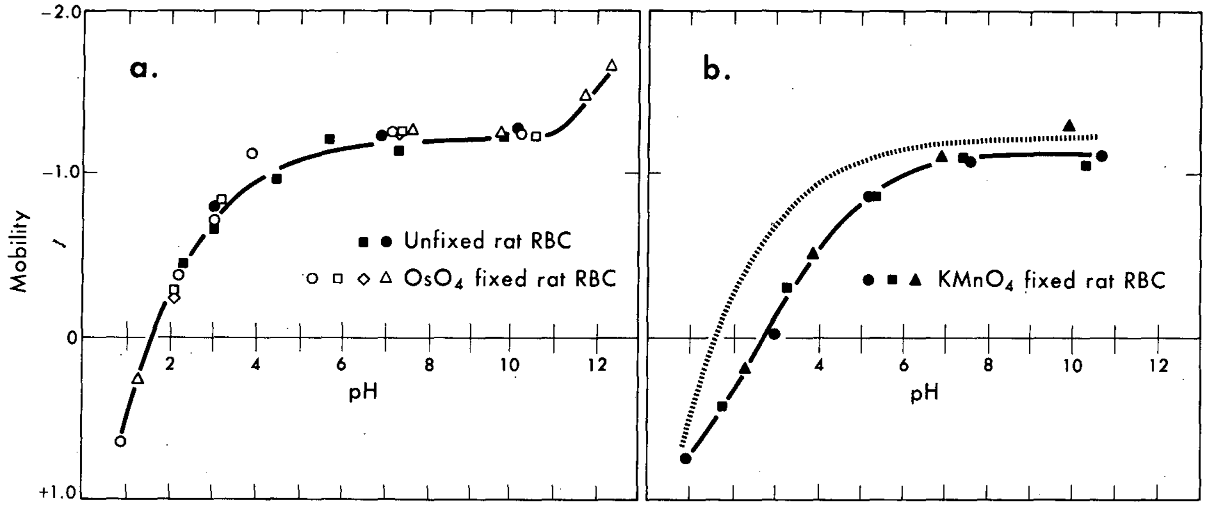

Figure 1a, 1b. Comparison of the mobility-pH curves for unfixed, OsO_4-fixed, and $KMnO_4$-fixed rat RBC. The dotted curve in 1b is a portion of the curve shown in 1a. The data indicated by the clear squares in 1a and by the dark squares in 1b were obtained with fixed cells dehydrated in ethanol.

MU-30523

electric current is essentially constant over such a small temperature range since the temperature coefficients of the viscosity and conductivity tend to cancel each other (9). The value of the mobility at 25°C can therefore be obtained by using the value of the conductivity at 25°C in the mobility calculations. For this reason all conductivity measurements were made in a water bath thermostated at 25°C.

RESULTS

At ionic strength 0.145, the mobility-pH curve for OsO_4-fixed rat RBC is identical to the curve for normal, unfixed rat RBC in the region where data can be obtained for the latter. (A slight shift in the magnitude, but not the shape, of the curve was found if the 2% OsO_4 solution was made with distilled water rather than with Standard Buffer.) Fig. 1a shows the combined results of four experiments with the OsO_4-fixed cells and two experiments with the unfixed cells. This curve is qualitatively identical to that first found by Furchgott and Ponder for human RBC (10) over the portion of the pH range from about 1.6 to 11.0. Fig. 1b shows that the mobility-pH dependence of $KMnO_4$-fixed RBC is qualitatively different from that of OsO_4-fixed (or unfixed) RBC. The difference between the two types of fixed cells is greatest below pH 7.0.

The dependence of mobility upon ionic strength is shown in Fig. 2 where the mobility of fixed and unfixed RBC, at pH 7.3 ± 0.2, is plotted as a function of the reciprocal of the Debye-Hückel constant, κ. At 25°C, $\kappa = 0.327 \times 10^8 \times \left(\frac{\Gamma}{2}\right)^{1/2} cm^{-1}$, where $\frac{\Gamma}{2}$ is the ionic strength. This method of displaying the ionic

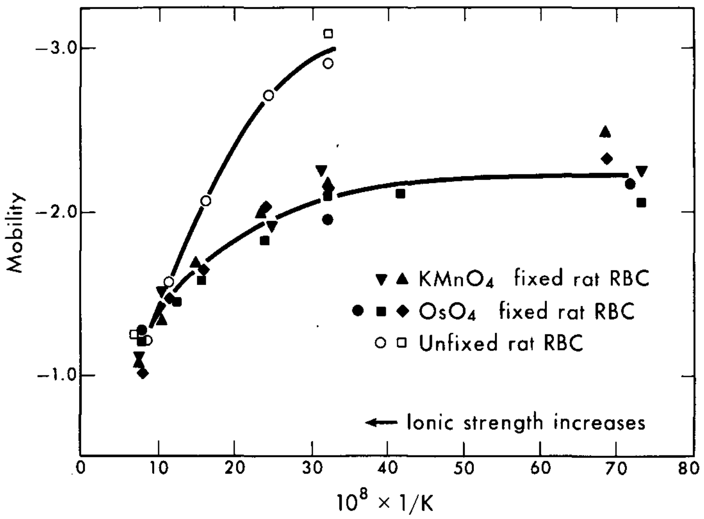

Figure 2. Mobility of fixed and unfixed rat RBC at pH 7.3 ± 0.2 as a function of the inverse of the Debye-Hückel constant. The Debye-Hückel constant, κ, is equal to $0.327 \times 10^8 (\frac{\Gamma}{2})^{1/2} cm^{-1}$ at 25°, where $\frac{\Gamma}{2}$ is the ionic strength. All mobility values have been corrected to the viscosity of water.

MU-30522

strength data was used by Furchgott and Ponder (10), and has been further discussed by Brinton and Lauffer (9). While the data obtained with both types of fixed RBC appear to fall on the same curve, there is a marked difference between this curve and that found for the unfixed RBC. Data have not been included for the unfixed RBC at the lowest ionic strengths ($\frac{1}{\kappa} > 30 \times 10^{-8}$ cm) because it was not possible to obtain reproducible values for the mobility from experiment to experiment. It was observed that for unfixed rat RBC the value of the mobility at these low ionic strengths was extremely sensitive to small variations in the initial pH, among other factors.

A remarkable feature of the fixed RBC, noted in the course of these experiments, was their great stability at the low pH's and low ionic strengths. No change in the mobility was exhibited throughout the period of observation (which was as long as 20 min), even at the extreme pH's of 0.9 or 12.3 or in ionic strengths as low as 0.00725. In addition, Table 1 shows that the mobility of OsO_4-fixed cells is restored to normal (within experimental error) when the cells are returned to Standard Buffer after a 5-min exposure to low pH or to low ionic strength. This reversibility experiment could not be performed with the OsO_4-fixed cells after exposure to pH 12.3 because of lysis at that pH (see below). Similar experiments were not attempted with the $KMnO_4$-fixed RBC as the majority of our interest has been centered about the characterization of the OsO_4-fixed RBC.

In contrast to the great stability of the fixed cells at low pH, it has long been known that the unfixed cells show rapid changes in acid solutions. For example, Furchgott and Ponder (10) noted that unfixed RBC undergo rapid hemolysis below pH 2.0, at which time the ghosts instantly acquire a positive mobility. At pH's above 2.0 but below 4.0 to 4.5, they observe (as have various

Table 1. Mobility of OsO_4-fixed rat RBC measured in Standard Buffer following 5-min exposure to the indicated solution conditions

pH = 0.90 ionic strength 0.145	pH = 7.0 ionic strength 0.00725	Standard Buffer
-1.24	-1.20	-1.28

authors since that time) that the mobility of unfixed RBC also becomes more positive with time. Such changes occur more slowly the higher the pH. An example of the time dependence of the mobility at pH 3.1 ± 0.1 is shown for unfixed rat RBC in Fig. 3. This figure shows the experimental reproducibility throughout one day: aliquots of the same RBC stock suspension were diluted in the low pH solutions at 20 min and at 210 min after the blood was first drawn. Such curves are, however, only semi-quantitatively reproducible from day to day.

In addition, we have observed that the unfixed RBC are rapidly and completely dissolved at pH's above 11.0. The stability of guinea pig RBC (1) and human RBC (2) at low ionic strengths has been rather carefully examined by other authors. Heard and Seaman have presented a complete map of the pH and ionic strength regions of stability for human RBC (2). We have not attempted such a complete mapping with the unfixed rat RBC in this study.

A word should be said about the morphological appearance of the fixed compared to the unfixed cells. Immediately after OsO_4 fixation, the cells appeared to be either sphered or oval in shape. Only a small percentage had the form of an ideal biconcave disk. If the OsO_4-fixed cells were stored at room temperature in the 0.145 M NaCl solution for several days, they gradually reassumed the form of a biconcave disk. At pH 11.8 and 12.3 the freshly fixed cells were swollen and greatly elongated by the time observation commenced.

The fixed cells are also considerably more resistant to alkali than are the unfixed. Lysis occurs only slowly at pH 11.8; it is complete in 2 to 3 min at pH 12.3, though intact ghosts still remain. The mobility of the ghosts appeared identical to that of the intact cells. Neither swelling nor lysis occurred in the OsO_4-fixed cells at pH's below 11.8.

The $KMnO_4$-fixed RBC appear, at a magnification of 200 diameters, to be smooth spheres about four or five microns in diameter. At higher magnification, however, it is seen that they are actually uniformly crenated spheres. The $KMnO_4$-fixed cells undergo a reversible swelling accompanied by a loss of crenation when placed in ethanol or in aqueous solutions of pH 8.0 or greater. The tonicity and the ionic strength do not appear to affect the shape of these

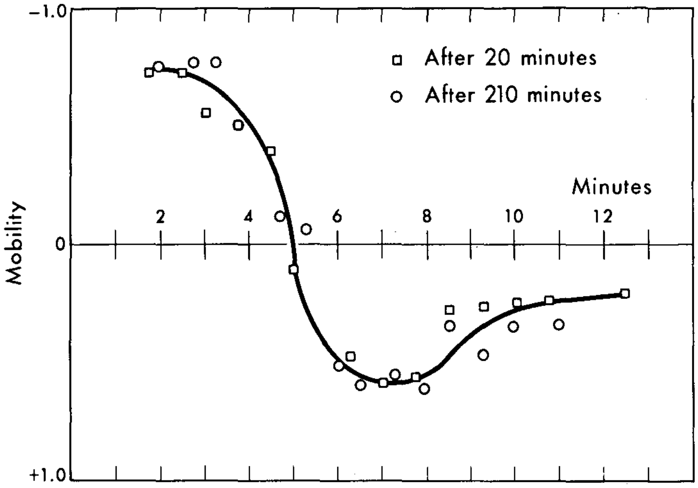

Figure 3. Time-change in the mobility of rat RBC suspended in 0.145 M NaCl at pH 3.1 ± 0.1. Zero time corresponds to the instant at which an aliquot of the 10% stock cell suspension was diluted 100-fold in the acid solution. Aliquots of the same stock suspension were diluted in the acid solution 20 min (squares) and 210 min (circles) after the blood was drawn.
MU-30521

objects. These observations on the various morphological changes have, as yet, no explanation.

DISCUSSION

MOBILITY-pH DATA WITH OsO_4-FIXED CELLS. The mobilities of the OsO_4-fixed rat RBC were shown in Fig. 1a to be identical to those of the unfixed cells, throughout the entire range of pH over which a comparison can be made. Thus the surface structures, at least the charge-determining ones, are not altered by this "drastic" treatment. Furthermore, OsO_4-fixed RBC have been found to be very stable at low pH, even down to pH 0.9. This remarkable stability has made it possible for the first time to obtain measurements of the reversible mobility of RBC below their isoelectric point at pH 1.6 (ionic strength 0.145) and at a pH as high as 12.3. In this way it has been possible to demonstrate two new features of the mobility-pH curve for RBC at ionic strength 0.145. First of all, it is shown that these cells (reversibly) acquire a positive mobility below their isoelectric point with no indication of an inflection point in the mobility-pH curve, down to pH 0.9. Second, it is found that the mobility increases in absolute value above pH 11.0. It is believed that these new features represent "real" properties of the cell surface, i.e., properties that are present at a physiological pH in the unfixed cells. The identity between the mobility of fixed and unfixed RBC, and the reversibility of the mobility of the fixed RBC are the basis of this belief. In particular, the positive mobility found below pH 1.6 cannot be ascribed to positively charged products of hydrolysis at that pH, as the mobility at pH 7.4 is not affected by exposing the fixed cells to pH 0.9 for 5 min.

The stability in the mobility of the OsO_4-fixed RBC at low pH is accompanied by other equally remarkable features. The fixed cells do not appear to be morphologically altered upon suspension in distilled water, upon dehydration in absolute ethanol, or upon air-drying (from distilled water) on a glass slide. Similarly it has been observed that the fixed cells will not stain appreciably with eosin, even after being boiled for 5 min. Unfixed RBC, however, take on an intense pink color in the eosin solution after incubation in hot (not boiling) water for less than 1 min; if boiled they disintegrate completely. In view of the apparent impermeability (to a small dye molecule) and stability under the stresses of low pH, low osmotic pressure, dehydration, and extreme heat, it is perhaps reasonable to assume that the OsO_4 has "cemented" together the membrane of the RBC.

The ability of OsO_4-fixed (human) RBC to bind specific antibody has been studied by Bessis, Bricka, and Breton-Gorius (11). They found that this binding ability was unaffected by OsO_4 fixation although agglutination was considerably reduced. This latter fact they ascribed to the rigidity of the fixed cells. The unaltered binding of specific antibody is a very sensitive indication that the structures on the surface of the RBC (at least the binding sites) have not been altered by the OsO_4 treatment. A similar conclusion has already been drawn from the electrophoretic identity of the fixed and unfixed cells.

It is instructive at this point to consider what is known about the chemical reactions of OsO_4 with biological materials. Unsaturated lipids react quite rapidly with OsO_4, whereas saturated lipids do not (12). Proteins also react with OsO_4, although often at a considerably slower rate than lipids react (13). Carbohydrates do not react at all (12). The bulk of the chemical evidence suggests that OsO_4 fixes biological materials by reacting with carbon-carbon double bonds to form an addition compound, possibly as a crosslink between molecules.* If so, this could help explain why the structure of the RBC is so greatly stabilized by OsO_4 fixation. Similarly the fact that both the antibody-binding structures and the charge-determining structures are unaffected by OsO_4 fixation is explainable on the basis of the above quoted chemistry. The blood group antigens are thought to be carbohydrate in character (15). In addition the evidence is that an acidic carbohydrate (sialic acid) is responsible for a large portion of the net charge on RBC. This last point is discussed in further detail below.

At first examination, Fig. 1a looks like the mobility-pH curve of an amphoteric substance that is characterized by both strongly acidic and strongly basic groups. The carboxyl group of sialic acid seems to compose a substantial fraction of the strongly acidic groups. Sialic acid itself apparently accounts for no more than 100% of the <u>net</u> charge at pH 6.8. The net charge will, however, be less than the total charge from all strongly acidic groups because of the presumed basic component of the cell surface. Thus, referring to Fig. 1a there must be a comparable number of strongly acidic groups, A_sH, of a different type.

*Alternative suggestions have been made recently for hydrophylic OsO_4-binding sites (14), pp. 34, 54.

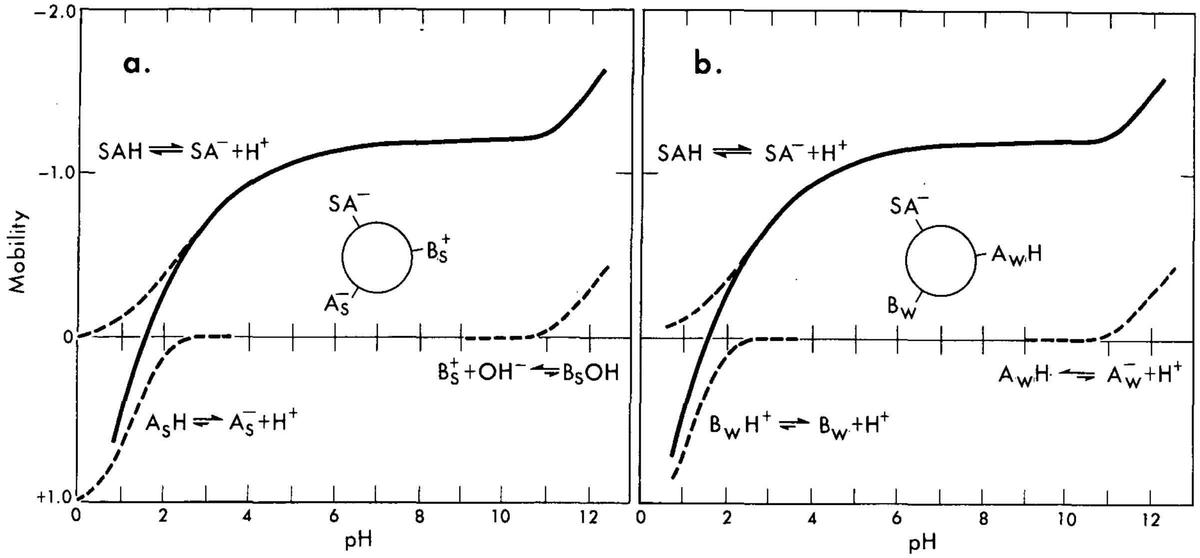

Figure 4a, 4b. Schematic representation of the acid-base characteristics of the rat RBC surface. The complete mobility-pH curve is shown as the solid curve, and the dissociation of the various acids and bases is indicated by the dashed curves. Figure 4a indicates the dissociation of sialic acid (SAH), a second strong acid (A_sH), and a strong base (B_sOH). Figure 4b indicates the dissociation of sialic acid (SAH), the proton binding of a weak base (B_w), and the dissociation of a weak acid (A_wH). The charged state of the groups at pH 7.4 is indicated by the schematic RBC surface in the center of each figure.

MU-31385

These would be responsible for the continued loss of negative charge as they become neutralized at the extreme low pH's. The net positive charge, which results below pH 1.6, is to be ascribed to the positive groups B_s^+ of the strong base B_sOH, at the outer surface of the RBC. Similarly the greater negative charge (i.e., mobility) above pH 11.0 is to be ascribed to the neutralization of these strongly basic groups. This model is summarized in a schematic fashion in Fig. 4a.

The above would seem to be the likely interpretation to be drawn from the mobility-pH data were it not for the data of Heard and Seaman that led them to the conclusion that the RBC surface was strictly anionic in nature at pH 7.4 (2,7,16). This conclusion appears to rule out the above interpretation of the mobility-pH curve. An alternative interpretation, which is in agreement with the anionic hypothesis, can be constructed as follows. The positive mobility at very low pH is ascribed to the presence of a very weak base, B_w, at the outer surface. The equilibrium reaction

$$B_w + H^+ \rightleftharpoons B_wH^+$$

would then be driven to the right at low pH. Similarly, the larger negative mobility above pH 11.0 would have to be ascribed to the presence of a very weak acid, A_wH. The reaction

$$A_wH \rightleftarrows A_w^- + H^+$$

would then be driven to the right at high pH. This model is summarized in a schematic fashion in Fig. 4b.

This second interpretation becomes all the more attractive when the structure of sialic acid is taken into careful consideration. In addition to the carboxyl group, the molecule contains an amide group, which is expected to behave as a weak base (Noller, p. 196) (17). The pK's for proton binding of peptides and amides, reported by Goldfarb, Mele and Gutstein (18), further support this suggestion. In addition, any of the hydroxyl groups of this sugar could behave as a weak acid. Glucose, for example, has a pK at 12.0 (19). Therefore, sialic acid itself appears to have all the qualitative features necessary to explain the entire mobility-pH curve from pH 0.9 to pH 12.3. This immediately suggests the possibility that sialic acid alone is responsible for the surface charge of (rat) RBC throughout this entire pH range. It is, of course, not safe to speak of "the RBC" as if RBC of every species were the same. According to the work thus far published (4,5), considerable species variation exists with regard to the types of sialic acid present in RBC and the degree to which the mobility of RBC can be decreased after removal of the sialic acid through incubation with the receptor destroying enzyme, (RDE). This enzyme specifically hydrolyses the O-ketosidic bond between sialic acid and other sugars (6). It is not yet clear whether the residual negative mobility after RDE treatment can be ascribed to 1) sialic acid that was not susceptible to the action of this enzyme, 2) other anionic groups that were originally present in addition to sialic acid, or 3) anionic groups that are exposed on the removal of sialic acid.

MOBILITY-pH DATA WITH $KMnO_4$-FIXED CELLS. It has been shown in Fig. 1b that the mobility-pH curve of the $KMnO_4$-fixed rat RBC is quite different from the curve for OsO_4-fixed (and unfixed) RBC. Although the two curves are very nearly the same in the pH range 7.0 to 11.0, the general shapes of the two curves below pH 7 are quite different, and the isoelectric point of the $KMnO_4$-fixed cells is one pH unit higher than that of the OsO_4-fixed cells. It is therefore concluded that the mobility-pH curve of $KMnO_4$-fixed rat RBC reflects a change in the pK of the anionic groups rather than an increase in the number of cationic groups (at pH 7.4). A suggestion can be made as to what chemical reaction lies behind this apparent change in pK based on the known reaction of $KMnO_4$ with carbohydrate (Noller, p. 121) (17):

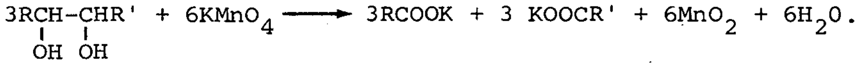

$$3\underset{\text{OH}}{\text{RCH}}-\underset{\text{OH}}{\text{CHR}'} + 6KMnO_4 \longrightarrow 3RCOOK + 3\ KOOCR' + 6MnO_2 + 6H_2O.$$

It is possible that $KMnO_4$ reacts with the carbohydrate at the cell surface in such a way that the carboxyl group of sialic acid is split off and a second carboxyl group is created to take its place. It must be pointed out, however, that $KMnO_4$ could just as well be reacting with the proteins or the lipids of the cell membrane to accomplish the same results. The recent observations of Eddy and Johns (pp. 53-54) (14) are consistent with this latter view.

IONIC STRENGTH DATA. The fact that the mobility-pH curve at ionic strength 0.145 is identical for the unfixed RBC and for the OsO_4-fixed RBC has been interpreted to mean that the two objects are identical with respect to their surface charge. Consequently it may seem surprising to find that the mobilities of the fixed and the unfixed cells vary in a radically different manner with changing ionic strength. On the other hand the mobility-ionic strength curve for the $KMnO_4$-fixed cells appears to be identical to that of the OsO_4-fixed cells. Inasmuch as all three types of objects have very nearly the same mobility at ionic strength 0.145 (and pH 7.4), it might be expected that all three would have the same mobility at other ionic strengths. The mobility is governed by the equation (9)

$$\mu\eta = \sigma_Q(\frac{1}{\kappa} + a_i)$$

where

σ_Q = charge per unit surface area
η = viscosity
a_i = radius of the counterion.

Some possible explanations of the difference in the ionic-strength curves (unfixed versus fixed) are as follows: 1) The unfixed RBC surface may be changing at the lower ionic strengths. This suggestion gains some support from the fact that the isoelectric point of the unfixed RBC increases considerably as the ionic strength decreases. The alternative possibility that the fixed RBC surface is changing at the lower ionic strengths seems unlikely in view of the stability of these cells and in view of the fact that the RBC fixed by two different methods show the same ionic-strength behavior. 2) The fixed cells may have an "electrophoretic" radius (as discussed in some length by Brinton and Lauffer (9)) different from that of the unfixed RBC. This possibility would provide a convenient explanation. Unfortunately there seems to be no theoretical justification for the use of any radius in the equations of electrophoresis other than the gross radius of the whole particle. 3) There could be a difference in the penetrability to counterions, as discussed by Haydon (20). This seems unlikely to be a satisfactory answer because the two curves should be different from each other by a similar factor throughout the entire range of ionic strength. 4) The conductivity of the fixed cells might be increased to the point where it becomes comparable to that of the surrounding medium at the lower ionic strengths. Then the mobility as a function of ionic strength will be governed by the equation (9)

$$\mu\eta = \sigma_Q(\frac{1}{\kappa} + a_i)\ \frac{2\sigma}{2\sigma + \sigma'},$$

where

σ = conductivity of the medium, a function of the ionic strength

σ' = conductivity of the particle.

According to this explanation, the conductivity of the unfixed RBC is always much less than that of the surrounding medium; therefore the mobility of the unfixed RBC would always be greater than or equal to the mobility of the fixed RBC. This fourth explanation could be tested by suitable measurements of the high frequency electrical impedance of these cells. (It should also be pointed out that the extreme low ionic strengths could have a different effect on mobility. After a period of time, this stress may cause the unfixed RBC membrane to become somewhat more permeable. The conductivity of the cell would correspondingly increase and as a result the mobility would decrease. This may in fact be the proper explanation of the irreversible decrease in the mobility with time at low ionic strength, reported for guinea pig RBC (1) and human RBC (2)).

THE EMERGING PICTURE OF THE CHARGE-DETERMINING STRUCTURE OF THE RBC. Furchgott and Ponder were the first to make measurements of what probably corresponds to the true isoelectric point of intact human RBC. The value of 1.7 reported by them was considerably lower than what they found for either the extracted lipid or the extracted protein fractions of the RBC ghosts (10). Low values of the isoelectric point of other mammalian cells have also been reported (21,22,23). The Ehrlich ascites cells studied by Cook, Heard, and Seaman (24) and the liver cells studied by Bangham and Pethica (23) are the only mammalian cells reported to have an isoelectric point above 3.0. Furthermore, the studies of Heard and Seaman with various monovalent anions (2) and studies on the effects of aldehyde treatment (7) imply that there are no cationic groups contributing to the net charge of human RBC at pH 7.4.

If the charged groups of either the lipid or the protein are to be responsible for the charge on the surface of RBC, these groups must be ordered in a very special way so that the isoelectric point of the whole is less than that of any of its components taken separately. In addition, Heard and Seaman's experiments and the approximate constancy of the mobility between pH 6.0 and 11.0 argue that groups that would be positively charged at pH 7.4 and groups with pK's in the range 6.0 to 11.0 must be effectively prevented from dissociating, i.e., they must be "folded" away in the surface structure.

The alternative explanation is that the lipid and protein of the cell membrane structure play a relatively minor role in the determination of net charge. In this picture, they are sufficiently far back from the surface of shear that their counterions move with the cell as a whole, and they are thus effectively undissociated. The charge on the surface of the RBC must then be dominated by other substances whose dissociable groups have only extremely low and extremely high pK values. The importance of sialic acid in determining the surface charge of human RBC (3,4,5) has been discussed in great detail in the literature. The suggestion to be made from the present study is that sialic acid may be completely responsible for the normal charge on the surface of RBC. This substance has no cationic groups at pH 7.4, and it appears to have all the acid-base characteristics necessary to explain the entire mobility-pH curve from pH 0.9 to 12.3.

SUMMARY

Mobility-pH curves at ionic strength 0.145 and mobility-ionic strength curves at pH 7.3 are reported for OsO_4-fixed, $KMnO_4$-fixed and unfixed rat RBC. OsO_4 fixation imparts great stability to the RBC, permitting extension of mobility measurements down to pH 0.9 and up to pH 12.3. The pH-mobility curves for OsO_4-fixed and for unfixed cells are identical over the entire range for which data can be obtained for unfixed RBC. Both types are isoelectric at pH 1.6. The OsO_4-fixed cells: a) reversibly acquire a positive charge below pH 1.6 and b) acquire an increased (negative) mobility above pH 11.0. These two new features are believed to represent intrinsic properties of the normal unfixed RBC. The entire extended mobility-pH curve appears consistent with the idea that outer-surface sialic acid (N-acylated neuraminic acid) is solely responsible for their charge (electrophoretic) characteristics.

$KMnO_4$-fixed RBC show considerably altered pH-mobility (hence surface) characteristics, compared with OsO_4-fixed and unfixed RBC. This is ascribed to differences in chemical reactivity of OsO_4 and $KMnO_4$. Mobilities of both kinds of fixed cells are virtually identical at all ionic strengths at pH 7.3 but are lower than those of the unfixed cells at lower ionic strengths.

ACKNOWLEDGEMENTS

The support of the U.S. Atomic Energy Commission, through the Lawrence Radiation Laboratory, is gratefully acknowledged.

REFERENCES AND NOTES

1. Bateman, J. B., and Zellner, A.; Arch. Biochem. Biophys. 60:44, 1956.
2. Heard, D. H., and Seaman, G. V. F.; J. Gen. Physiol. 43:635, 1960.
3. Cook, G. M. W.; Heard, D. H., and Seaman, G. V. F.; Nature 191:44, 1961.
4. Eylar, E. H.; Madoff, M. A.; Brody, O. V., and Oncley, J. L.; J. Biol. Chem. 237:1992, 1962.
5. Seaman, G. V. F., and Uhlenbruck, G.; Arch. Biochem. Biophys. 100:493, 1963.
6. Gottschalk, A.: The Chemistry and Biology of Sialic Acids and Related Substances, London, Cambridge University Press, 1960, p. 99.
7. Heard, D. H., and Seaman, G. V. F.; Biochim. Biophys. Acta 53:366, 1961.
8. Hartman, R. S.; Bateman, J. B., and Lauffer, M. A.; Arch. Biochem. Biophys. 39:56, 1952.
9. Brinton, C. C. Jr., and Lauffer, M. A.: Electrophoresis, New York, Academic Press Inc., 1959, Ch. 10.
10. Furchgott, R. F., and Ponder, E.; J. Gen. Physiol. 24:447, 1941.

11. Bessis, M.; Bricka, M., and Breton-Gorius, J.; Compt. Rend. Soc. Biol. 147: 369, 1953.
12. Bahr, G. F.; Exptl. Cell Res. 7:457, 1954.
13. Hayes, T. L.; Lindgren, F. T.; Gofman, J. W.; Spaulding, S. W., and World, J. P.; Semiannual Report, Donner Laboratory, Lawrence Radiation Laboratory, UCRL-10683, 1962.
14. The Structure and Function of the Membranes and Surfaces of Cells, edited by D. J. Bell and J. K. Grant, Biochem. Soc. Symp. No. 22, London, Cambridge University Press, 1963.
15. Morgan, W. T. J.; Proc. Roy. Soc. Lond. B 151:308, 1960.
16. Seaman, G. V. F., and Heard, D. H.; J. Gen. Physiol. 44:251, 1960.
17. Noller, C.: Textbook of Organic Chemistry, Philadelphia, W. B. Saunders Co., 1951.
18. Goldfarb, A. R.; Mele, A., and Gutstein, N.; J. Am. Chem. Soc. 77:6194 1955.
19. West, E. S., and Todd, W. R.: Textbook of Biochemistry, 2nd Ed., New York, Macmillan Co., 1957, p. 57.
20. Haydon, D. A.; Biochim. Biophys. Acta 50:450, 1961.
21. Bangham, A. D.; Pethica, B. A., and Seaman, G. V. F.; Biochem. J. 69:12, 1958.
22. Wilkins, D. J.; Ottewill, R. H., and Bangham, A. D.; J. Theoret. Biol. 2: 265, 1962.
23. Bangham, A. D., and Pethica, B. A.; Proc. Roy. Phys. Soc. Edinburgh 28:43, 1960.
24. Cook, G. M. W.; Heard, D. H., and Seaman, G. V. F.; Exptl. Cell Res. 28:27, 1962.

Based in part on the dissertation of Robert M. Glaeser submitted in partial fulfillment of the requirements for the degree of Doctor of Philosophy. Available as Lawrence Radiation Laboratory Report UCRL-10898, 1963.

Received September, 1963.

Rapid Continuous Electrophoretic Concentration of Dilute Protein Solutions

Howard C. Mel, Hans F. Loken and Joan Manning

During the course of electrophoretic studies on serum proteins, it became necessary to concentrate dilute separated fractions for subsequent analysis. The mildest possible procedure was desired in order to reduce the chances of any irreversible alterations to the proteins. It therefore seemed advantageous to restrict the process so that the macromolecules would remain in unheated aqueous solution, not contacting foreign surfaces or organic solvents. Concentration methods are basically separation methods. A survey of existing protein separation procedures (1) indicates that most are excluded by the above restrictions. One of the few procedures suitable for concentration is ultracentrifugation, but long handling times (24 hr or more) and relatively limited capacity are undesirable features.

The particular applicability of stable-flow free-boundary (STAFLO) electrophoresis for concentration has already been pointed out, and a rapid fourfold concentration (and separation) of very dilute dyes reported (2). In work with biological colloids the need for concentration procedures arises frequently because a) species of interest commonly occur in dilute form in large fluid volumes and b) most separation procedures themselves lead to (unwanted) dilution of species being separated. This short communication describes our solution to the problem, using a specific example. The differences from the previously reported dye example are: a) use of a natural protein mixture, b) more concentrated sample solution (wt %), c) larger sample flow rate, d) shorter steady-state residence time (in the flow-cell), e) higher concentration factor, and f) concentration effected without separation.

MATERIALS AND METHODS

The theory and practice of STAFLO-electrophoresis are given in detail elsewhere (3). The bulk liquid in a horizontal flow-cell (Fig. 1) has its flowing strata stabilized, in a steady state configuration, by hydrodynamic principles rather than by use of a supporting medium. In the vertical electric field (transverse to the flow), charged components move according to a variety of migration principles (3, paper III). Dilute, normal human serum was chosen as a broadly representative complex sample. Six ml, dialyzed 4 hr against distilled water, were diluted with distilled water to 1,100 ml and introduced

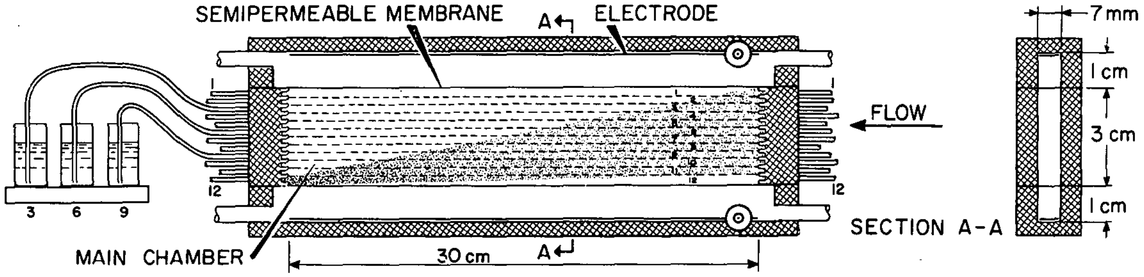

Figure 1. Schematic diagram of STAFLO flow-cell. In the idealized concentration experiment shown, the sample enters through inlets Nos. 1 - 11 and (the solute) all leaves through outlet No. 12. Theoretical concentration factor: sample inlets/sample outlets = 11:1.

MU-20112B

into inlets Nos. 1 - 11 (see Fig. 1). Specific resistance of the sample (at $25.5^{\circ}C$) was 10.4×10^{4} ohm cm. The top electrode compartment solution was stock high-resolution (TRIS) buffer (LKB, Stockholm) diluted $\sim 4 \times 10^{-2}$ with distilled water to a specific resistance (at $25.5^{\circ}C$) of 0.52×10^{4} ohm cm, pH = 8.8. Inlet solution No. 12 and the bottom electrode compartment solution were this same buffer, containing 2% (wt/vol) sucrose.

Inlet solutions Nos. 1 - 12 were each pumped at 0.47 cc/min; total sample flow rate was 5.2 cc/min. Top and bottom electrode solutions flowed at 27 ml/min. The top (Pt foil) electrode was 120 V negative relative to the bottom electrode; current was 3.75 mA. Collection was terminated after 68 cc of sample had flowed, and the fractions were then analyzed spectrophotometrically.

RESULTS AND DISCUSSION

Optical densities (O.D.) of those inlet and outlet solutions that showed appreciable absorption are given in Table 1. The first comparison to be made is the concentration factor achieved in outlet No. 12, compared with the inlet sample (in Nos. 1 - 11). This factor is 0.354 x 10/0.352 = 10.1. The migration time <u>for any given molecule</u> is 11.2 min, which is the steady state residence time under the above flow conditions. Material balance comparison can also be made: No. 12 outlet contains 0.354 x 10 = 3.54 O.D. units, or 91.4% of the input O.D. (0.352 x 11); No. 11 outlet contains 4.9% of the input O.D.

This concentration is based on the principle of the free-solution "conductivity barrier" (3, paper III). Since the conductivity of inlet solution No. 12 is approximately 20 times greater than that of inlet solutions Nos. 1 - 11, downward electrophoresis of the proteins nearly stops when they reach the position of the 11-12 boundary. In this manner, the proteins are kept away from the lower (dialysis tubing) "wall", and concentration of a mixture can be

Table 1. Optical density (O.D.) of inlet and outlet solutions measured in a 1- by 1-cm cell in a Beckman DK-1 recording spectrophotometer at the protein absorption maximum, O.D. 280 mμ; in TRIS buffer, pH 8.8

Solution	O.D.
Inlets Nos. 1 - 11	0.352
Outlet No. 12, diluted 1/10 in top buffer	0.354
Outlet No. 11	0.189

effected without fractionation (the 3.7% of unaccounted-for sample may represent a small amount reaching the "wall" and adhering to it). With the high electrical field strength in the flow-cell, even relatively low-mobility components are seen to migrate very rapidly. The increased mobility of proteins at lower ionic strengths is also useful in minimizing migration time (4). Summing up the result of this paper: a ten-fold concentration of dilute human serum has been accomplished in aqueous solution at room temperature (it can be cooled if desired), with an 11-min residence time and a sample flow rate of 5.2 cc/min.

In cases where time and stress of handling must be kept to a minimum (e.g., because of lability of molecules or molecular complexes) STAFLO-concentration offers real advantages compared with most other methods. A variety of dialysis procedures that have proved useful for protein concentration can involve relatively little short-term stress (though some macromolecular contact with the membrane is required), but the times involved are often considerable. For example, Hofsten and Falkbring report a processing time of 30 hr for their 8-fold concentration of a 1,000-ml bacterial extract (5).

The permissible ranges in dilution, flow rate, electrical current, and other important variables in the STAFLO system have not been determined, but undoubtedly wide variations are possible from the arbitrarily chosen values used in this example. If higher concentration factors are desired, an apparatus with more outlets (e.g., 24) may be used; recycling could also be employed. Because of the steady-state nature of the migration process, total capacity can be increased, theoretically at will, simply by allowing the apparatus to run as long as necessary. The method has been shown to be generally applicable to a variety of charged species, from small ions up to micron-sized objects (such as living cells).

ACKNOWLEDGEMENTS

The support of the Atomic Energy Commission through the Lawrence Radiation Laboratory, is gratefully acknowledged.

REFERENCES AND NOTES

1. Analytical Methods of Protein Chemistry. Vol. 1, The Separation and Isolation of Proteins, edited by P. Alexander and R. J. Block, New York, Pergamon Press, 1960.
2. Mel, H. C.; J. Chem. Phys. 31:559, 1959.
3. Mel, H. C.; "Stable-Flow Free Boundary Migration and Fractionation of Cell Mixtures: I, II, III," J. Theoret. Biol., 1964, in press.
4. Tiselius, A., and Svensson, H.; Trans. Faraday Soc. 36:16, 1940.
5. Hofsten, B. v., and Falkbring, S. O.; Anal. Biochem. 1:436, 1960.

Dr. Hans F. Loken and Joan Manning are associated with the Department of Medicine, University of California, San Francisco. Professor Loken's present address: Sentral Sykehuset, Kristiansand, S., Norway.

Received September, 1963.

Continuous Free-Flow Fractionation of Cellular Constituents in Rat Bone Marrow

Howard C. Mel, Linda T. Mitchell and Bo Thorell

Bone-marrow cells are known to have great heterogeneity in size and other physical properties, as well as in morphology, function, and biochemistry (1-4). This heterogeneity complicates biological, biochemical, and biophysical studies on this tissue. For example, the elusive stem cells certainly constitute a very small fraction of the total marrow population, and yet transplantation experiments must generally be performed using whole marrow. Similarly in immunological studies of transplantation antigens and graft-versus-host reactions, a small percentage of the cells may determine the primary biological interactions (5). In such situations two developments would appear highly useful: 1) An unambiguous, reproducible physical classification of the cellular constituents in heterogeneous mixtures in the tradition established, for proteins by Svedberg (sedimentation rate) and by Tiselius (electrophoretic mobility). This should provide a physical framework for discussing the often ambiguous morphological classes of cells. 2) Preparative separation of large numbers of cells of the different types, for direct investigation of their characteristic biological properties.

A start has been made for achieving both of these objectives simultaneously. In a previous publication results were presented on apparently anomolous flow-sedimentation behavior of nucleated and non-nucleated cells in normal rat bone marrow (6). This behavior led to the slower sedimentation of erythrocytes than of other fractions in the cell mixture. A range of uncorrected sedimentation rates (in Svedbergs) for individual cell types was also reported. In the present paper we wish to describe the more detailed continuous preparative fractionation of rat bone marrow as judged by morphological criteria.

MATERIALS AND METHODS

PREPARATION OF SAMPLE. Male, Long-Evans rats, each weighing approximately 200 g, are stunned by a sudden blow on the head, decapitated by guillotine, then allowed to exsanguinate. The six long bones are quickly removed, both ends punctured with a No. 18 hypodermic needle and the marrow forced out in chunks or in a single plug, using 3 to 4 cc of chilled isotonic saline for each bone. The marrow chunks are dispersed mechanically by forcing the suspension through a No. 60 gauge stainless wire mesh, followed by filtration through a nylon mesh filter bag, then expulsion through a No. 25 hypodermic needle. The cells are centrifuged at 3°C for 5 min at 125 times gravity, then resuspended in saline and made up to the starting sample concentration of 2.6×10^7 cells/cc. At higher cell concentrations with the particular gradient solutions described below, the previously described "clump sedimentation" phenomenon is observed (7,8).

A variety of suspending liquids has been tried in place of isotonic saline. We observed that if a "more physiological" liquid was employed (e.g., Hanks' solution) the cells again became "sticky," and it was difficult or impossible to break up the clumps completely. If a "less physiological" liquid was employed (e.g., isotonic sugar) the cell condition deteriorated. Since the success of the fractionation procedure depends upon achieving a non-clumpy single-cell suspension (yet the cells must not be damaged in the process) considerable care must be taken at each step of the handling procedure.

A single rat handled as above yields about 7×10^8 marrow cells. By eosin Y staining (9) these cells generally test over 90% viable.

FRACTIONATION PROCEDURE. The method employed is stable-flow free-boundary (STAFLO) sedimentation (10,7,8), an extension of the earlier STAFLO electrophoresis (11) to the use of a gravitational force field. A multilayer, horizontally flowing, free liquid system is stabilized by hydrodynamic feedback principles rather than by use of any solid supporting medium (10). This condition leads to a special kind of plug-laminar horizontal flow. The gravitational force acts transverse to the flow in the vertical sense, leading to a downward sedimentation movement of cells. Each cell follows a resultant pathway through the main chamber of the flow-cell determined by the horizontal flow rate (~ the same for all cells) and the vertical sedimentation rate (different for different cells) (8). If the cell sample is put into the top inlet, an idealized steady-state migration pattern would resemble the wedge-shaped shaded area in Fig. 1, a schematic drawing of the flow-cell. In practice, patterns closely resembling that of Fig. 1 are often seen. (The RBC have been indicated in the figure as the slowest sedimenting component.) The electrodes shown in Fig. 1 have not been used in the present study concerned only with sedimentation.

The inlet solutions feeding the flow-cell are isotonic in saline and contain graded amounts of dextran. They are made by diluting six percent Injection Dextran in Normal Saline (Cutter Laboratories, Berkeley, Calif.). The flowing layers are numbered 1-12 from top to bottom and have dextran compositions (in weight/volume percent) as follows: No. 1, 0%; No. 2, 0% (cell-sample solution); No. 3, 0.50%; No. 4, 0.65%; No. 5, 0.80%; No. 6, 0.88%; No. 7, 0.95%; No. 8, 1.03%; Nos. 9 and 10, 2.1%; Nos. 11 and 12, 3.1%. Under the

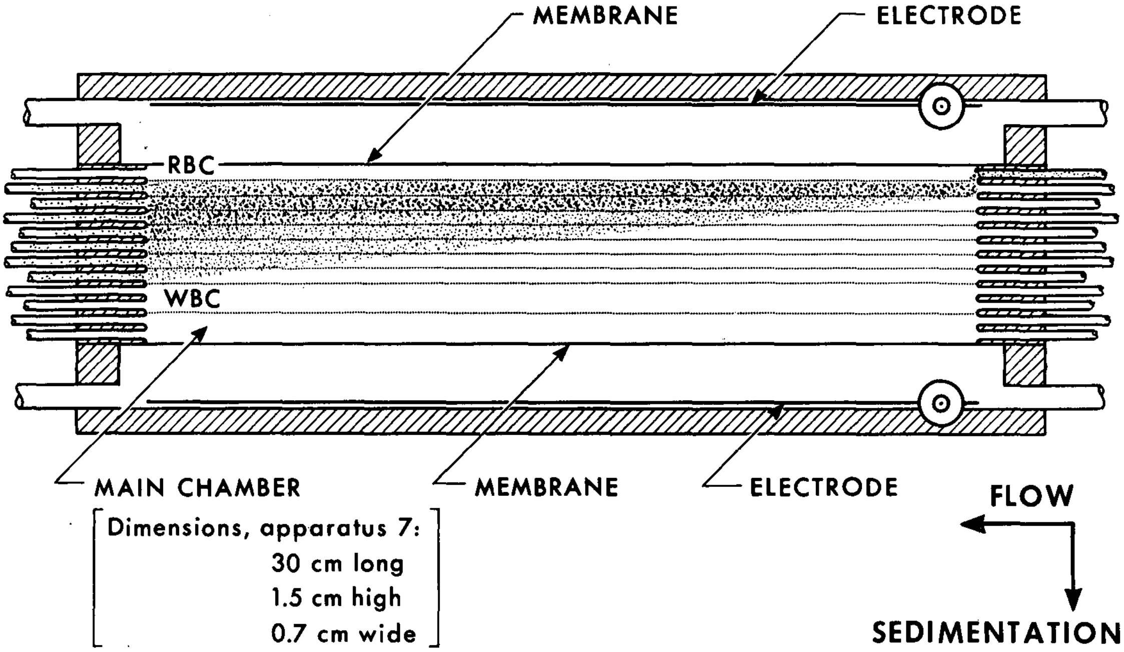

Figure 1. STAFLO flow-cell showing ideal cell sedimentation pattern.
MU-32018

experimental conditions employed in these experiments, few of the cells sediment below the 8th outlet. The stronger density gradients at the 8-9 and 10-11 boundaries provide a "density shelf" to catch most of those that do. If any large clumps are not disrupted during the sample preparation they may sediment all the way to the bottom. The light horizontal lines inside the main chamber (Fig. 1) indicate the initial discontinuities in dextran composition in adjacent layers. At later times (downstream distances) diffusion smooths these boundaries, though less with large molecules like dextran than with small molecules like sucrose. Dextran is preferred to sucrose as an inert density-gradient-producing solute because it has negligible effect on the osmotic composition of the solution. Presence of even these small amounts of colloid undoubtedly contributes to making a favorable solution environment for the cells.

Solutions are pumped into the main chamber by a rack of 12 ganged syringes. The cell-sample syringe is slowly stirred magnetically. The importance of a small-diameter feed-in tube for the cell sample has already been discussed (10). In order to reduce variations in horizontal linear flow rate near the inlet, caused by this inlet tube having a smaller diameter than that of the others, the cell-sample solution is actually introduced through inlet No. 1. Since this solution has a higher density than the "layer No. 1" saline (actually introduced through inlet No. 2), the two solutions interchange positions immediately upon entering the flow-cell (see Fig. 1). Without careful examination of the immediate inlet region, this exchange is not noticed: the top one-twelfth layer of the main chamber is clear, the second twelfth contains the cells. The surprisingly smooth nature of such a doubly bending and crossing inlet flow pattern has been illustrated in the photograph of alternating dye streams, taken in the pre-steady-state set-up period (7). To conserve sample during the set-up period, saline is initially substituted for the cell suspension. When the steady-state flow pattern is established, the sample is switched in its place.

The flow rate, identical for all solutions, was chosen to give a steady state residence (sedimentation) time of 32 min in the 30- by 1.5- by 0.7-cm main chamber. This gives a sample flow of 2.2×10^6 cells/min. Generally about 10 cc of each outlet fraction have been collected.

EXAMINATION OF FRACTIONS. Fractions are often examined directly and photographed using phase contrast microscopy. Because of the greater detail to be seen and the greater general familiarity of most workers with stained smears, the results in this paper are based on counts made from smears. Each fraction is centrifuged and the supernatant removed by suction. A drop of aged rat serum is added to each tube, the pellet is gently resuspended, and several smears are made from each fraction. When viability counts are to be made, a portion of the wet pellet is used for that purpose.

After air drying, the slides are first fixed-stained for hemoglobin with Ralph's stain (12). One set is then panoptically counterstained with Jenner-Giemsa stains, a second set with Giemsa alone. The remaining smears are fixed and retained as spares.

The following morphological classifications have been used:

1. Erythrocytes (RBC).
2. "Erythroblasts" (EBL): this designation for any nucleated erythroid cell showing a positive Ralph reaction.
3. Mature Granulocytes (WBC): segmented, or "band" (large, thin-ringed nucleus) granulocytes.
4. "Myelocytes" (MYEL): only used for distinctly granulated, non-segmented (or non-"band") myeloid cells; includes promyelocytes and metamyelocytes; generally larger than WBC.
5. "Immatures" (IM): cells not fitting the other classifications, probably corresponding to "blast" cells; generally large.
6. Lymphocytes (L): used for lymphocytes of all sizes.
7. "Small Blues" (S.B.): "small round cells," "naked nuclei"; unidentified ~RBC-sized cells with blue nucleus and scanty cytoplasm.
8. "Damaged": cells damaged beyond recognition as one of the above classes; many resemble the "amorphous pinkish patches" of Ramsell and Yoffey (13).

These classifications were chosen to minimize morphological ambiguities rather than to maximize the detailed descriptive information. The most likely remaining ambiguities are: a) confusion between the largest lymphocytes and immatures; b) uncertainty about "small blues" (we tentatively group these with "erythroblasts" rather than with lymphocytes or elsewhere--see remarks in next section). Also, no sharp boundaries exist in a continuous development sequence so distinction between early myelocytes and immatures, and between late myelocytes and WBC must be somewhat arbitrary. From the repeatability of the experimental results, it is believed these ambiguities do not lead to serious errors in assignment to the above classes.

RESULTS

The results of the differential counts for a single experiment (RTM-19) are presented in Fig. 2. The data are plotted as the percentage of the total cells in each fraction that is of the given type.

For a comparison of different runs, results for three experiments run under the same conditions are plotted in Fig. 3. "Damaged" cells (not shown) were usually less than five percent, though in a few instances they were as high as 10% of a fraction. In Fig. 3, lymphocytes are shown separately from the immatures. The slides for Fig. 3 were recounted several times over intervals of weeks or months, and a number of them counted independently by more than one person, in order to have some data involving an irreducible minimum of subjectivity. The results obtained were similar to those found in a large number of repeat experiments in which only normal care in counting was exercised.

The number of cells/cc in each collection fraction (averaged for three duplicate runs) is shown in Table 1. A comparison of total cells/cc in all collection fractions with the initially measured starting sample concentration reveals a 53% recovery of cells.

In a number of experiments, collection fractions were stained with eosin Y. "Viabilities" commonly run 90% or more, with values rarely lower than 60%. (The few cells sedimenting below outlet No. 8 often do show lower than 60% viability.) There has been some suggestion of a systematic variation in viability, but this needs further investigation and will not be discussed in this paper.

We find relatively few lymphocytes in the rat marrow, so curves (Im + L) in Fig. 2 and (Immature) in Fig. 3 show no qualitative difference. In grouping the "small blues" with "erythroblasts" instead of with lymphocytes we are being less consistent with the conclusions of Ramsell and Yoffey (13) (who reported many lymphocytes in the marrow of their Lister Hooded rats) than with those of

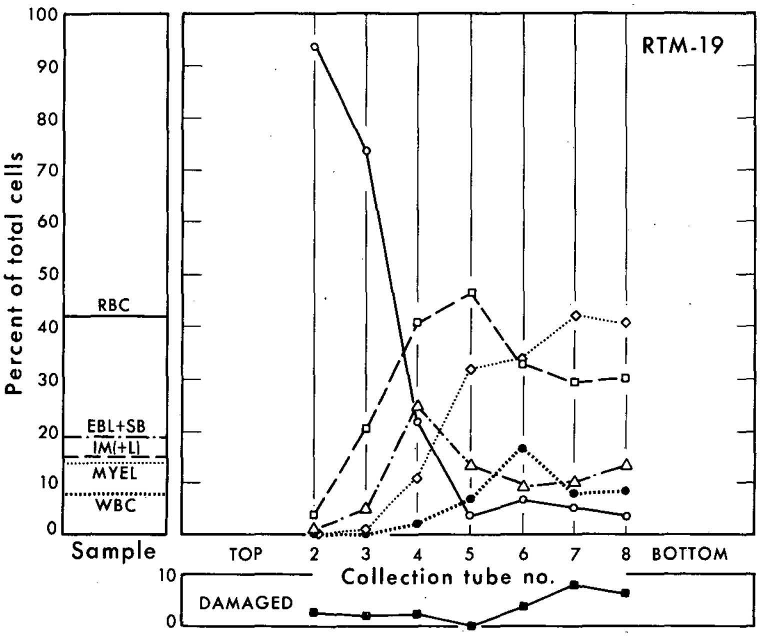

Figure 2. Relative compositions of collection fractions and sample in rat-marrow experiment RTM-19.
MU-32016

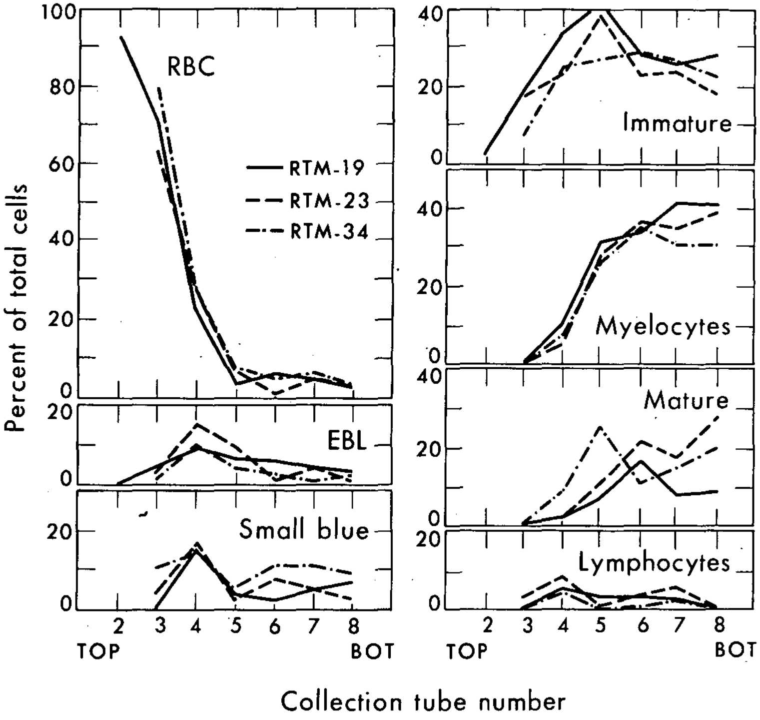

Figure 3. Comparison of fraction compositions for three duplicate STAFLO-sedimentation experiments on rat bone marrow.
MU-32017

Table 1. Total cells/cc in collection fractions
(averages for 3 runs)

Collection fraction no.	2	3	4	5	6	7	8
Numbers of cells (units: 10^5 cells/cc)	1.5	53	50	24	11	4.2	2.6

Schooley and Kelly (14) and Schooley, Bryant, and Kelly (15). In any case, relatively little should be concluded about the migration properties of lymphocytes from these experiments. For fractionation-migration studies of lymphocytes, lymph rather than marrow is the logical starting tissue.

Note that our results are reported in terms of percentages of total cells in each fraction, whereas most authors report percentages of nucleated cells. Because the physical process of STAFLO-sedimentation used involves all the cells, we prefer to take the total-cell population as our basis.

DISCUSSION

Immediately upon starting these experiments, when it was obvious that some fractionation of the marrow was occurring, a choice of directions had to be made: either (I) to devote the major effort to a systematic study of the effects of different gradients, flow rates, electrical fields, and the like on "sharpening" the peaks like those in Figs. 2 and 3, or (II) to investigate the physical reproducibility of the migration/separation process by running a large number of repeat experiments, limiting classification and analysis of the data to a small number of cell types.

We chose the second objective as our initial one, believing that demonstrated experimental reproducibility is a primary prerequisite for use of a new method. Furthermore, with a complex mixture, such as marrow, it is difficult to predict the outcome of biological experiments using different fractions, without actually performing the experiments with each fraction. Thus, extensive systematic work on "improving" the fractionation would very likely be premature at this point. In addition, re-examination of the present data according to different classifications would lead to different-looking cell-distribution curves (in the fractions) even without changing any experimental parameters. (This reclassification can always be made later if desired.) Consequently, after a few preliminary experiments gave us conditions leading to an interesting appearing fractionation, these conditions were adopted for the whole subsequent series. When the biological consequences of the present fractionation are in hand, the study of point (I) will undoubtedly be desirable. (For more discussion on experimental design, see references 7, 8, and 10.)

Table 2. STAFLO-sedimentation, composite of experiments RTM 19-37

Cell type	Maximum, in collection tube no.	Maximum percent	Starting samples, average percent
RBC	2, (3)	94	45.4
Erythroblasts + S.B.	4, (2nd pk. in 6?)	33	19.6
Immatures	4-5	46	17.5
Myelocytes	6-8	53	12.3
Mature WBC	6-8	30	8.4

The results in Fig. 2 covering a single experiment indicate immediately that major changes of composition have been achieved relative to the starting sample, and that great variations in composition have been achieved in the different collection fractions. Fig. 3 shows the experimental reproducibility of the migration/fractionation behavior of the different cell classes in the three most carefully scored duplicate runs, carried out with different animals at different times. (As previously mentioned, the results from these three runs were typical of those of the whole group of runs.) Considering biological variability, the numerous steps in handling and the previously described remaining ambiguities in morphology, these results appear quite encouraging. The cells fall broadly into classifiable and separable categories, according to physical (STAFLO-sedimentation) properties.

The data of experiment RTM 19 (Fig. 2) indicate the following enrichments and depletions for the different cell classes: RBC, range of 93.3% to 3.5%, cf. starting 42.1%; erythroblasts + S.B., range of 23.9% to 0.7%, cf. starting 19.6%; immatures (+ L), range of 45.7% to 3.4%, cf. starting 14.8%; myelocytes, range of 41.8% to 0%, cf. starting 14.6%; WBC, range of 16.1% to 0%; cf. starting 7.9%.

A composite of data from 17 repeat experiments indicates the persisting patterns shown in Table 2. The erythrocytes are always most concentrated near the top (fractions Nos. 2, 3). Erythroblasts + S.B. have always shown a peak in fraction No. 4, and quite often a second peak in fraction No. 6. The possibility of this being a meaningful bimodal distribution merits further investigation. With few exceptions, immatures reach a maximum in fractions Nos. 4 or 5. The myelocytes and mature granulocytes almost always rise to their maximum in the lower fractions Nos. 6-8; we have not seen a systematic separation between these two classes. For each class, relatively high maximum concentrations were achieved, in some cases more than 50% (Table 2). These maxima may be compared with the average starting sample compositions included in Table 2.

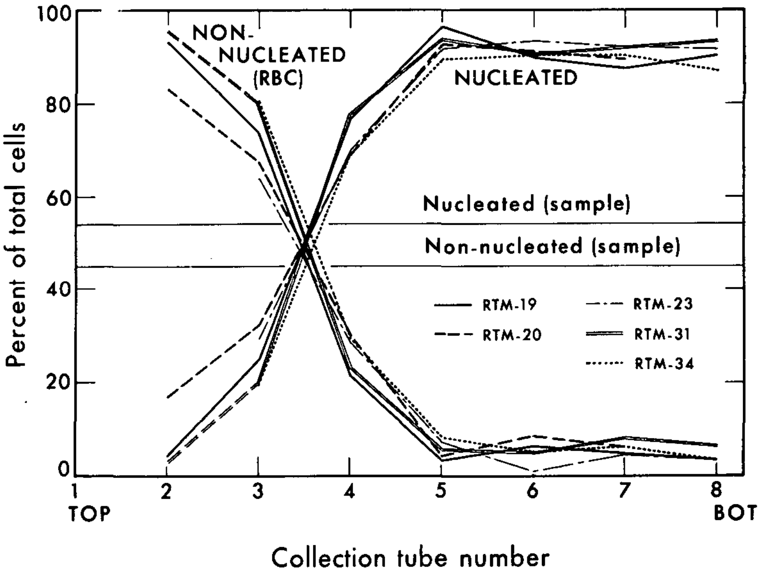

Figure 4. Separation of erythrocytes (RBC) from nucleated cells in rat bone marrow by 1-g STAFLO-sedimentation.
MU-30203A

Qualitatively, the interclass relationships of the starting sample average figures have also held for all the individual samples. For an idea of the quantitative variations involved, we can compare the sample values for RTM 19 (Fig. 2) with the composite average figures in Table 2. For a particular class, e.g., erythrocytes, the range in sample values for all experiments reported in Figs. 2-4 has been from 42.1% to 49.1% (cf. the 45.4% average).

Data on total cells/cc in each fraction were determined for a number of runs. Variations were observed to occur, particularly if significant numbers of cell clumps survived the sample preparation procedure. The data in Table 1 can be considered well representative of the present series of experiments. Fractions Nos. 3 and 4 contain approximately equal numbers of cells, and each contains more cells than any of the other fractions. The very large change in composition between fractions Nos. 3 and 4 (Figs. 2, 3) is therefore particularly noteworthy. This change can be seen perhaps even more clearly by considering, as in Fig. 4, only the two simple classes: RBC and nucleated, for which reliable data are much more easily obtained. Results are included from five experiments in Fig. 4. The high degree of physical reproducibility observed when using only this simple classification has been a feature of all our experiments. The physical basis for this particular type of differential migration has been discussed previously (6).

From the preparative standpoint, sufficient numbers of cells of any of the fractions Nos. 2-8 (for most common purposes) are relatively easy to obtain without changing the present steady-state parameters. In order to obtain 10^7 cells of an immature-rich fraction No. 4 (using the figures of Table 1) 2 cc would have to be collected. For the highest RBC-percentage fraction

Table 3. Examples of enrichment by STAFLO-sedimentation

Ratio of cell types	Values of ratio			Fraction and experiment
	Starting sample	Collected fraction		
Immature/mature WBC	1.73	∞	in No. 3	(RTM-19)
RBC/all nucleated	0.74	21.7	in No. 2	(RTM-19)
All nucleated/RBC	1.19 av.	∞	in No. 5-8	(RTM-22)
EBL* (+ S.B.*)/MYEL* + WBC	0.97 av.	6.1	in No. 4	(RTM-23)

*EBL = erythroblasts; S.B. = "small blue"; MYEL = myelocytes.

(No. 2), collection of about 67 cc would provide 10^7 cells. RBC sometimes account for as much as 80% of the cell-rich fraction No. 3, however, (Fig. 4). If it is desired to increase the number of RBC in the upper fractions, a small adjustment to the horizontal level of the flow-cell can accomplish this.

In order to quantitate the relative enrichments achieved in this series of STAFLO-sedimentation experiments, one can calculate (from Fig. 2 and all similar curves) ratios of different cell types in all collection fractions. For the ratio (immatures/WBC), a maximum value of approximately ∞ has been obtained, compared with a starting value of 1.73; for the ratio (RBC/nucleated cells), a maximum of 21.7 has been obtained, cf. a starting value of 0.74; for the ratio (nucleated/RBC) a maximum of approximately ∞ has been obtained, cf. the average starting value of 1.19; for the ratio (EBL + S.B./MYEL + WBC), i.e., identifiable nucleated red cells to identifiable nucleated whites, a maximum of 6.1 has been obtained compared with the average starting ratio of 0.97. These figures are tabulated in Table 3, together with the experiment and fraction in which each was obtained.

As previously noted, less than 100% of the nominally injected cells are recovered in the collection fractions. In these experiments, recoveries have generally ranged between 50% and 80%. Part of the loss undoubtedly lies in the not-completely-ideal single-cell nature of these naturally "sticky" marrow cells. Any clumps present will sediment much faster than individual cells, and a few are sometimes seen reaching the bottom of the main migration chamber. This also appears to be the most likely explanation for the 3-to-6% "background" of RBC usually observed in the lower collection fractions (Fig. 4). (In one older experiment with an RBC-impoverished sample, values of 0% RBC were found in tubes 5 and beneath.)

The great majority of work reported on the separation of blood cells and bone-marrow cells has been concerned with blood. No systematic review of the literature will be attempted here. Allfrey (16) has reviewed literature prior to 1959. Recent remarks by DeDuve (17) and Beaufay and Berthet (18) are relevant to general biophysical problems of cell separations, particularly those based on centrifugation (the most common approach). In an interesting paper dealing with bone marrow, Goodman (19) further reviews the literature and presents her own experimental results. A very recent report is by Stoloff and Weiss (20). The cell separation problem is a difficult one, and Goodman's observation that none of the past approaches has yielded a satisfactory separation from the standpoint of purity, high yield and cell viability, appears still to be true today.

It is beyond the scope of this paper to pursue in detail the physical aspects of the complex sedimentation process giving rise to Figs. 2 and 3. For the representation of Fig. 4, the sedimentation-rate differences could be ascribed primarily to differences in cell size (6). For representations of Figs. 2 and 3, either size or density apparently can be the controlling factor. For example, the erythroblasts + S.B. in fraction No. 4 are smaller than the immatures in fraction No. 5, i.e., are segregated by size. On the other hand, the mature WBC in fraction No. 6 are smaller than the myelocytes in the higher fraction No. 5, i.e., density appears to be the controlling factor here. Other examples could also be given as illustration. In any case, the differential migration and separation is of the sedimentation rate type, as contrasted with the usual equilibrium (centrifugation) methods for separating cells. Both size and density factors must enter into the rate-type migration. As pointed out elsewhere, however, "size" and "density" are ambiguous concepts when applied to living cells (18,6).

In STAFLO apparatus No. 7 used in these experiments each flowing layer is 1.25 mm thick (high) so that each outlet is on the average 1.25 mm below the outlet directly above. The cells, which enter the main chamber in the position of stream No. 2 and leave via outlet No. 2, must have sedimented between 0 and 1.25 mm, or an average of 0.625 mm, during the 32-min ($\sim$1/2 hr) residence time. Thus, the "average extreme sedimentation rate" for cells in collection fraction No. 2 must be approximately 0.625/1/2 = 1.25 mm/hour. Similar calculations can be made for the other collection fractions; the resulting values are tabulated in Table 4, both in mm/hour and in Svedbergs (S). (One Svedberg = 10^{-13} sec.) The values in S-units are seen to fall in the range 3.5×10^5 to 4.2×10^6. Comparison of Tables 2 and 4 gives the nominal S-rates corresponding to the different cell-type maxima.

In conclusion, it should be reemphasized that the migration-fractionation experiments reported here are in a relatively early stage. Nevertheless, one objective, to obtain an "interesting," reproducible, preparative fractionation of rat bone marrow, appears quite well met. Toward the other (analytical)

Table 4. Nominal sedimentation rates for various collection fractions

Collection fraction no.	Average extreme sedimentation rate (mm/hr)	(10^5 Svedbergs)
2	1.25	3.5
3	2.5	7
4	5.0	14
5	7.5	21
6	10.0	28
7	12.5	35
8	15.0	42

objective--to provide a physical classification for the different cell types--we can offer the above uncorrected, nominal S-rates. Although this characterization represents only a partial achievement of our objective, it may be useful (8,6). As far as we know, other data of this kind have not yet been reported. It is hoped that eventually it will be possible to correct such data to some kind of "standard conditions." When it becomes clear what kind of improved separation may be required for a given biological purpose, it appears very likely that such an improvement can be achieved. To this end, a systematic study of different gradients, macromolecular content, pH, sample concentrations and flow rates, as well as the combined use of electric and gravitational fields (8), should prove very fruitful.

SUMMARY

A single-cell suspension of normal rat bone marrow is prepared mechanically. This suspension is continuously fractionated in free solution, under sedimentation rate conditions, using 1g only. With a sample flow of 2.2×10^6 cells/min and a 32-min steady-state residence time in the stable-flow free-boundary (STAFLO) flow-cell, the cells exit almost entirely into 7 of the 12 collection bottles. Maximum numbers of different cell types are observed, with good repeatability, in approximately descending order from top to bottom as follows: erythrocytes, "erythroblasts," "immatures," "myelocytes" and mature granulocytes. Major changes are effected relative to the starting marrow composition, and very large relative enrichments are achieved for certain cell types. In addition to the rapid, mild, preparative aspect of this study, nominal sedimentation rates can be assigned for the different collection fractions, in the range of 3×10^5 to 4×10^6 Svedbergs, thus making a start on a simple physical classification of the cellular elements in this complex tissue.

ACKNOWLEDGEMENTS

The support of the U.S. Atomic Energy Commission, Lawrence Radiation Laboratory is gratefully acknowledged.

REFERENCES AND NOTES

1. Bessis, M.: Cytology of the Blood and Blood-Forming Organs, New York, Grune & Stratton, 1956.
2. Wintrobe, M. M.: Clinical Hematology. 5th Ed., Philadelphia, Lea & Febiger, 1961.
3. Braunsteiner, H., and Zucker-Franklin, D.: The Physiology and Pathology of Leukocytes, New York, Grune & Stratton, 1962.
4. Yoffey, J. M.: Quantitative Cellular Haematology, Springfield, Ill., Charles C. Thomas, 1960.
5. Wolstenholme, G. E. W., and Cameron, M. P.: Ciba Foundation Symposium on Transplantation, Boston, Little, Brown and Co., 1962, various authors, e.g., pp. 41 and 207.
6. Mel, H. C.; Sedimentation Properties of Nucleated and Non-Nucleated Cells in Normal Rat Bone Marrow, Nature 200:423, 1963; Semiannual Report, Donner Laboratory, Lawrence Radiation Laboratory, UCRL-11033:69, 1963.
7. Mel, H. C.: Stable-Flow Free-Boundary Migration and Fractionation of Cell Mixtures, II: Laminar Flow and Density Gradient Stability; J. Theoret. Biol., March, 1964, in press.
8. Mel, H. C.: Stable-Flow Free-Boundary Migration and Fractionation of Cell , Mixtures, III: Migration Principles--Sedimentation and Electrophoresis; J. Theoret. Biol., March, 1964, in press.
9. Schrek, R.; Am. J. Cancer 28:389, 1936.
10. Mel, H. C.: Stable-Flow Free Boundary Migration and Fractionation of Cell Mixtures, I: Apparatus and Hydrodynamic Feedback Principles; J. Theoret. Biol., March, 1964, in press.
11. Mel, H. C.: J. Chem. Phys. 31:559, 1959; Science 132:1255, 1960.
12. Ralph, P. H.; Stain Technol. 16:105, 1941.
13. Ramsell, T. G., and Yoffey, J. M.; Acta Anat. 47:55, 1961.
14. Schooley, J. C., and Kelly, L. S.; Semiannual Report, Donner Laboratory, Lawrence Radiation Laboratory, UCRL-10683:114, 1962.
15. Schooley, J. C.; Bryant, B. J., and Kelly, L. S.; in The Kinetics of Cellular Proliferation, edited by F. Stohlman, Jr., New York, Grune and Stratton, 1959, p. 213.
16. Allfrey, V.; in the Cell, Vol. 1, edited by J. Brachet and A. E. Mirsky, New York, Academic Press, 1959, p. 193.
17. De Duve, C.; in Methods of Separation of Subcellular Structural Components, edited by J. K. Grant, Biochemical Society Symposium No. 23, Cambridge, Cambridge University Press, 1963, p. 1.
18. Beaufay, H., and Berthet J.; in Methods of Separation of Subcellular Structural Components, edited by J. K. Grant, Biochemical Society Symposium No. 23, Cambridge, Cambridge University Press, 1963, p. 66.
19. Goodman, J. W.; Exp. Cell Res. 21:88, 1960.
20. Stoloff, I. L., and Weiss A. J.; in Abstracts of Conference on Bone Marrow Transplantation and Irradiation Protection, C. C. Congdon, chairman,

Atlantic City, New Jersey, April 16, 1963; Blood 22:501, 1963.

This paper is based in part on a talk presented at the Conference on Bone Marrow Transplantation and Irradiation Protection, Atlantic City, New Jersey, April 16, 1963.

Dr. Bo Thorell is professor of pathology at the Karolinska Institute, Stockholm.

Received November, 1963.

Scintillation Camera with 11-inch Crystal

Hal O. Anger

The scintillation camera is a sensitive electronic instrument that produces pictures of the distribution of gamma-ray and positron-emitting isotopes (1-5). It is being used to localize tumors, to show the shape, size, and location of organs, and to illustrate and measure functions of organs in human subjects. The pictures are similar to those produced by medical radioisotope scanners. However, the scintillation camera operates without any mechanical scanning motion. The instrument is 3 to 20 times more sensitive than mechanical scanners with focused collimators. The higher sensitivity permits a reduction in isotope dosage or a reduction in the examination time.

A unique advantage of the scintillation camera over mechanical scanners is its sensitivity to all parts of its field of view at all times. This permits the use of isotopes with very short half lives, as well as tracer compounds with rapid biological turnover. This property, in combination with the high sensitivity, permits taking sequences of still pictures or time-lapse motion pictures to show the movement of isotopes in physiological processes. In addition, a quantitative readout of the amount of isotope present in a given part of the subject as a function of time can be obtained. Methods for obtaining the quantitative readout will be reported at a later date.

This paper contains a brief general description of the scintillation camera and the three types of image-producing collimators that can be used with it. A detailed description is given of the new image detector that uses a sodium iodide crystal, 11-1/2 in. in diameter by 1/2 in. thick, and a bank of 19 phototubes. The circuits that compute the position of scintillations are also described in some detail. Examples of pictures taken with the instrument show the results obtained in clinical use with the various collimating methods.

GENERAL DESCRIPTION

A block diagram of the instrument is shown in Fig. 1. The scintillation camera consists essentially of a) a collimator for producing a gamma-ray image of the subject, b) a large flat sodium iodide crystal that transforms the gamma-rays into a pattern of scintillations, c) a hexagonal array of phototubes spaced a short distance away from the crystal, d) a computing circuit that determines the position and the brightness of scintillations in the crystal, e) a pulse-

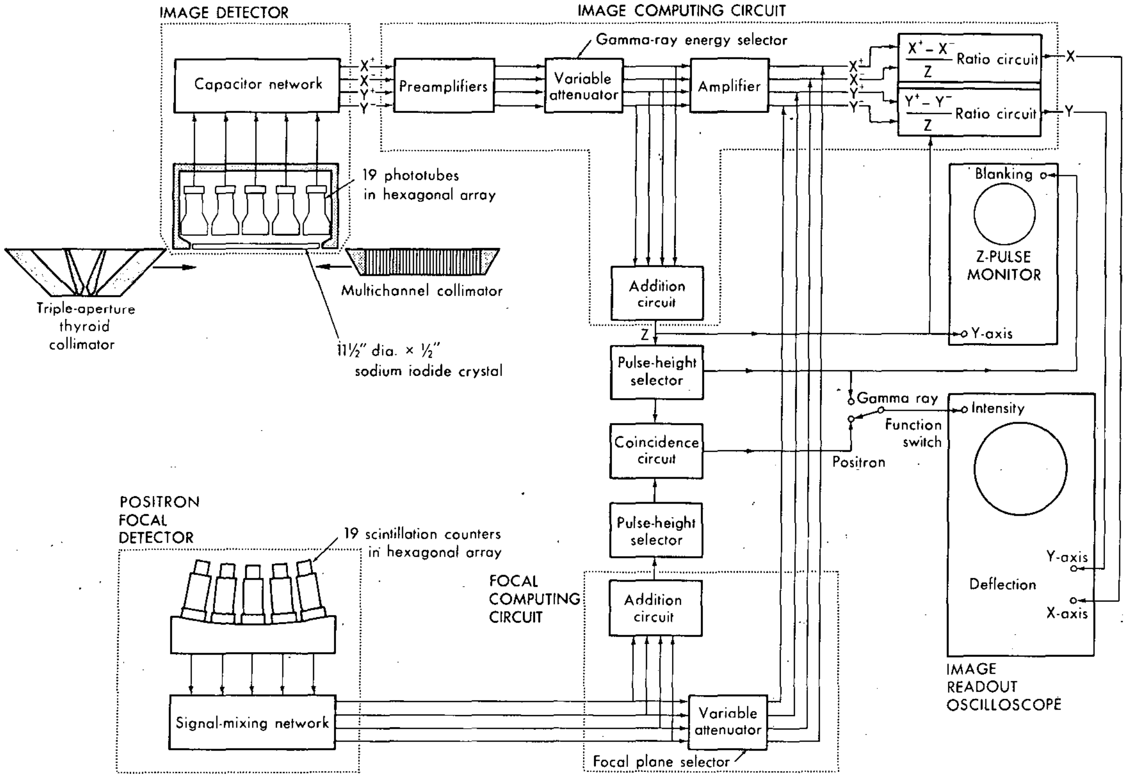

Figure 1. Block diagram of scintillation camera with multichannel collimator, triple-aperture pinhole collimator, and positron focal detector.

MUB-1973

height selector, f) a cathode ray oscilloscope that receives signals from the computing circuit and reproduces the desired scintillations as bright points of light in their proper locations on the cathode ray tube and g) an optical camera for recording these flashes of light as dots on photographic film.

The bank of phototubes is coupled to the sodium iodide crystal through an optical light guide so that the phototubes view overlapping areas of the scintillator. When a scintillation occurs, the resulting light divides among the phototubes, the closest tubes receiving the most light. All the phototubes simultaneously give pulses that are proportional in amplitude to the amounts of light received. The duration of each pulse is approximately one microsecond, which is short compared with the average time interval between scintillations.

The pulses from the phototubes are combined in the electronic circuits described below, and three output signals are obtained. Two of the signals are X and Y position signals, which deflect the beam of the cathode ray tube to a point corresponding to the location of the scintillation in the crystal. The third signal, the Z signal, is proportional only to the brightness of the scintillation. This signal goes to the pulse-height selector, which is adjusted to pass only the scintillations within the photopeak of the isotope employed. The output of the pulse-height selector goes to the grid of the cathode ray tube where it turns on the beam momentarily after the beam has been properly positioned by the X and Y signals.

Thus, the cathode ray tube presents a continuous readout of photopeak scintillations occurring in the crystal. The location of each flash of light on the cathode-ray tube screen corresponds quite accurately with that of the original scintillation, as shown later in this report. The flashes are photographed over a period of time with a Polaroid or other type of camera, and the resulting picture shows the distribution of activity in the subject. Exposure times last from 30 sec to 15 min or more, and 1,000 to 100,000 or more dots are recorded on each picture. An oscilloscope camera with several lenses is used to obtain simultaneously several images with graded densities. Thus a wide range of exposure times can be used with the assurance that one of the images will be properly exposed.

COLLIMATION METHODS

Three different methods of collimation can be used to project images of a radioactive subject on the sodium iodide crystal. They are (a) pinhole collimation, (b) multichannel collimation and (c) positron coincidence collimation.

PINHOLE COLLIMATORS. A pinhole collimator consists of an aperture at the end of a conical lead shield. Gamma rays that enter the aperture continue traveling in straight lines to form an inverted image of the subject at the scintillator. This type of collimator provides the best sensitivity and resolution for small subjects because the subject can be positioned close to the aperture and a magnified image is projected on the scintillator. The sensitivity is inversely proportional to the square of the distance from the aperture to the subject. This type of collimation is not efficient for large subjects because they must be positioned farther away. The single-aperture pinhole collimators have been described (6,7) and the geometric resolution and efficiency discussed (2,4) in previous publications.

For some purposes, pinhole collimators with more than one aperture are used (5). For the human thyroid gland, a special pinhole collimator with three apertures is now being clinically tested. The central aperture projects a conventional view of the entire thyroid gland on the central portion of the scintillator. At the same time, the left aperture projects an enlarged oblique view of the left lobe on the left portion of the scintillator. This view is enlarged because the left aperture is closer to the subject than the central one. The right aperture projects an enlarged view of the right lobe. Therefore, three different views of the thyroid are obtained simultaneously. This arrangement provides increased chances of seeing a nodule in or near the thyroid because

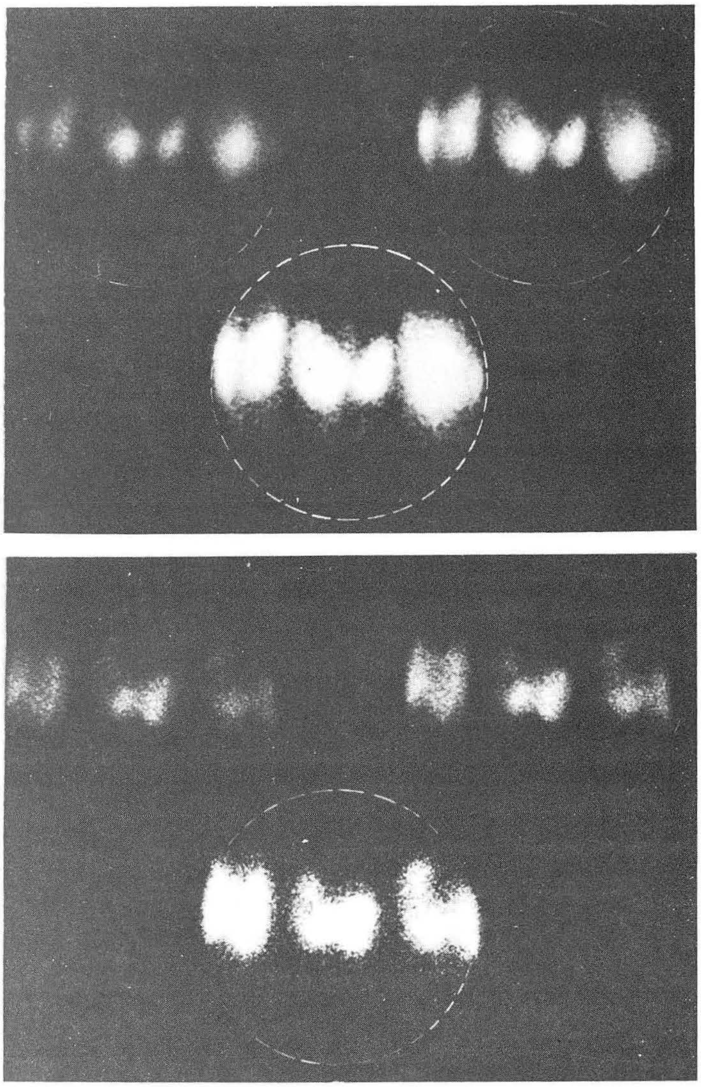

Figure 2. Pictures of the thyroid gland taken with the triple-pinhole collimator. A frontal and two oblique views are taken simultaneously in three different density grades.

three views are provided in one exposure, each lobe is viewed from two different angles, and increased detail is visible in the two enlarged views. The large size of the image detector and its high resolution make this type of collimator feasible. Figure 2 shows pictures of the human thyroid gland taken in 5 min with the triple-aperture pinhole collimator, using a 50μC dose of I^{131}. From left to right in each image are shown 1) an enlarged oblique view of the patient's left lobe, 2) a frontal view of the entire gland, and 3) an enlarged oblique view of the right lobe. The three graded-density images of each subject were obtained simultaneously by means of a 3-lens oscilloscope camera (5).

MULTICHANNEL COLLIMATORS. This type of collimator has also been described in previous publications (1,3,5,8-12). As now used, it consists of a thick lead plate with a thousand or more parallel holes. The collimator is located as close to the image-detector crystal as possible, and the subject is placed as close as possible to the other side of the collimator. It rejects gamma rays from the subject except those that travel through the holes of the collimator, and an image of the subject results. This collimation method gives the best combination of sensitivity and resolution for larger organs. The field of view with the present image detector is 9 to 10 in. in diameter, which is large enough to allow simultaneous visualization of both kidneys in most patients. Multichannel collimators are also being used to localize brain tumors, to show substernal and thyroglossal extensions of the thyroid and hot nodules in the neck with a single exposure, and to show the liver in one view when the liver is not enlarged. Pictures of the above organs can be taken in about one-fifth to one-tenth the time necessary when using a focused-collimator mechanical scanner.

Pictures of kidneys in two human subjects are shown in Fig. 3. The subjects each received 100 µC of Hg^{203} Neohydrin, and the exposure time was 5 min. The six graded-density images of each subject were obtained in a single exposure by means of a six-lens oscilloscope camera with graded lens apertures.

POSITRON COLLIMATION. A coincidence-collimation system yields the best combination of sensitivity and resolution for positron emitters. Brief descriptions have been given of an early version of the positron scintillation camera (2) and of the present form (5). The subject is placed as close as possible to the image-detector crystal, and the focal detector, consisting of one or more scintillation counters, is located a distance away on the opposite side of the subject. No collimator in the usual sense is used.

Positron emitters produce two simultaneous 0.51-MeV gamma rays that travel away from their point of origin in opposite directions. When one gamma ray strikes a counter in the focal detector, the other impinges on the image detector. A straight-line relationship exists between the focal detector, the point of origin of the two gamma rays and the point of impingement on the image detector. A coincidence circuit detects the simultaneous pulses from these events and allows the scintillation in the image detector to be displayed on the oscilloscope. No other scintillations are shown. The focal detector is a focal point for all the gamma-ray pairs that form an image of the subject. Therefore, a slightly enlarged image of the subject is projected on the image detector.

Nineteen scintillation counters are employed in the focal detector in order to obtain better resolution of thick subjects. This permits sharp focus on the deeper planes within the subject by the following method. When gamma rays are detected by the center counter of the focal detector, the coincident scintillations in the image detector are shown on the oscilloscope without

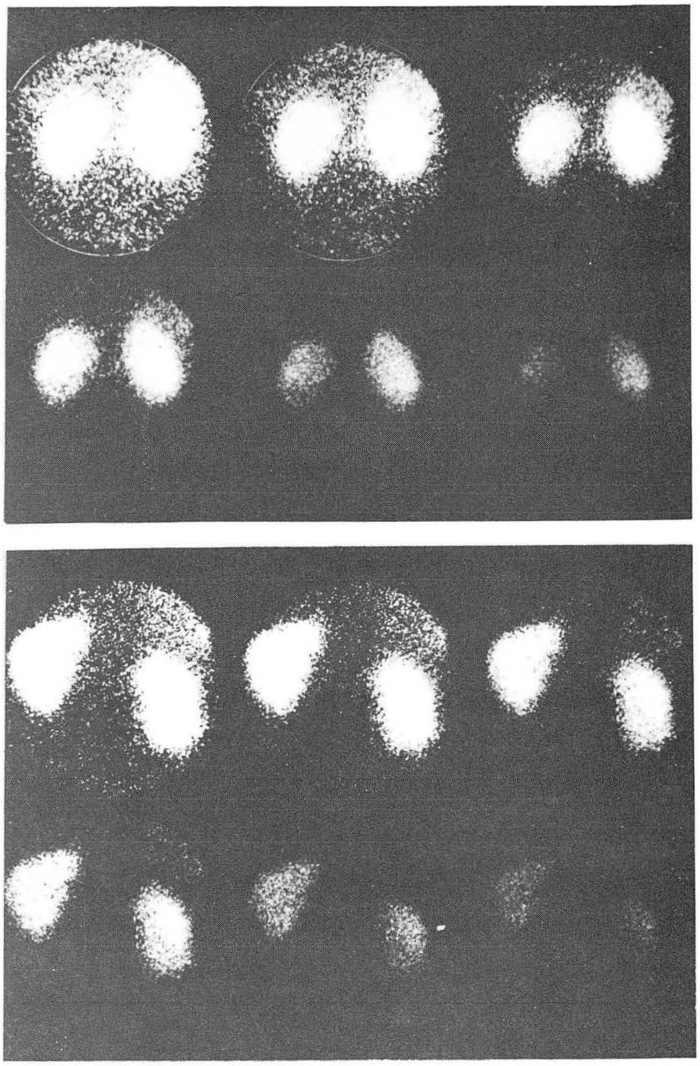

Figure 3. Pictures of human kidneys taken with the multichannel collimator. Exposure time was 5 min.

change of location. However, when a gamma ray is detected by any other counter, a correction signal shifts the position of the flash on the oscilloscope. The direction and amplitude of the correction signals are such that a point source located on a given plane is imaged at a single point on the oscilloscope, even though it is imaged at a different place on the image detector by each of the nineteen counters.

The plane at which best focus occurs can be set to any depth in the subject by the focal plane selector, an attenuator that varies the strength of the correction signals. Although the parts of the subject lying on the plane of best focus are clearest, phantom studies have shown that small sources 2-1/2 in. above or below the plane of best focus are still well defined (13) when the focal detector is at its usual location 24 in. away from the image detector

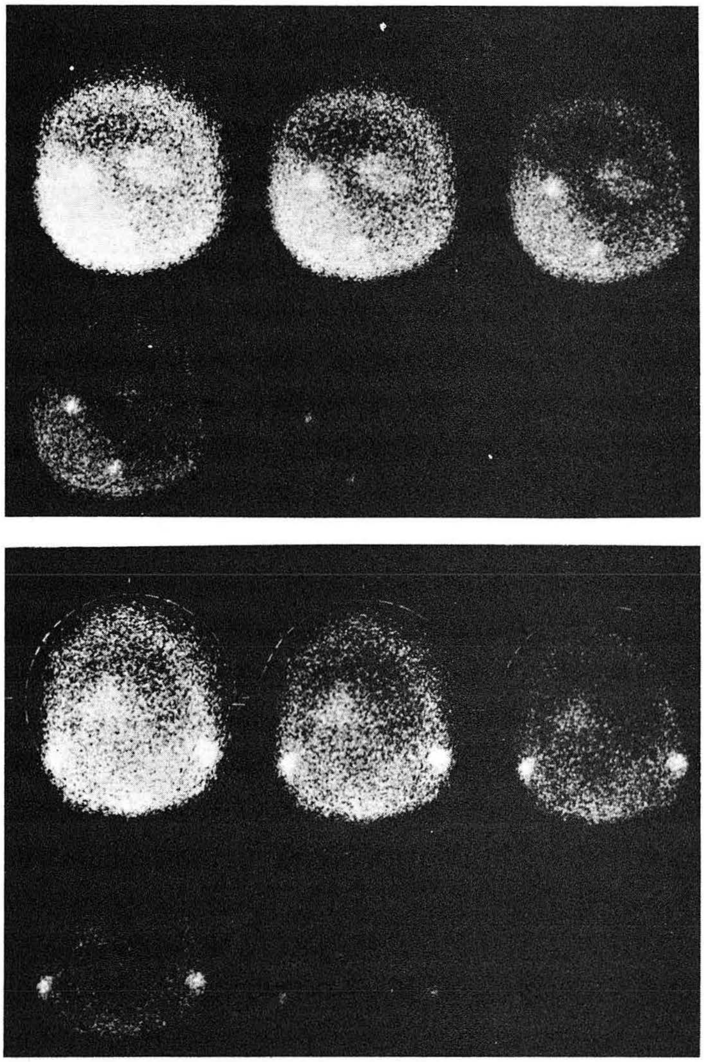

Figure 4. Brain-tumor pictures taken with the positron scintillation camera and Ga^{68} EDTA. Exposure time was 10 min.

crystal. With this collimation method, the scintillation camera is about 20 times as sensitive as a conventional focused-collimator scanner. At the same time better resolution at and near the plane of best focus is obtained. The application of the positron scintillation camera to brain-tumor localization with Ga^{68} EDTA has been described in a preliminary paper (14). Brain tumor pictures are obtained in 5 to 10 min with very low radiation dose to the patient. Figures 4a and 4b show 10-min lateral and frontal views of a brain tumor patient. A large tumor is visible in each view, together with two small marker sources taped to anatomic landmarks on the patient. The tracer compound has a half-life of 68 min and is obtained from a positron cow. The positron scintillation camera is also being used to map the location of functioning bone marrow in humans and small animals with 8-hr Fe^{52} (15). The positron camera will be more fully described in a later paper.

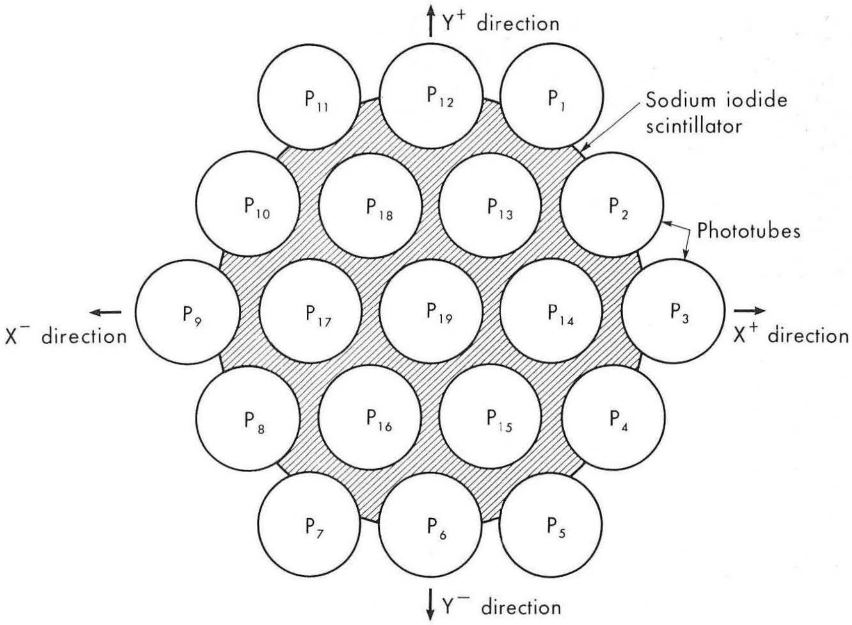

Figure 5. Plan view of phototubes and scintillator.
MU-31622

IMAGE DETECTOR AND COMPUTING CIRCUITS

The image detector consists of a solid sodium iodide crystal 11-1/2 in. in diameter by 1/2 in. thick, a bank of nineteen 3-inch-diameter RCA 8054 phototubes arranged in a hexagonal pattern (Fig. 5), and the capacitor network (Fig. 6 and Table 1). The phototubes are coupled to the crystal by a transparent optical light guide 1-1/2 in. long. Light that would normally fall on the spaces between phototubes is reflected by a beveled white surface acting as a light deflector. The dimensions of the light deflector and the phototube-to-crystal spacing are critical in obtaining optimum performance of the image detector.

The output signal from each phototube goes directly to the capacitor network where pulses from the 19 phototubes are converted to four output signals, which carry all the necessary pulse-height and position information. The four output signals are called the X^+, X^-, Y^+ and Y^- signals. The X^+ signal is obtained by adding signals P_1, P_2, etc. from the phototubes in the following way:

$$\begin{aligned} X^+ = {} & 0.03\ P_1 + 0.035\ P_2 + 0.04\ P_3 + 0.35\ P_4 + 0.03\ P_5 \\ & + 0.02\ P_6 + 0.01\ P_7 + 0.005\ P_8 + 0.005\ P_{10} + 0.01\ P_{11} \\ & + 0.02\ P_{12} + 0.025\ P_{13} + 0.03\ P_{14} + 0.025\ P_{15} + 0.015\ P_{16} \\ & + 0.01\ P_{17} + 0.015\ P_{18} + 0.02\ P_{19}. \end{aligned} \tag*{1)}$$

The magnitude of signal taken from each phototube to form the X^+ signal is proportional to the position in the plus X direction of that phototube in the array. Similarly, the X^-, Y^+, and Y^- signals are obtained by adding signals proportional to the locations of the phototubes in the other three directions.

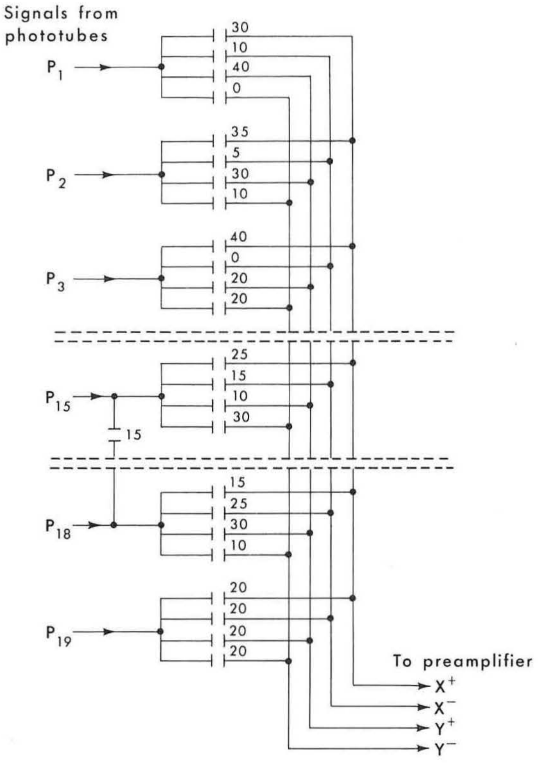

CAPACITANCES GIVEN IN PICOFARADS

Figure 6. Diagram of portion of capacitor network.
MU-32494

In all cases the capacitance between a given phototube and an output signal lead is directly proportional to the signal to be transferred. A portion of the capacitor network is illustrated in Fig. 6, and the values of all the capacitors in the network are given in Table 1.

When the capacitor network consists only of the elements described in equation 1), the picture has a small amount of "barrel" distortion in which the center elements are slightly too far apart. This effect is due to the finite number of phototubes in the array and reflection of light from the edge of the crystal. The addition of the three compensating capacitors shown at the right of Table 1 largely eliminates this distortion. With the compensating capacitors, the position accuracy is such that scintillations occurring within a 9- to 10-inch-diameter area are, for all practical purposes, linearly shown on the cathode ray tube. Outside this area, at the extreme edge of the picture, the flashes are still compressed together. However, the 9- to 10-inch-diameter linear area obtained is still adequate for nearly all the usual diagnostic purposes.

The X and Y position signals, which direct the beam of the cathode ray oscilloscope to the position of the original scintillation, are obtained from the X^+, X^-, Y^+ and Y^- signals by taking the ratio

Table 1. Capacitor network values (given in picofarads)

Phototube	+X	-X	+Y	-Y	P_{16}	P_{17}	P_{18}
P_1	30	10	40	0			
P_2	35	5	30	10			
P_3	40	0	20	20			
P_4	35	5	10	30			
P_5	30	10	0	40			
P_6	20	20	0	40			
P_7	10	30	0	40			
P_8	5	35	10	30			
P_9	0	40	20	20			
P_{10}	5	35	30	10			
P_{11}	10	30	40	0			
P_{12}	20	20	40	0			
P_{13}	25	15	30	10	15		
P_{14}	30	10	20	20		15	
P_{15}	25	15	10	30			15
P_{16}	15	25	10	30			
P_{17}	10	30	20	20			
P_{18}	15	25	30	10			
P_{19}	20	20	20	20			

2A) $$X = \frac{X^+ - X^-}{Z} \qquad Y = \frac{Y^+ - Y^-}{Z}$$

where Z is defined in equation 3).

An alternative method of obtaining the X and Y signals is by simple subtraction,

2B) $$X = X^+ - X^- \quad \text{and} \quad Y = Y^+ - Y^-$$

The latter equations are valid only if scintillations of approximately equal brightness are shown on the cathode ray tube. This condition is fairly well met by the use of the pulse-height selector. Fortunately, the pulse-height resolution of the scintillation camera is excellent because of the solid sodium iodide crystal and high light-collection efficiency. Therefore a relatively narrow window accepts nearly all the photopeak. Even so, an improvement in resolution is now obtained near the edges of the picture by taking a ratio in accordance with Equation 2A). The difference signal of Equation 2B) was used in earlier scintillation cameras.

The Z signal, which is proportional only to the brightness of the scintillation without regard to where the scintillation occurs in the image-detector crystal, is obtained by adding the same four signals,

3) $$Z = X^+ + X^- + Y^+ + Y^- .$$

The Z signal is sent to the input of the pulse-height selector, and the output of the pulse-height selector is sent to the grid of the cathode ray tube in the oscilloscope. Normally, the grid potential of the cathode ray tube is such that the beam is cut off. When a photopeak scintillation occurs, the X and Y signals position the beam, and then the signal from the pulse-height selector turns the beam on momentarily, reproducing the scintillation on the cathode ray tube screen.

In the initial adjustment of the scintillation camera, the gain of the phototubes must be equalized, so that scintillations of equal brightness at any point in the scintillator give Z pulses of equal amplitude. To accomplish this, a collimated gamma-ray source is aimed at the scintillator area directly below each phototube in turn, and the gain of each tube is adjusted so that the photopeak is centered within the pulse-height-selector window. The adjustments are made by observing a monitor oscilloscope display of the Z signal at the input to the pulse-height selector. The photopeak forms a bright narrow line on the Z display, as shown in Fig. 7a, when a strong beam of monoenergetic gamma rays is aimed at the scintillator. The pulses that pass through the window are blanked out, forming a prominent dark band through the photopeak line as shown in Fig. 7b (16).

For alignment purposes, the pulse-height-selector window is made very narrow, and the phototubes are adjusted as described so that the photopeak line is centered on the window. The sequence is repeated several times because the adjustments are interdependent. After this, the phototube voltages are kept constant. No readjustment of the phototubes is normally needed over long periods of time. The scintillation camera is tuned to isotopes of different gamma-ray energy by means of an attenuator located in the X^+, X^-, Y^+, and Y^- leads, as shown in Fig. 1. The attenuator is called the "gamma ray energy selector" and covers the range from 0.10 to 0.67 MeV.

When pictures are being taken, the pulse-height-selector window is widened to accept most of the photopeak as shown in Fig. 7b. It is important

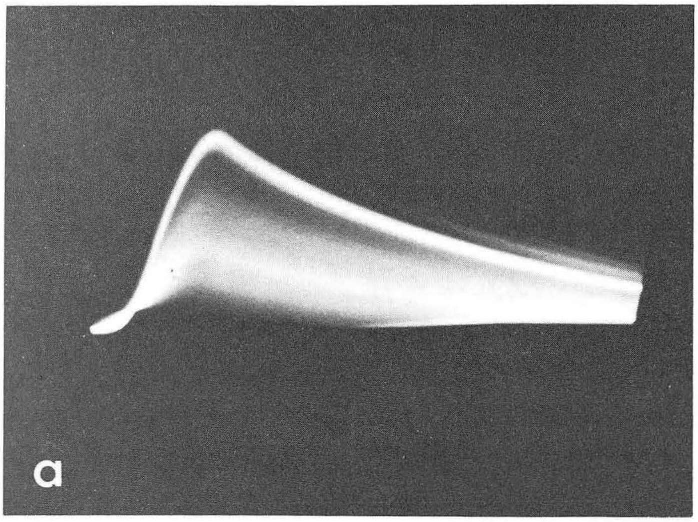

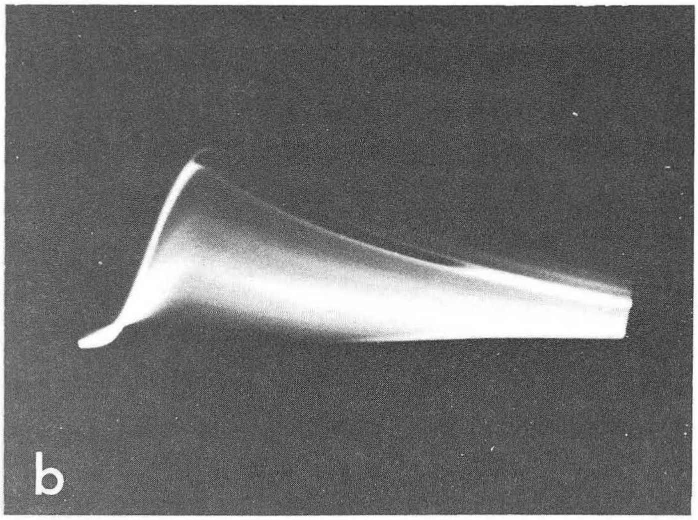

Figure 7a. Monitor oscilloscope display of Z pulses at input to pulse-height selector.
Figure 7b. Same display with pulses that pass pulse-height selector blanked out.

for the window to coincide accurately with the photopeak of the isotope being used, because under these conditions maximum sensitivity and maximum rejection of scattered gamma rays are obtained (17). This is especially important for thick subjects. The Z-pulse display of Fig. 7 provides an accurate and rapid method of making this adjustment.

RESOLUTION AND SENSITIVITY OF IMAGE DETECTOR

The following important advantages result from the use of a solid sodium iodide crystal of moderate thickness, rather than a thick crystal or mosaic: (a) position resolution is such that picture elements 3/16 to 1/4 in. wide can be resolved, (b) excellent pulse-height resolution is obtained, (c) the images have no mosaic pattern superimposed, and (d) collimators that pass gamma rays at oblique angles can be used with minimum loss of position resolution.

A 1/2-inch-thick scintillator offers better position resolution than a thicker scintillator partly because multiple scattering of gamma rays in the scintillator is minimized. Some gamma rays produce a Compton event, after which the secondary gamma ray travels a distance in the scintillator and produces a photoelectric event. The addition of these simultaneous scintillations results in a single Z pulse that is equal in magnitude to primary photoelectric scintillations and is therefore accepted by the pulse height selector. A single flash is placed on the cathode ray tube at the center of intensity of the two events. If the secondary gamma ray travels only a short distance before absorption, no appreciable resolution loss results, but if the distance is large, the misplacement of the flash is appreciable. For practical purposes, the resolution lost by gamma-ray scattering in sodium iodide is quite small, except for thick crystals at high gamma-ray energies. Thinner crystals allow more of the secondary gamma rays to escape. The event is then rejected by the pulse-height selector and is not shown on the cathode ray oscilloscope. Multiple scattering is discussed in detail elsewhere (18).

Another important advantage of a solid crystal is the excellent pulse-height resolution obtained. This is apparent from the Z-pulse display in Fig. 7 and from numerical measurements of the pulse-height spectrum. With the present image detector, the half width of the photopeak at half maximum is 8.7% for Cs^{137} and 13.8% for Hg^{203} when the entire scintillator is irradiated with gamma rays. The high resolution is due to the close optical coupling between the crystal and phototube bank and the resulting high light-collection efficiency. Good pulse-height resolution has the important advantage that a narrow pulse-height-selector window can be used, providing maximum rejection of gamma rays scattered by the subject and the collimator and maximum reduction of background from cosmic rays and stray radioactivity. Crystal mosaics do not usually give good pulse-height resolution because the light-collection efficiency is lower and the light output varies from one mosaic element to another.

Another major advantage of solid scintillators is the absence of a mosaic pattern superimposed on the image. This is important because the pattern of a mosaic scintillator distorts the fine detail of the images unless the elements are very small. This was shown in an experimental image detector employing a crystal 1/4 in. thick and cut into a mosaic of 1/8-inch-square elements. The fine detail of the images was distorted even by these small elements. Solid scintillators also permit the use of a variety of multichannel collimators with different hole spacings. It is not necessary to match the collimator grid to the crystal mosaic to avoid Moire effects.

Finally, scintillators of moderate thickness have the further advantage that they permit the use, with minimum resolution loss, of collimators in which gamma rays travel at oblique angles. The triple-aperture pinhole collimator

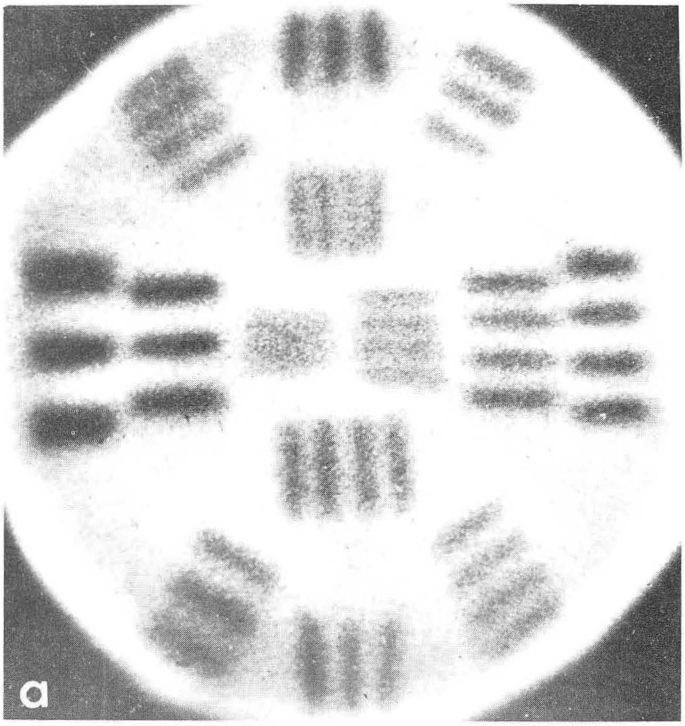

Figure 8a. Image-detector resolution pictures taken with tungsten bar pattern and radioactive point source.

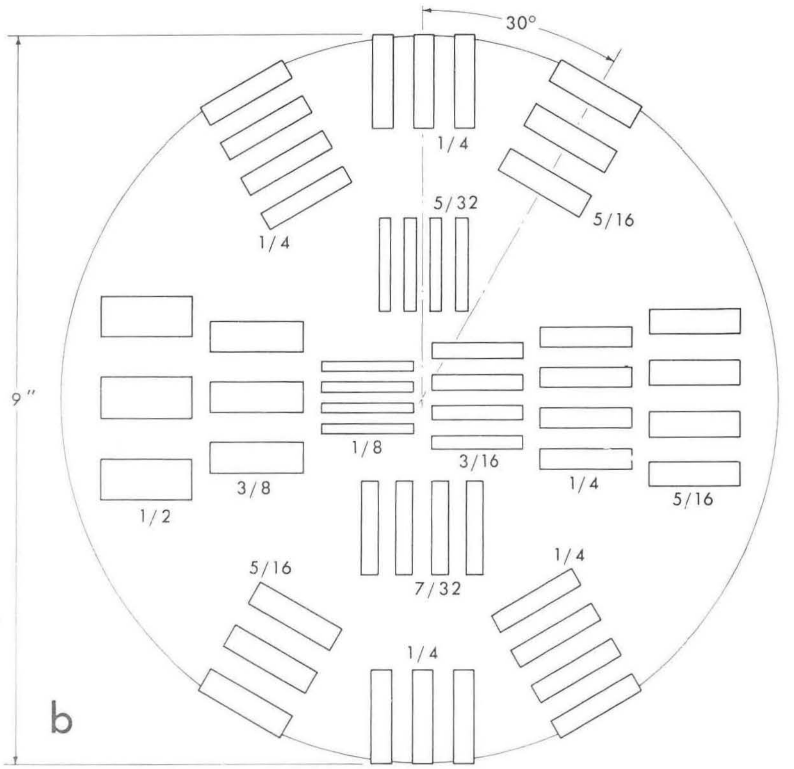

Figure 8b. Diagram of tungsten bar pattern.
MU-32599

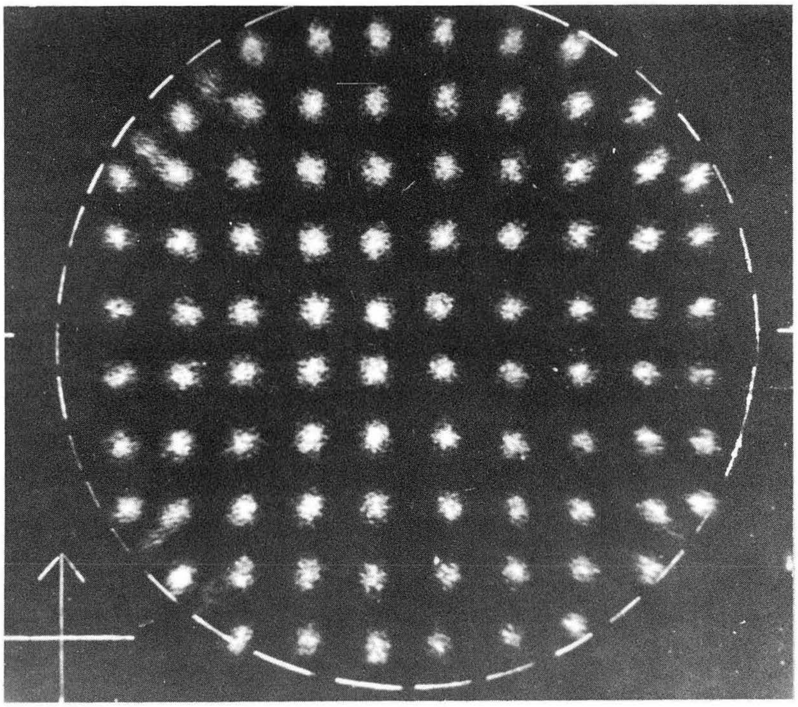

Figure 9. Test pattern showing position linearity and useful area of image detector.

and the multichannel collimator are two examples. When the latter collimator is used with thick scintillators, resolution is lost from spreading of the gamma-ray image after the gamma rays go through the collimator. This is a purely geometric effect that is quantitated in a report on multichannel collimator design (19).

A test picture illustrating the position resolution obtained from the present image detector is shown in Fig. 8a. An array of tungsten bars that effectively absorbed 80% or more of the gamma rays was placed close to the image detector. The size and spacing of the bars is shown in Fig. 8b. The image detector was irradiated with 0.36 MeV gamma rays from a point source located a few feet away.

Near the center of the picture, the 3/16-in. bars can be barely resolved and the 7/32-in. bars are clearly resolved. The 1/4-in. bars are also resolved in the more difficult area at the edge of the picture. Since the useful area of the image detector is 9 to 10 in. in diameter, 1/4-in. resolution corresponds to 1,000 picture elements. This is much better than the resolution offered by mosaics consisting of a few hundred crystals.

Tests show that the 1/4-in. tungsten bars can still be resolved at 0.16 MeV in the central area. Because of statistical variations in light photon collection and electron multiplication in the phototubes, the resolution of the

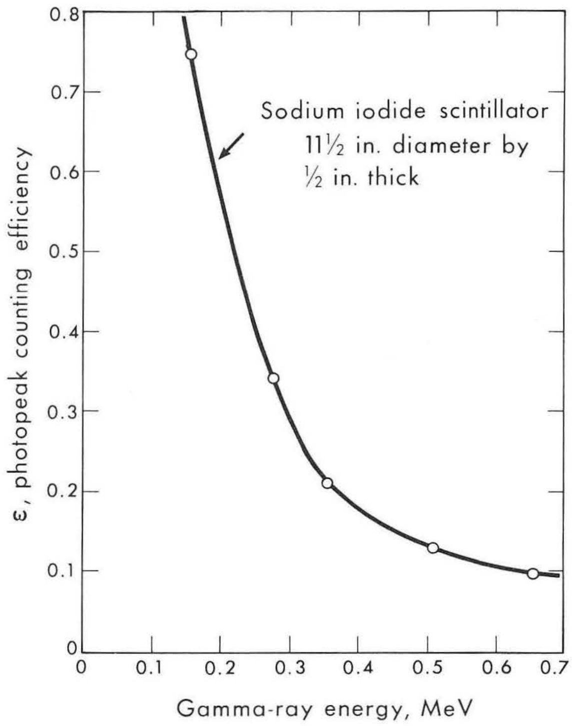

Figure 10. Photopeak detection efficiency of 1/2-inch-thick sodium iodide crystal in scintillation camera.

MU-31625

image detector is best for the higher energy gamma rays. From theoretical considerations, the resolution-distance should vary as the inverse square root of the gamma-ray energy.

A test pattern illustrating the position linearity of the image detector is shown in Fig. 9. This pattern was produced by an array of highly collimated gamma-ray beams aimed at the scintillator. The center-to-center spacing of the beams was 1 in. The resulting picture shows the linearity achieved and also that the diameter of the linear area exceeds 9 in.

The measured photopeak counting efficiency ϵ of the 1/2-inch-thick sodium iodide crystal is given as a function of gamma-ray energy in Fig. 10 where ϵ is defined as the fraction of gamma rays of a given energy incident on the scintillator that produce a dot on the picture. Points on the curve were obtained by counting calibrated sources of Ce^{139}, Hg^{203}, I^{131}, Ge^{68} and Cs^{137} at a known distance from the scintillator. The pulse-height selector was set to its usual width so that it accepted nearly all the photopeak. The counting efficiency varies from 75% at 0.16 MeV to 10% at 0.66 MeV. When used with the efficient collimators described earlier, these efficiencies are high enough to give excellent overall sensitivity to the scintillation camera.

The important characteristics in any instrument that images the distribution of radioisotopes are high overall sensitivity, good position resolution, low background counting rate, maximum rejection of scattered gamma rays, and an adequately large field of view. The scintillation camera, by using a solid scintillator of moderate thickness and the collimators described, gives a good combination of these factors.

ACKNOWLEDGEMENTS

The clinical examples were obtained with the collaboration of Dr. Alexander Gottschalk. Mr. Philip Yost and Mr. Yukio Yano provided technical assistance.

This work was done under the auspices of the U. S. Atomic Energy Commission.

REFERENCES

1. Anger, H. O.; Rev. Sci. Instr. 29:27, 1958.
2. Anger, H. O.; in Medical Radioisotope Scanning, Vienna International Atomic Energy Agency, 1959, p. 59.
3. Anger, H. O.; Radiation Image Device, U.S. Patent 3,001,057, 1961.
4. Mallard, J. R., and Myers, M. J.; Phys. Med. Biol. 8:165, 1963.
5. Anger, H. O.; Nucleonics 21, No. 10:56, 1963.
6. Copeland, D. E., and Benjamin, E. W.; Nucleonics 5:44, 1949.
7. Anger, H. O.; Nature 170:200, 1952.
8. Johansson, S. A. E., and Skanse, B.; Acta Radiol. 39:317, 1953.
9. Kellershohn, C., and Pellerin, P.; Nucleonics 13, No. 12:34, 1955.
10. Bender, M. A., and Blau, M.; J. Nuclear Med. 1:195, 1960.
11. Bender, M. A., and Blau, M.; Nucleonics 21, No. 10:52, 1963.
12. Mallard, J. R., and Myers, M. J.; Phys. Med. Biol. 8:183, 1963.
13. Gottschalk, A., and Anger, H. O.; Semiannual Report, Donner Laboratory, Lawrence Radiation Laboratory, UCRL-11033, 1963.
14. Anger, H. O., and Gottschalk, A.; J. Nuclear Med. 4:326, 1963.
15. Van Dyke, D.; Anger, H., and Pollycove, M.; this report, p.6.
16. Harris, C. C.; Eason, H. O.; Francis, J. E. Jr., and Bell, P R.; J. Nuclear Med. 1:280, 1960.
17. Allen, H. C., and Risser, J. R.; Nucleonics 13:28, 1955.
18. Anger, H. O., and Davis, D. H.; this report, p.86.
19. Anger, H. O.: Scintillation Camera with Multichannel Collimators, in preparation.

Received December, 1963.

Gamma-Ray-Detection Efficiency and Image Resolution in Sodium Iodide

Hal O. Anger and Donald H. Davis

Several reports have been published on the gamma-ray-detection efficiency of sodium iodide (1-3). In this report, calculated photoelectric, Compton, and photopeak efficiencies are given at several gamma-ray energies for large flat NaI crystals of various thicknesses. Additional quantities are given which are of interest when NaI scintillators are used to produce images of the distribution of gamma rays The additional information concerns the degradation in position resolution caused by scattering of gamma rays in the scintillator.

In the scintillation camera (4-8), gamma-ray images are thrown on a scintillator by pinhole collimators, multichannel collimators and positron coincidence techniques. A bank of multiplier phototubes and a computing circuit determine the center of luminous intensity of each scintillation or each group of simultaneous scintillations. Then a single flash is shown on a cathode-ray tube at a location corresponding to the center of intensity of the light produced. A pulse-height selector tuned to the photopeak allows only photopeak events to be shown on the cathode-ray tube. This reduces the background count from stray radioactivity and gamma rays that have been scattered in the subject.

The overall resolution of the scintillation camera is limited by (a) the geometry involved in the formation of the gamma-ray image by the collimator, (b) the translation of that image into light by the scintillator and (c) the subsequent reproduction and recording of the image. In this paper, the loss of resolution due to scattering in the scintillator will be considered in detail.

TYPES OF GAMMA-RAY INTERACTIONS

When a gamma ray impinges on a scintillator, any of the following interactions can occur.

PHOTOELECTRIC INTERACTIONS. In this kind of event, the gamma ray disappears, and a photoelectron absorbs all the energy of the gamma ray. Light is emitted along the path of the electron, but the path length of the electron is very short. For instance, the range of a 0.36 MeV photoelectron is 0.25 mm in sodium iodide (9). In calculations in this paper all the light is assumed to come from the point where the interaction occurred. At the lower gamma-ray energies, photoelectric interactions are the main contributors to the photopeak of the pulse-height spectrum.

ONE OR MORE COMPTON INTERACTIONS FOLLOWED BY ESCAPE OF A SECONDARY GAMMA RAY FROM THE CRYSTAL. In this kind of event, part of the energy of the original gamma ray is transferred to a Compton electron, and the remaining energy is carried away by a secondary gamma ray. If the secondary gamma ray escapes the scintillator, the event does not contribute to the photopeak of the pulse-height spectrum. The effect of these events on image resolution was not considered in these calculations because it was assumed they would be rejected by pulse-height selection.

ONE OR MORE COMPTON INTERACTIONS WITHIN THE CRYSTAL FOLLOWED BY PHOTOELECTRIC INTERACTION OF A SECONDARY PHOTON. These events contribute to the photopeak, since all the energy of the original gamma-ray is absorbed in the scintillator. The scintillation from the first Compton electron is correctly positioned on the path of the original gamma ray, but the other scintillations are located a distance away. The computing circuit of the scintillation camera places a single flash on the oscilloscope at a point corresponding to the center of intensity of the simultaneous scintillations. These multiple Compton-photoelectric events are the main contributor to the photopeak at the higher gamma-ray energies.

The probability of this kind of event as a function of the perpendicular distance from the primary event to the center of intensity was calculated. It will be seen in the results to follow that the misplacement of the center of intensity is appreciable only for high-energy gamma rays and very thick scintillators.

DISCUSSION

The amount of resolution loss due to scattering in the scintillator is shown graphically in Fig. 1. A limited number of gamma-ray energies and crystal thicknesses are shown in these curves.

The curves show the relative numbers of events occurring in various intervals of $\tilde{r}$, where $\tilde{r}$ is the perpendicular distance from the primary gamma ray to the center of intensity of the light produced. Primary photoelectric events are included and are shown as the shaded ordinate to the left of $\tilde{r} = 0$. The curves are all normalized to equal photopeak-detection efficiency (equal area under the curve), since their purpose is to show only the position resolution obtained.

The curves in Fig. 1 show that for a crystal half an inch thick the center of intensity of practically all events is confined within a circle of

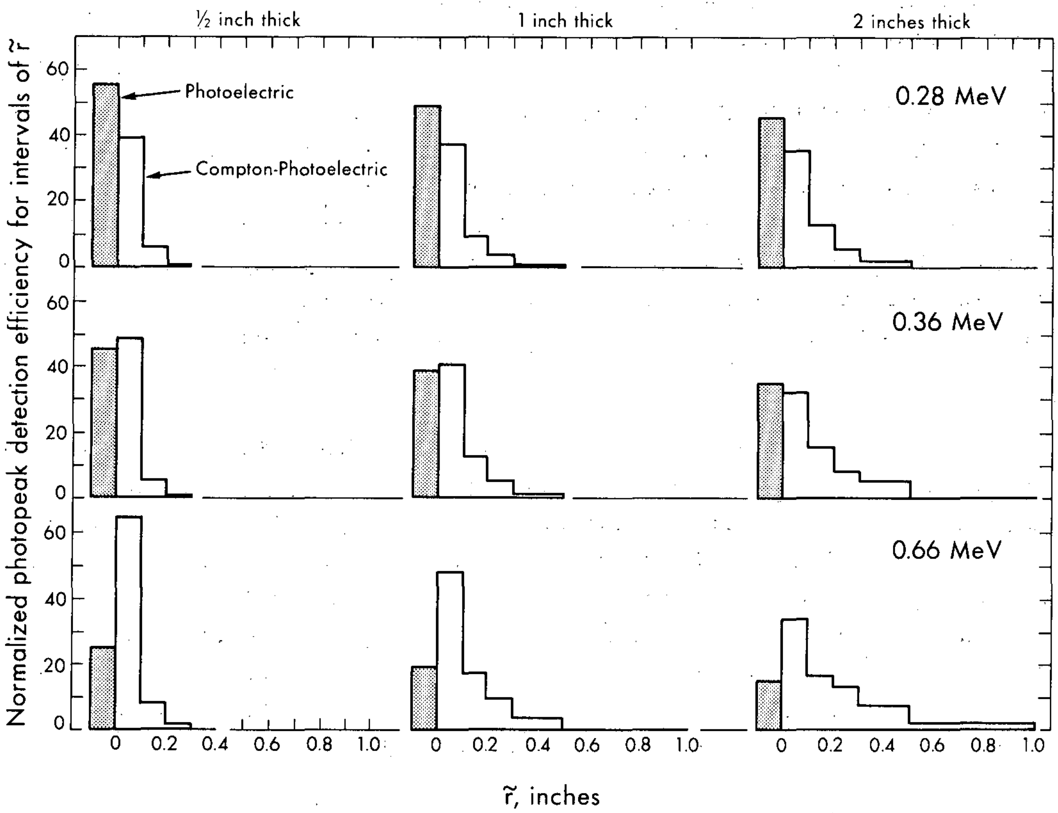

Figure 1. Loss of position resolution due to multiple gamma-ray photopeak interactions in 1/2, 1, and 2-inch thick sodium iodide at 0.28, 0.36, and 0.66 MeV.

MUB-2189

0.1 in radius for gamma rays up to 0.66 MeV. For a crystal two inches thick some degradation occurs at 0.28 MeV and considerable loss at 0.66 MeV. Calculations showed that for a 2-in. crystal at 0.66 MeV, the center of intensity of 52% of the photopeak events is outside a radius of 0.1 in. and that 10% are outside a radius of 0.5 in. In general, the scattering in crystals of moderate thickness is less than the amount quoted by others (7,10). Curves of gross detection efficiency and photopeak-detection efficiency are shown in Figs. 2 and 3.

The photopeak-detection efficiency of a NaI crystal eleven and a half inches in diameter and 0.46 in. thick has been measured by counting calibrated gamma-ray sources at known geometry. The sources were Ce^{139} (0.166 MeV), Hg^{203} (0.28 MeV), I^{131} (0.36 MeV), Ge^{68} (0.51 MeV), and Cs^{137} (0.66 MeV). The pulse-height-selector window was set so that nearly all the photopeak was accepted. Measured efficiencies were 75%, 34%, 22%, 13%, and 10% respectively. The measured value is some 80% to 95% of the calculated value. The discrepancy is probably caused by a) loss of photopeak pulses that were outside the pulse-height

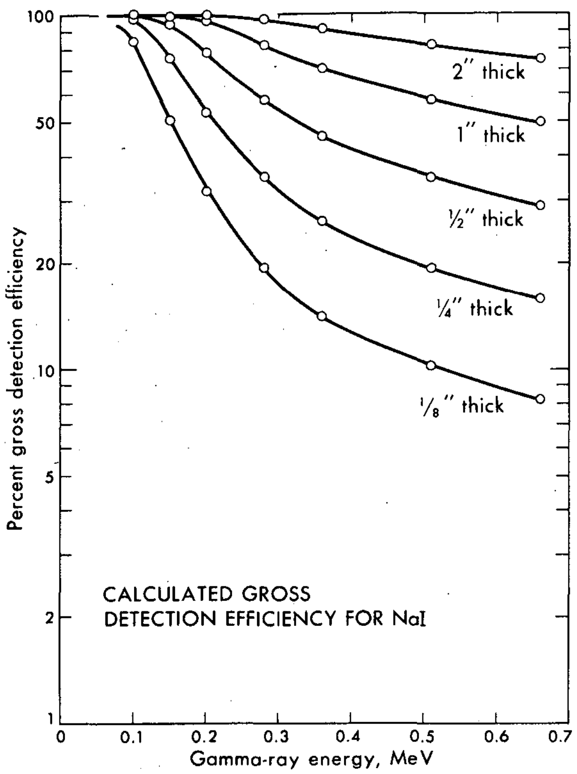

Figure 2. Calculated probability of gamma-ray interactions of any kind in sodium iodide 1/8 to 2 in. thick.

MU-32922

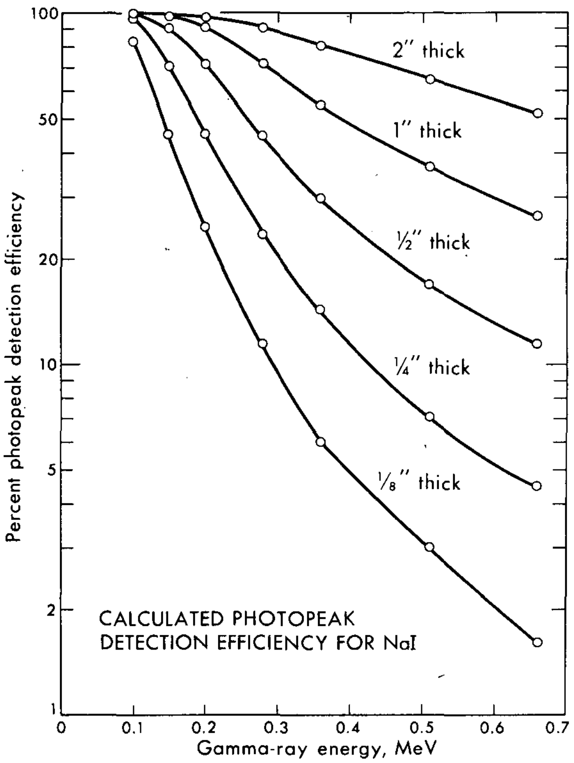

Figure 3. Calculated probability of photopeak interactions in large sodium iodide crystals 1/8 to 2 in. thick.

MU-32921

selector window, b) loss of recoil electrons from the surface of the scintillator, and c) the simplifying assumptions made in the calculations.

If a thick mosaic crystal is used without shielding between the elements, the efficiency and scattering data obtained here still apply. If a thick mosaic crystal is used with gamma-ray shielding between small elements, the data indicate that quite a large number of Compton-photoelectric events will be changed to ordinary Compton events as far as light output is concerned.

SUMMARY

Photoelectric, Compton, and photopeak efficiencies are calculated at several gamma-ray energies for large flat sodium iodide crystals in which the thickness ranges from one-eighth to two inches. In addition, the loss of position resolution by gamma-ray scattering within the scintillator is calculated because of its importance in the design of gamma-ray imaging devices such as the scintillation camera. An examination of the data shows the advantage of using low-energy gamma rays for imaging whenever possible. These gamma rays

are efficiently detected by solid sodium iodide scintillators half an inch thick with little loss of position resolution from multiple scattering of gamma rays in the scintillator. In the higher energy range, a choice must be made between a thin scintillator with its relatively good position resolution and low detection efficiency, or a thick crystal with higher detection efficiency and less satisfactory resolution.

ACKNOWLEDGEMENTS

This work was carried out under the auspices of the U.S. Atomic Energy Commission.

REFERENCES AND NOTES

1. Berger, M. J., and Doggett, J.; Rev. Sci. Instr. 27:269, 1956.
2. Miller, W. F., Reynolds, J., and Snow, W. J.; Argonne National Laboratory Report ANL-5902, 1958.
3. Vegors, S. H., Marsden, L. L., and Heath, R. L.; Phillips Petroleum Co., Atomic Energy Division, IDO-16370, 1958.
4. Anger, H. O.; Rev. Sci. Instr. 29:27, 1958.
5. Anger, H. O.; in Medical Radioisotope Scanning, International Atomic Energy Agency, Vienna, 1959, p. 59.
6. Anger, H. O., and Gottschalk, A.; J. Nucl. Med. 4:326, 1963.
7. Mallard, J. R., and Myers, M. J.; Phys. Med. Biol. 8:165, 1963.
8. Anger, H. O., Nucleonics 21, No. 10:56, 1963.
9. Ramm, W. M.; in Radiation Dosimetry, edited by Gerald J. Hine and Gordon L. Brownell, New York, Academic Press, 1956, p. 278.
10. Bender, M. A., and Blau, M.; Nucleonics 21, No. 10:52, 1963.

An enlarged version of this paper will be published in a forthcoming issue of Review of Scientific Instruments.

Received December, 1963.

Interrelationships Between Serum Lipids, Serum Lipoproteins and Lipoprotein Composition

Frank T. Lindgren, Norman K. Freeman and Robert D. Wills

For many years, blood lipids have been studied by a wide variety of techniques. An important goal of these analytical efforts has been the evaluation of the relative importance of these lipids and lipoproteins in relation to arteriosclerosis. From the purely chemical viewpoint, the measurement of the total serum concentration of esterified and unesterified cholesterol has until recently generally been regarded as the most important chemical measurement for evaluating coronary risk and potential efficacy of therapy. However, with the development of improved analytical methods for glycerides (1,2), the importance of this lipid class is becoming widely recognized as an independent aspect of the problem of arteriosclerosis. Furthermore, since nearly all the blood lipids exist in the form of lipoproteins, which vary greatly in physical size and chemical composition, it is essential to consider the interrelationships between any or all of these entities. The lipoproteins that appear to be significantly related to coronary arteriosclerosis are the low-density lipoproteins comprising the entire S_f 0-400 lipoprotein spectra (3). From the point of view of analysis by ultracentrifugation (4) or refractometry (5), these lipoproteins may be appropriately grouped into the glyceride-rich S_f 20-400 and the cholesterol-rich S_f 0-20 lipoproteins.

In this study, an attempt was made to find significant relationships between serum lipid and lipoprotein measurements in a population of normal males. In addition, the chemical composition of each of the major lipoprotein classes has been reexamined, and the data have been correlated with the total serum-lipid and lipoprotein determinations.

METHODS

Non-fasting blood sera were obtained in the morning from a group of normal males, 35 to 49 years old and working at the Livermore site of Lawrence Radiation Laboratory. Low-density lipoproteins were isolated ultracentrifugally and quantitated by precision refractometry (5). This method measures the S_f 0-10^5 lipoproteins ($0.92 < \sigma\text{'s} < 1.006$ g/ml*) and the total low-density S_f 0-10^5 lipoproteins ($0.92 < \sigma\text{'s} < 1.063$ g/ml). Thus, the S_f 0-20 lipoproteins are

---

*All densities are given at 20°C.

Table 1. Serum lipid and low-density lipoprotein values 32 normal males, 35 to 49 yrs (values in mg/100 ml)

Measurement	Mean	Standard deviation	Standard error
S_f 0-10^5	590	158	29
S_f 20-10^5	173	124	23
S_f 0-20	417	91	17
Total lipid	796	158	29
Triglycerides	172	97	18
Total cholesterol	251	45	8
Phospholipids	267	39	7
A.I.$_{\Delta n}$	75	26	5

obtained by difference between these two lipoprotein groups. Lipoproteins for detailed chemical analysis were fractionated by three consecutive stages of preparative ultracentrifugation (6), in which the initial salt-solution densities (before ultracentrifugation) were 1.006 g/ml, 1.070 g/ml, and 1.218 g/ml. In the latter two cases, NaBr was used to provide the density increment.

Sera and lipoprotein fractions were extracted with chloroform-methanol using a procedure patterned after that of Sperry and Brand (7), and the total lipids were measured gravimetrically. Infrared spectrometry of the total lipid extract (8) yielded values for total phospholipids, total cholesterol, total esterified fatty acids, and total lipids. After removal of phospholipids by adsorption on silicic acid, glycerides and cholesteryl esters were measured simultaneously (9) in the remaining lipid mixture. Infrared measurements were made using a Perkin-Elmer 421 grating-type instrument, which provided the high resolution and accurate wave-length settings necessary for the simultaneous glyceride and cholesteryl ester analysis.

RESULTS AND DISCUSSION

Table 1 presents a summary of the lipid and lipoprotein data evaluated from 32 normal non-fasting male sera. The mean values and their standard deviation suggest that this population is not in any way unusual and that it, therefore, represents a fairly typical male group of 35 to 49 years, selected from the American population. For example, this group exhibits a mean serum cholesterol of 251 mg/100 ml and a mean serum glyceride of 172 mg/100 ml.

In order to evaluate the interrelationships between each of these lipid and lipoprotein measurements, Pearson product-moment correlation coefficients

Table 2. Correlation coefficients for
low-density lipoproteins and serum lipids
32 normal males, 35 to 49 yrs

	S_f 0-10^5	S_f 20-10^5	S_f 0-20	Total lipids	Triglycerides	Total cholesterol	Phospholipids
S_f 20-10^5	0.82						
S_f 0-20	0.63	0.07*					
Total lipid	0.96	0.80	0.58				
Triglycerides	0.82	0.99	0.08*	0.82			
Total cholesterol	0.73	0.30*	0.86	0.77	0.32*		
Phospholipids	0.82	0.54	0.68	0.90	0.57	0.90	
A.I.$_{\Delta n}$	0.97	0.94	0.41	0.94	0.94	0.57	0.73

*Not significant. Significant at 5% level, remainder significant below 1% level.

were calculated and are shown in Table 2. Several of these relationships are worthy of comment. First, an unusually high correlation (r = 0.99) exists between the levels of the S_f 20-10^5 lipoproteins and the total serum glyceride. Although the S_f 20-10^5 lipoproteins are composed of about 55% glycerides by weight, they account for (on the average) about 60% of the total serum glycerides. Second, in contrast to this, a correlation coefficient of only 0.86 is obtained between total serum cholesterol and the S_f 0-20 lipoproteins. These lipoproteins are approximately 50% by weight cholesterol and are responsible for the transport of approximately 60% of the total serum cholesterol. It should be noted that of all the serum-lipid measurements, total serum lipid (10) is best correlated with the total low-density lipoproteins and the Atherogenic Index (3). Another relationship observed for this group of normal males is a rather high correlation (r = 0.90) between serum cholesterol and serum phospholipid.

Several lipoprotein and lipid values are conspicuous by their relative independence one from another. For instance, the absence of a relationship between the glyceride-rich S_f 20-10^5 and the cholesterol-rich S_f 0-20 lipoproteins is striking. As one might expect from the chemical composition of these classes, no significant relationship was observed between serum glyceride and serum cholesterol.

Fig. 1 illustrates the very high degree of correlation observed between the S_f 20-10^5 lipoproteins and serum glycerides. In view of this unexpectedly pronounced relationship, it was thought pertinent to explore further the possible

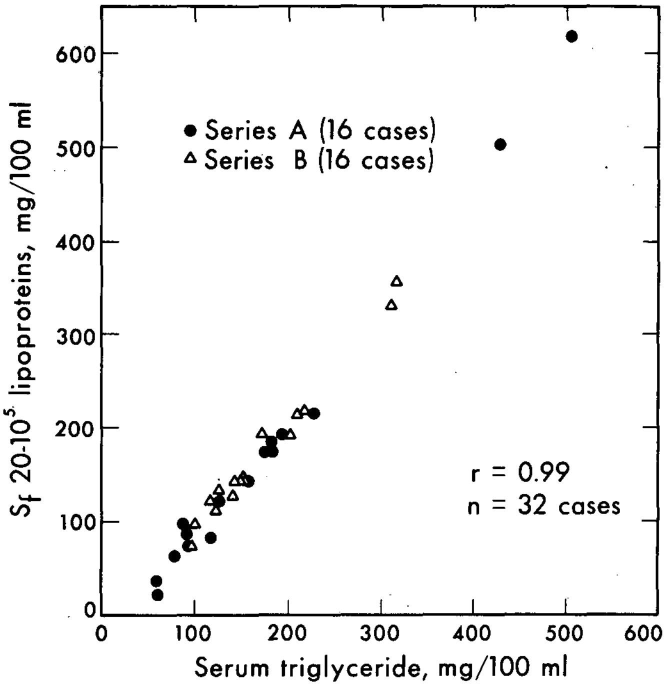

Figure 1. Relationship between serum concentration of the S_f 20-10^5 lipoproteins and serum glyceride.

MU-31426

reasons for this virtual identity of measurement between these two serum-lipid and lipoprotein variables. Therefore, of the original thirty-two serum samples, the second series of sixteen (taken consecutively) was separated into the S_f 20-10^5, S_f 0-20, and HDL_{2+3} lipoprotein fractions. Separate statistical analysis of series A and B revealed essentially the same degree of correlation between the S_f 20-10^5 lipoproteins and serum glyceride ($r = 0.99$). For subpopulations A and B, the mean and standard deviation of serum glyceride were 171 ± 64 mg/100 ml and 173 ± 122 mg/100 ml, respectively.

The percentage composition of glycerides and cholesteryl esters of the total lipid extracted from each lipoprotein fraction was determined. Table 3 presents the results of these composition studies. Of particular interest is the possible relationship between the level of S_f 20-10^5 lipoproteins (or serum glyceride) and the glyceride content of the three major lipoprotein fractions. No definitive correlation was observed between the level of S_f 20-10^5 lipoproteins and the weight percentage of glyceride contained in this lipoprotein class. On the other hand, a correlation coefficient of $r = 0.70$ (significant at the 5% level) was observed between the level of S_f 20-10^5 lipoproteins and the glyceride content of the S_f 0-20 lipoproteins. However, a rather striking relationship ($r = 0.90$) was observed between the S_f 20-10^5 lipoproteins and the glyceride content of the high-density lipoproteins (significant at the 1% level). Figs. 2 and 3 illustrate these relationships for S_f 0-20 and HDL_{2+3} lipoproteins, respectively. Although the number of samples was limited, there is a suggestion that the glyceride composition of the HDL_{2+3} lipoproteins

Figure 2. Relationship between glyceride composition of the S_f 0-20 lipoproteins and serum concentration of S_f 20-10^5 lipoproteins.

MU-31428A

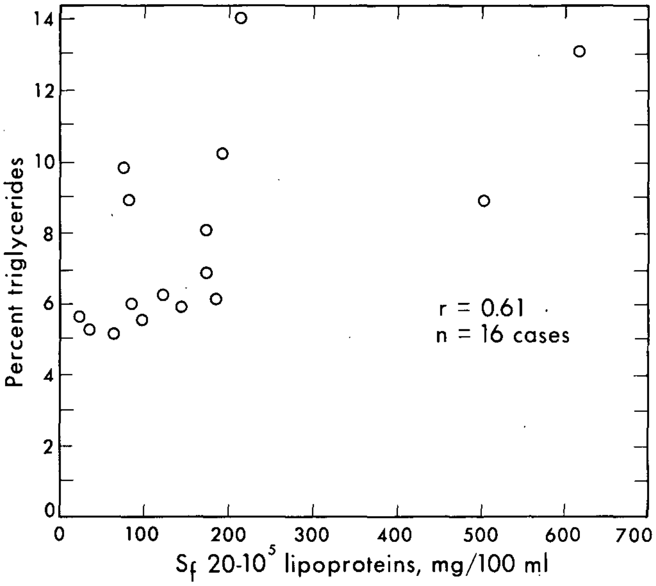

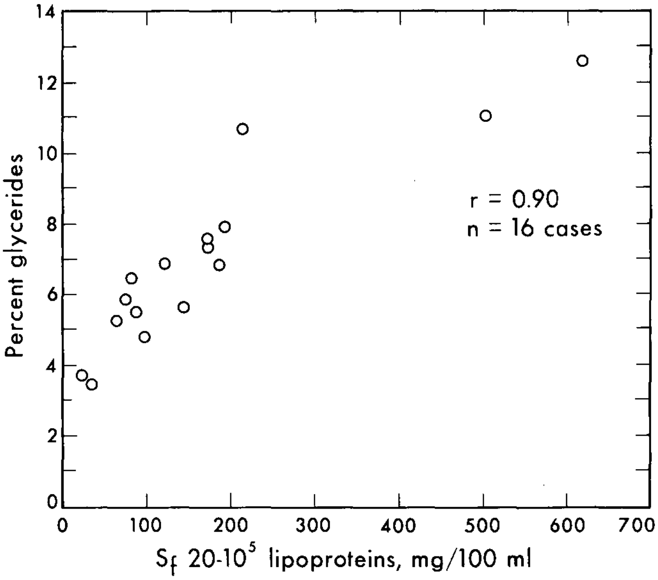

Figure 3. Relationship between glyceride composition of HDL_{2+3} lipoproteins and S_f 20-10^5 lipoprotein concentration.

MU-31427A

Table 3. Comparison of serum lipid and lipoprotein values with lipoprotein composition

	Serum concentration mg/100 ml			Lipoprotein composition (% of total lipid)					
				S_f 20-10^5		S_f 0-20		HDL_{2+3}	
Sample	S_f 20-10^5	TG	CE	TG	CE	TG	CE	TG	CE
1	191	193	315	50.0	20.6	10.2	56.0	7.9	45.8
2	185	184	390	60.0	18.8	6.1	58.4	6.8	45.0
3	23	60	321	*	*	5.6	55.4	3.7	46.9
4	173	177	249	62.0	20.4	8.0	58.2	7.7	44.4
5	618	505	346	65.0	21.2	13.1	55.0	12.6	40.3
6	81	117	313	53.0	22.3	8.9	51.7	6.5	43.9
7	502	427	416	60.5	22.4	8.9	57.5	11.0	41.0
8	64	79	303	51.7	26.2	5.2	58.0	5.3	47.4
9	98	87	268	50.4	26.4	5.5	56.8	4.8	44.3
10	75	97	249	52.9	22.8	9.8	54.0	5.9	44.0
11	144	157	457	54.7	25.1	5.9	55.4	5.6	45.6
12	173	181	360	60.2	24.8	6.8	55.3	7.3	45.0
13	121	129	426	52.3	30.7	6.2	54.6	6.8	46.6
14	35	60	304	64.8	31.2	5.3	56.5	3.5	48.7
15	87	91	265	56.8	28.3	6.0	55.4	5.5	45.4
16	214	228	312	56.4	27.8	14.0	51.1	10.7	41.2
Mean values (±S.D.)	174±157	173±122	331±62	57.4±4.6	24.6±3.7	7.8±2.7	55.6±2.0	7.0±2.5	44.7±2.3

*Insufficient quantity (ca. 0.5 mg) for adequate analysis.

reach a saturation level. This would seem to occur when the serum concentration of S_f 20-10^5 lipoproteins is in excess of 500 mg/ml. Of course, all these observations have assumed that the procedure for fractionating these lipoproteins does not disturb the lipid composition of each lipoprotein class. However, it is possible that in the high concentrations of salt used, some redistribution of components of the lipid moiety may occur among those lipoproteins present.

What are the implications of these relationships? Although these composition studies were restricted to 16 non-fasting males, the results, nonetheless, suggest (at least in the normal male 35 to 49 years old) that the high-density lipoproteins may be much more actively involved in the transport of glyceride than previously was thought to be the case. Earlier evidence for this was obtained from the acute oil ingestion studies of Nichols _et al_. (11) that indicated the potentially important, early incorporation of fed glyceride into the glyceride moiety of the high-density lipoproteins. In addition, recent high-density lipoprotein experiments of Ashworth and Green (12) suggest a wide range of binding capabilities for these lipoproteins, including a high capacity for binding glycerides. Further, in a more controlled _in-vitro_ environment, quantitative uptake and binding of glycerides by high-density lipoproteins from

S_f 20-10^5 lipoproteins and artificial glyceride-containing emulsions have been observed by Nichols (13). The exact nature of this glyceride binding by high-density lipoproteins is not entirely resolved, although the affinity for lipids of the de-lipidized high-density lipoprotein has been observed by Scanu and Hughes (14).

SUMMARY

The interrelationships between the low-density lipoproteins and the total serum level of the commonly measured lipids (total lipid, total cholesterol, phospholipid, and glycerides) were evaluated for 32 normal males (ages 35 to 49 years). A most striking relationship ($r = 0.99$) was observed between the level of the S_f 20-10^5 (very low-density lipoproteins) and total serum glyceride. Chemical-composition studies indicated that the level of the S_f 20-10^5 lipoproteins (or total serum glyceride) was positively correlated with the percentage composition of glyceride in two lipoprotein classes--the S_f 0-20 and the HDL_{2+3} lipoprotein class. The highest degree of correlation ($r = 0.90$) was observed for the high-density lipoproteins, suggesting their potential importance in the transport and metabolism of glycerides.

REFERENCES

1. Van Handel, E., and Zilversmit, D. B.; J. Lab. Clin. Med. 50:1952, 1957.
2. Carlson, L. A.; Acta Soc. Med. Upsaliensis 64:208, 1959.
3. Gofman, J. W.; Strisower, B.; deLalla, O.; Tamplin, A.; Jones, H., and Lindgren, F.; Modern Med. 11:119, 1953.
4. deLalla, O., and Gofman, J.; in Methods of Biochemical Analysis, Vol. 1, edited by D. Glick, New York, Interscience, 1954, p. 459.
5. Lindgren, F. T.; Nichols, A. V.; Wills, R. D.; Wing, L., and Gullberg, J. E.; Lawrence Radiation Laboratory Report UCRL-10794, 1963.
6. Freeman, N. K.; Lindgren, F. T., and Nichols, A. V.; in Progress in the Chemistry of Fats and Other Lipids, vol. 6, edited by R. T. Holman, W. O. Lundberg, and T. Malkin, London, Pergamon Press Inc., 1963, p. 215.
7. Sperry, W. M., and Brand, F. C.; J. Biol. Chem. 213:69, 1955.
8. Freeman, N. K.; Ann. N.Y. Acad. Sci. 69:131, 1957.
9. Freeman, N. K.; Semiannual Report, Donner Laboratory, Lawrence Radiation Laboratory, UCRL-10683, 1963.
10. Nichols, A. V.; Lindgren, F. T., and Gofman, J. W.; Geriatrics 12:130, 1957.
11. Nichols, A. V.; Rehnborg, C. S.; Lindgren, F. T., and Wills, R. D.; J. Lipid Res. 3:320, 1962.
12. Ashworth, L. A. E., and Green, C.; Biochim. Biophys. Acta 70:68, 1963.
13. Nichols, A. V.; this report, p. 113.
14. Scanu, A., and Hughes, W. L.; J. Biol. Chem. 235:2876, 1960.

Received August 1963.

An Improved Method for the Computer Analysis of Gas-Liquid Chromatograms

Alicia M. Ewing, Pamela P. Walker, Robert D. Wills and Frank T. Lindgren

With the increased application of gas-liquid chromatography as an analytical tool, the calculation, tabulation, and analysis of gas-liquid chromatograms can become a time-consuming data-processing task. A variety of techniques is available for the calculation of areas under each chromatographic peak, such as planimetry, triangulation (1), the product of peak height and retention time (2-4) and mechanical and electronic integration. Recently, a completely automatic procedure for computation of gas chromatographic data has been presented (5). This procedure, although elegant, requires conversion of detector voltage output to a frequency, storage of this information on a magnetic tape and, finally, presentation of this chromatographic information directly into a computer. Since such elaborate facilities are not generally available, a semiautomated analysis of gas chromatographic data has been developed, which requires a minimum of manual data transcription from the actual chromatogram. This method provides for absolute mass calibration, analysis of standard mixtures with correction of preexisting calibration factors, peak height correction for the contribution of interfering peaks in the same neighborhood (6) and subtraction from a sample chromatogram of contaminating components as obtained from an appropriate base line blank run.

METHODS

The procedure for the analysis of gas-liquid chromatograms, described in this paper, is an extension of a previously described method (3). Although our application is for the analysis of the methyl esters of long chain fatty acids, it is anticipated that this method would be applicable to the gas-liquid chromatographic analysis of hydrocarbons, steroids, amino acids, sugars, etc. The manual work consists of drawing an appropriate base line on the chromatogram and measuring peak height, retention time and recorder amplification (or attenuation) for each component on the chromatogram. The full use of this program assumes that for a set of chromatograms there is available an absolute calibration. This is achieved either by carefully controlling the injection volume (our method) or by utilizing an internal standard (7).

COMPUTER INPUT

Input to the program, which runs on the IBM 7094 computer, consists of punched cards that are transferred to magnetic tape by the IBM 1401 computer. However, any large capacity, high-speed computer with appropriate accessory equipment would be suitable to handle this program. An input deck for a typical chromatogram consists of a single header card, plus one card for each component. The header card, which is easily distinguished from other input cards by a negatively coded identification number, is used to specify the type of run and any special corrections or parameter changes desired. In addition to an identification number, the other cards contain retention time, peak height and recorder amplification for each component. The program requires that these cards are arranged in order of increasing magnitude of retention time, and that methyl stearate time is coded negative for easy identification.

COMPUTER OUTPUT

Output from the 7094 program is written on a magnetic tape that is subsequently printed on the 1401. In addition to identifying and descriptive information printed for each chromatogram, all input values and all calculated values are printed for each peak. For convenience, the output record for each chromatogram is headed by two statements, one describing the maximum extent of calculations currently possible and another describing the output data requested for the chromatogram. An example of the format for the computer output is illustrated in Fig. 1.

COMPUTER CALCULATIONS

Figure 2 shows a logical flow chart of program operation for all types of chromatographic input data. As an illustration, the following is the approximate sequence of calculations made by the computer for an input chromatogram where all corrections are desired:

1. All peak heights are normalized to a reference recorder amplification; in this case, to 10" full scale = 1.07×10^{-7} ampere detector current.
2. Retention times (relative to a standard such as methyl stearate, cholestane, etc.) are calculated for each component.
3. Peak heights are corrected for overlapping peaks.
4. First and second order relative masses are calculated and summed; percentages are calculated for each component. This series of calculations includes two correction functions.
5. The palmitate calibration factor is applied to the second-order relative mass for each component to give a first estimate of absolute mass for each component.
6. Absolute masses for all components identifiable with components in the preceding multicomponent calibration run are corrected by the associated calibration factor, giving a second absolute mass; a corrected absolute mass is summed and percentages calculated.

```
SET  4815, SAMPLE RUN                              16 DEC 1963

PROGRAM PERMITS CALCULATION OF ALL INPUT OPTIONS
INPUT SPECIFIES ALIQUOT RATIO =  10.0,    PEAK RESOLUTION DESIRED,    BASELINE CORRECTION DESIRED

 TIME    P.H.      AMPL   MASS 2    REL T   M2 PCT  AM2 PCT  AM3 PCT  ABS M 1  ABS M 2  ABS M 3

 3.43    0.05     10.00     0.02    0.233     0.11     0.12     0.13     0.01   0.       0.

 4.65    0.06     10.00     0.03    0.316     0.17     0.26     0.26     0.01   0.02     0.

 6.30    0.04     10.00     0.03    0.429     0.15     0.17     0.09     0.01   0.       0.01

 8.25    1.55     10.00     1.46    0.561     7.79     8.73     8.86     0.63   0.63     0.62

 9.80    0.08     10.00     0.09    0.667     0.47     0.52     0.54     0.04   0.       0.

11.15    0.39    100.00     0.05    0.759     0.26     0.29     0.21     0.02   0.       0.01

12.86    0.25    100.00     0.04    0.875     0.19     0.21     0.22     0.02   0.       0.

14.70    3.63    100.00     0.59    1.000     3.13     3.51     3.17     0.25   0.25     0.22

16.92    2.82     10.00     5.07    1.151    26.97    28.01    28.62     2.18   2.02     2.00

21.37    4.56     10.00    10.58    1.454    56.25    53.31    54.79     4.54   3.84     3.82

25.55    0.36    100.00     0.12    1.738     0.62     0.69     0.42     0.05   0.       0.03

28.57    0.71    100.00     0.26    1.944     1.36     1.53     1.22     0.11   0.       0.09

34.20    0.15    100.00     0.06    2.327     0.33     0.37     0.38     0.03   0.       0.

44.00    0.20    100.00     0.10    2.993     0.55     0.61     0.63     0.04   0.       0.

49.75    0.30    100.00     0.17    3.384     0.93     0.83     0.28     0.07   0.06     0.02

58.24    0.20    100.00     0.14    3.962     0.72     0.81     0.17     0.06   0.       0.01

                           18.80                                         8.07   7.19     6.98
```

Figure 1. Printed output for a sample run with all corrections performed. The three left columns repeat the input data for ease of cross reference. Absolute mass values of "0." indicate that no correction was performed at this level.

7. Absolute masses of all components identifiable with contaminating components on a preceding residue base line run are corrected by subtraction, taking into account sample dilution and injection volumes. A corrected third absolute mass is summed and percentages calculated for each component.

Steps 3, 5, 6, and 7 are optional. The entry of the appropriate calibration runs will initiate Steps 5 and 6, but these calculations may subsequently be skipped if the input deck contains an appropriate request card. Step 7 is utilized only if the program has a currently stored residue base line and the input requests this correction. Step 3 is entirely controlled by input request. At any point during the operation, the program will accept a new calibration run or a new residue base line, store it appropriately and use it as the basis for subsequent corrections.

Because both the multicomponent calibration and the residue correction involve the comparison of two chromatograms in which absolute retention time

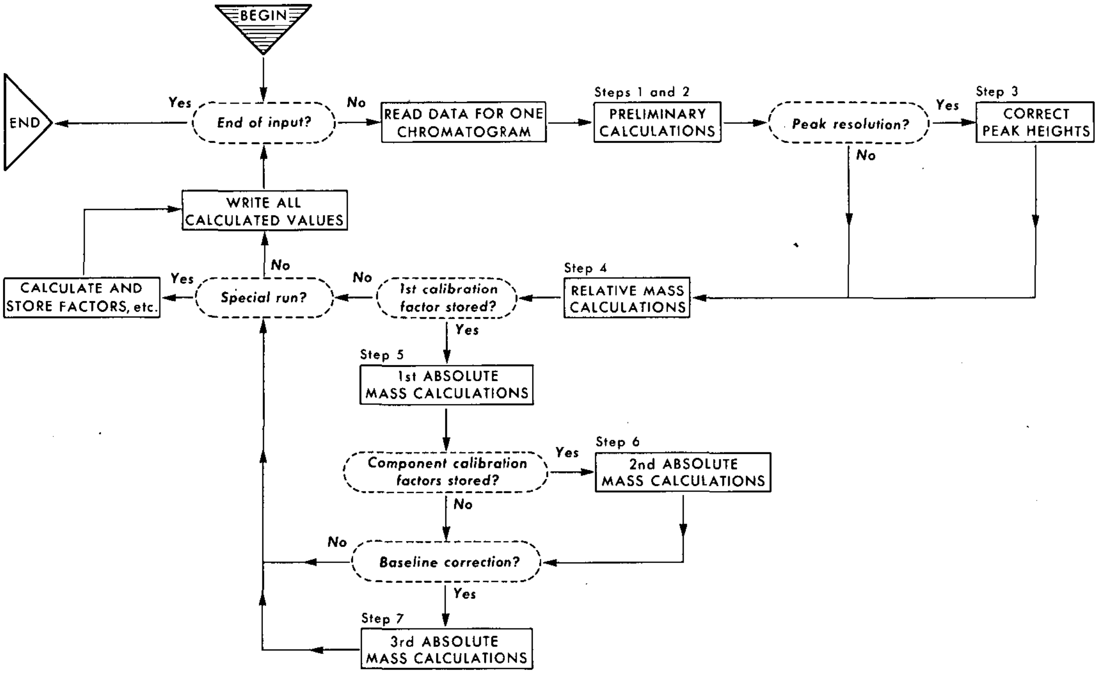

Figure 2. Logical flow chart of program operation for all chromatographic types. Dotted ovals denote decision making processes; rectangles represent nonbranching calculations.

MUB-2188

may vary considerably for a given component, comparisons are based on the essentially constant relative retention time (i.e. retention time divided by the reference component retention time). As our criterion for identifying a data input component (A) with a stored component (B), we have chosen:

$$(0.96 \times \text{Rel. time of B}) \leq \text{Rel. time of A} \leq (1.04 \times \text{Rel. time of B}).$$

If the input component fails to fall within this range, no correction is made.

The program reads the data for an entire chromatogram from the input tape into the computer and then performs the appropriate calculations. The entry of a palmitate calibration run, for example, besides initiating certain basic computations (normally Steps 1, 2, and 4) will cause the calculation and storage of the palmitate calibration factor (known absolute mass of palmitate divided by its calculated relative mass); in addition, palmitate relative time is stored for future program reference, and a switch is turned on to permit Step 5 calculations for subsequent chromatograms. (As used here, a switch is considered to be an internal routing device. It is set by the program to reflect a given situation or status and is subsequently used by the program to select automatically the correct sequence, or sequences, of calculations.) The procedure for a multicomponent calibration run is similar, but it produces a series of factors, each stored with its associated relative time. The factor for the jth component is calculated as:

$$F_j = \frac{(\text{known absolute mass percent})_j}{(\text{calculated mass percent})_j} \times \frac{1}{F_{\text{Palmitate}}} .$$

The residue base line is stored as an absolute mass--relative time pair for each component; in addition, the aliquot factor reciprocal (volume sample/volume injected) for this run is stored. If the base line correction is to be made, the appropriate aliquot factor reciprocal for such a sample is also required.

All calculations are performed in floating point arithmetic. Rounding occurs only at output time when calculations are complete for the current chromatogram.

COMPUTATION TIME

Complete calculations were performed for a set of 28 chromatograms, consisting of a total of 467 components, in 0.18 min. This represents a variety of run types and correction calculations. In general, execution time varies somewhat depending on the extent of the calculations desired. The loading time for this program is 0.28 min and is essentially constant.

DISCUSSION

The program in its present form includes checking routines to minimize errors and time loss caused by incorrectly coded or punched input decks. The discovery of such an error will cause a diagnostic message to be written on the output tape, calculations for this chromatogram will be deleted and the program will begin processing the next chromatogram.

Although Steps 5, 6, and 7 are optional calculations, they are not independent. For example, 1. the storage of a residue base line (as a series of absolute mass--relative time pairs) implies the previous entry of a palmitate calibration run, and 2. the proper calculation of the multicomponent calibration correction is similarly dependent, as it is applied to the first absolute mass calculation.

The problem of correct order of operations is handled by a set of program switches, each of which can be turned on only by the appropriately ordered entry of the associated run. For flexibility of operations, however, these switches may be turned off by the entry of appropriately coded input. Not only do the switches provide for the correct routing through the calculations, but they also prevent such erroneous calculations as would occur when an input chromatogram specified that a base line correction was desired when no residue base line had been stored.

Tables of the correction functions (3) based primarily on peak height and relative retention time are separately compiled into a machine language deck to permit easy additions and refinements. This facility is needed especially when using a chromatographic apparatus that has a nonlinear response, such as is the case with an argon beta-particle detector. Because the amount of bleed (8) and other chromatographic conditions also may effect the degree of this nonlinear response, it is essential to be able to compensate fully for this in the analysis of the gas-liquid chromatogram.

SUMMARY

An improved method for the computer analysis of gas-liquid chromatograms is presented. The analytical results are presented in terms of the relative mass, relative retention time, and percentage composition of each component of the chromatogram. In addition, the procedure provides for the optional calculation of absolute mass, correction of calibration factors, peak height correction for unresolved components and subtraction of contaminating components from each chromatogram.

ACKNOWLEDGEMENTS

This work was supported by Research Grants HE 01882-09 and HE 02029-08 from the National Heart Institute, Public Health Service, Bethesda, Maryland, and by the United States Atomic Energy Commission.

REFERENCES AND NOTES

1. James, A. T., and Wheatly, V. R.; Biochem. J. 63:269, 1956.
2. Pecsok, R. L.; Principles and Practice of Gas Chromatography, New York, John Wiley and Sons, Inc., 1959, p. 145.
3. Tandy, R. K.; Lindgren, F. T.; Martin, W. H., and Wills, R. D.; Anal. Chem. 33:665, 1961.
4. Carroll, K. K.; Nature 191:377, 1961.
5. Johnson, H. W.; Anal. Chem. 35:521, 1963.
6. Bartlet, J. C., and Smith, D. M.; Can. J. Chem 38:2057, 1960.
7. Napier, E. A.; Anal. Chem. 35:1294, 1963.
8. Lindgren, F. T.; Tandy, R. K.; Wills, R. D., and Nichols, A. V.; Circulation Res. 11:577, 1962.

Pamela P. Walker is a participant in the National Science Foundation Summer Fellowship Program.

Received December, 1963.

Infrared Micromethod for Serum Triglycerides and Cholesteryl Esters

Norman K. Freeman

In a method reported previously (1), triglycerides and cholesteryl esters of serum are analyzed simultaneously, using a high-resolution (grating) infrared spectrophotometer. A total lipid extract is first obtained from 1 ml of serum, and the phospholipids are separated from the mixture by adsorption on silicic acid. Infrared measurements are made on the nonadsorbed lipids in CCl_4 solution. From absorbances at the respective peak frequencies of their ester carbonyl groups, triglycerides and cholesteryl esters are calculated. This report describes two additional features of this analysis:

1. The applicability of a simplified extraction procedure;
2. feasibility of performing the analysis on 0.05 ml of serum.

The extraction procedure is essentially similar to that of Mendelsohn and Antonis (2). It combines in a single step the separate operations of extraction and adsorption. Van Handel and Zilversmit (3) have also given such a direct extraction method for serum glycerides, differing mainly in their choice of solvent and adsorbent. In the micromethod, the extraction procedure is scaled down for smaller quantities, and the infrared measurements are made in a microcell.

MATERIALS AND METHODS

The extraction solvent is isopropyl ether, reagent grade, further purified by allowing it to stand over activated alumina. (Mendelsohn and Antonis (2) recommend passage over an alumina column just prior to use.) Reagent grade CCl_4 is used without additional treatment for solutions to be measured by infrared. Silicic acid is 325 mesh, specially prepared for chromatography of lipids (obtained from Bio-Rad Laboratories, Richmond, California). Extractions are carried out in screw-cap vials of appropriate sizes, and the caps are fitted with Teflon liners to prevent contamination from the ordinary plastic liners. Infrared measurements have been made on a Perkin-Elmer Model 421 grating spectrophotometer.

DIRECT EXTRACTION OF NEUTRAL LIPIDS. Place a clean half-inch Teflon-covered magnetic stirring bar in a 40-ml vial. Add 3 g of silicic acid and 6.0 ml of isopropyl ether. While this mixture is stirring briskly on a magnetic stirring device, add 1.0 ml of serum dropwise from a pipette. Cap the vial and continue stirring for about five minutes, or until the slurry is smooth and uniform. Add 18.0 ml of isopropyl ether, cap the vial tightly, and shake on a mechanical shaker for 20 min. Centrifuge at 1,500 rpm for 10 min. Measure 16.0 ml of the clear supernatant into a clean dry vial and evaporate to dryness. Rinse down the walls of the vial with about 2 ml of isopropyl ether (or $CHCl_3$), and again evaporate to dryness.

EXTRACTION PROCEDURE FOR 0.05 ML OF SERUM. Place a clean three-eighth-inch Teflon-covered magnetic stirring bar in a 2-dram (8 ml) vial. Add 0.3 g of silicic acid and 1.0 ml of isopropyl ether. While this mixture is stirring briskly on a magnetic stirring device, add 0.05 ml of serum dropwise from a pipette. If the pipette is a micropipette of the type calibrated "to contain," rinse the pipette once with distilled water. Add the rinse water (0.05 ml) to the silicic acid slurry. Add 5.0 ml of isopropyl ether, cap the vial tightly, and continue the stirring for 20 min. Centrifuge the vial, measure 5.0 ml of the clear supernatant into a clean dry vial, and evaporate to dryness. Rinse the vial down with about 1 ml of solvent and reevaporate.

INFRARED MEASUREMENTS. The dried aliquot of extracted lipid is dissolved in an accurately measured volume of CCl_4 and the absorption cell of the spectrophotometer is filled with the solution. For the extract from 1 ml of serum, the volume of CCl_4 required is about 0.7 ml; but this may have to be adjusted if the measured absorbances are not within the range 0.2 to 0.6. The cell used in this case is nominally 1 mm in thickness, and a duplicate cell containing pure solvent is used in the reference beam of the spectrophotometer. Absorbance measurements are made at stationary frequency settings of 1745 and 1730 cm^{-1}. The slit width is 0.25 mm.

For the extract from 0.05 ml of serum, the volume of CCl_4 used is 0.20 ml. This is about the minimum amount required to fill the cell; but if dilution is necessary, the volume can be made larger. A Perkin-Elmer standard 3-mm microcell (NaCl windows) may be used; however, this work was done with a slightly modified version of it made in the laboratory shop. The instrument does not accommodate a duplicate microcell in the reference beam. Instead a cavity cell (Instrument Division, Barnes Engineering Co., Stamford, Conn.) of 3-mm thickness has been employed. The standard mounting for this cell is not perfectly rigid, so that some care must be exercised to be sure that it is positioned reproducibly. Alternatively, the measurements can be made without a reference cell if the reference beam is matched to the solvent-filled sample cell by a suitable attenuator.

Concentrations of triglycerides and cholesteryl esters are calculated from the absorbances measured at 1745 and 1730 cm^{-1} using the equations determined in calibration. Concentrations multiplied by the volume of CCl_4

give milligrams of each component in the aliquot. Dividing by the aliquot ratio (2/3 or 5/6) gives the weight of total component extracted, which can then be expressed as mg per 100 ml of serum by applying the appropriate volume ratio.

Blanks should be carried through the entire procedure and, if they are of significant magnitude as measured by infrared, corrections for them may be applied.

CALIBRATION. Calibration consists of determining the absorption coefficients (in the cell used) for both components at both frequencies. Absorbances were measured for CCl_4 solutions of pure triolein (Hormel Foundation) and pure cholesteryl oleate (Applied Science Labs), each at several concentrations. Average values of the absorption coefficients ($= \alpha = A/C =$ absorbance/concentration) over the expected range of concentration are used to calculate the equations which give concentrations explicitly. These equations are:

for the 1-mm cell

$$C_{TG} = 6.51\ A_{1745} - 1.37\ A_{1730}$$

$$C_{CE} = -4.02\ A_{1745} + 13.19\ A_{1730}$$

For the 3-mm cell

$$C_{TG} = 2.00\ A_{1745} - 0.38\ A_{1730}$$

$$C_{CE} = -1.16\ A_{1745} + 4.02\ A_{1730}$$

where C_{TG} = concentration of triglycerides

C_{CE} = concentration of cholesteryl esters

A = absorbance

These equations apply only to the particular sets of cells and instrumental operating conditions that have been used; other equations must be determined for any given set of cells and conditions.

RESULTS

In order to evaluate the direct extraction procedure at the 1-ml sample level, replicate analyses were carried out and the results compared with those obtained by the previously established method (1). A single randomly selected serum was analyzed in triplicate by both methods: first on the day of preparation, and subsequently, at five different times during the first two months thereafter. During this time, the serum was stored in a refrigerator at just above 0°C. Results of the analyses are given in Table 1. Blank corrections have not been applied since average values for blanks correspond to about 2% or less of either component in either method. For all determinations, the averages for each component agree within 3% between the two methods. Values obtained by the direct extraction procedure tend to be slightly lower, with somewhat more scatter.

Table 1. Comparison of direct extraction with total lipid extraction followed by adsorption of phospholipids. Values are serum concentrations in mg per 100 ml.

Date of analysis	Triglycerides Direct extraction	Triglycerides Extraction-adsorption	Cholesteryl esters Direct extraction	Cholesteryl esters Extraction-adsorption
10/17/63	163	164	353	353
	164	164	353	363
	165	171	353	356
10/22/63	160	168	350	359
	160	174	341	363
	157	178	347	341
10/30/63	167	167	365	366
	154	162	341	353
	154	166	344	350
11/6/63	188	172	389	348
	168	165	341	354
	171	171	351	353
11/13/63	171	160	341	362
	178	171	348	365
	156	177	371	375
11/26/63	163	170	333	345
	157	161	351	350
	140	162	323	363
Average	163	168	350	357
σ	±10	±5	±14	±8

The same serum sample was used to test the micromethod, and two sets of triplicate analyses are shown in Table 2. The values obtained by this procedure have been somewhat more erratic. If those given in Table 2 are compared with the averages in Table 1, it may be noted that triglycerides are generally 5-10% higher and cholesteryl esters are 5-10% lower. The same orders of differences have been found when lipids from the larger scale extraction were diluted by a factor of three and analyzed in the microcell. It would appear, therefore, that the extraction is probably not at fault, but that some factor related to the use of the microcell is responsible for the discrepancies. Some prepared mixtures have been analyzed and the results (Table 3) are 0 to 10% high in both components. This also suggests a sample handling or calibration problem.

DISCUSSION

The direct extraction procedure appears to yield results that are virtually as accurate but not quite as reproducible as those from the procedure consisting of extraction followed by an adsorption step. The larger standard deviations given in Table 1 can be attributed mainly to the presence of a few extreme values, although most of these are within an acceptably narrow range.

Table 2. Analyses of 0.05-ml aliquots of serum. Two triplicate runs on different days. (mg per 100 ml of serum)

Number	Triglycerides	Cholesteryl esters*
1A	171	340
1B	172	340
1C	202	382
2A	173	331
2B	178	333
2C	180	340

*A blank correction of 12 mg per 100 ml has been applied to the cholesteryl ester values.

Table 3. Analyses of prepared mixtures of triolein and cholesteryl oleate (values are in mg)

Mixture	Component	Amount	By analysis
No. 1	TO	0.086	0.094
	CO	0.203	0.213
No. 2	TO	0.086	0.092
	CO	0.324	0.340
No. 3	TO	0.171	0.171
	CO	0.203	0.230

The cause of the occasional random deviations is not clear, but it is expected that by careful attention to the details of manipulation it can be eliminated. The obvious virtue of this method is its extreme simplicity.

In scaling the method down by a factor of 20 in serum-sample size, the usual problems of small sample handling are encountered, e.g., contamination, small volume measurement, etc. Our preliminary data suggest that further work on these problems is needed to improve the reliability. A statistical evaluation is not possible from these limited data, but it appears that the method is capable of both accuracy and precision to within ± 10%.

SUMMARY

Further experience with an infrared spectrophotometric method for the determination of serum triglycerides and cholesteryl esters is reported. Two new aspects considered are the use of a single-step combined extraction and adsorption procedure, and the feasibility of analyzing 0.05-ml serum samples. The simplified extraction, in comparison with the two-step procedure, has been found to be substantially equivalent in accuracy and slightly poorer in precision. Analysis on the micro scale is a promising extension of the method, although preliminary results are not quite comparable with those from larger samples.

REFERENCES

1. Freeman, N. K.; Semiannual Report, Donner Laboratory, Lawrence Radiation Laboratory, UCRL-10683, 1962.
2. Mendelsohn, D., and Antonis, A.; J. Lipid Res. 2:45, 1961.
3. Van Handel, E., and Zilversmit, D.; J. Lab. Clin. Med. 50:152, 1957.

Received December 1963.

Osmium Tetroxide-Triglyceride Interaction as a Function of Degree of Unsaturation
An X-ray Fluorescence Study

Thomas L. Hayes and James N. Hawkins

Electron microscopy has depended to a large extent on the deposition of osmium compounds within tissue components in order to fix the tissue and enhance contrast. Several studies have been done on the chemical nature of this interaction (1-5), and the results of these experiments have materially aided in the interpretation of electron micrographs. In our continuing study of the reaction between osmium tetroxide and tissue components, we have investigated the interaction between lipoproteins and osmium tetroxide (1). We concluded from this study that the lipid moiety was responsible to a large extent for the interaction between lipoprotein and osmium tetroxide. The fatty acid double bond was thought to be a likely reaction site because osmium tetroxide will not stain saturated lipids but will react readily with unsaturated compounds. The present study is an attempt to measure the amount of osmium deposited in triglycerides containing various numbers of double bonds. Again, in this study, the method chosen for analysis of osmium was X-ray fluorescence as developed by Gofman (6).

MATERIALS AND METHODS

The triglycerides used in this study were triolein, trilinolein, and trilinolenin. These are glyceride esters of 18 carbon fatty acids containing one, two, and three double bonds in the 9, 9-12, and 9-12-15 positions, respectively.*

The triglyceride was dissolved in chloroform and dispersed in a filter-paper disk that could be used subsequently for osmium determination by X-ray fluorescence. The amount of lipid deposited in the paper was determined by calibrating the volume of chloroform taken up by the filter-paper disk in a standard dipping time and then using this value to determine the concentration of triglyceride necessary in the dipping solution to produce a sample containing 200 μg of triglyceride. The 1.132-inch diameter filter-paper disks were found to absorb 0.17 ml of chloroform solution in a 20-second dipping time. After dipping, the disks were dried at room temperature for 24 hr and then placed in a standard osmium tetroxide solution (1% osmium tetroxide, acetate

*Triolein, Cal. Bio. Chem., A Grade, assay 90%+. Trilinolein, Hormel Institute, University of Minnesota, assay 99%+. Trilinolenin, Hormel Institute, University of Minnesota, assay 99%+.

Table 1.

	µg triglyceride	µg Os	µg Os/µg triglyceride
Triolein	200	184	0.92
	200	182	0.91
Trilinolein	200	330	1.65
	200	251	1.26
Trilinolenin	200	512	2.56
	200	530	2.65

Veronal buffer, pH 7.4) for one-half hour. The disks were again dried sufficiently for the excess osmium tetroxide to evaporate and then placed in the Siemans X-ray fluorescence apparatus used. Analyses for osmium were made on the $L_{\beta 1}$ line (λ = 1.197 Å) with the following operating parameters: Tungsten tube, 50 kV, 38 mA, LiF monochromator, scintillation detector. Yields were 53 counts/min/µg of osmium. Standard counting error = 4 µg Os (6).

Control samples were prepared by the same procedure from chloroform solutions without triglycerides. Osmium standards were prepared from an aqueous osmium trichloride solution.

RESULTS

Table 1 shows the osmium content of the three triglycerides after reaction with osmium tetroxide for one-half hour. The results are given in terms of weight of triglyceride in the sample, the amount of osmium in the sample, and the ratio of µg osmium per µg triglyceride.

DISCUSSION

The amount of osmium found in triglycerides following the one-half hour reaction time used in this experiment was found to be approximately proportional to the number of double bonds in the molecule. An average of between one and two osmium atoms per double bond was found. These results, plus the fact that the saturated triglyceride tristearin does not react with osmium tetroxide, would support the hypothesis that the double bonds of fatty acids represent a major site of osmium tetroxide reaction.

SUMMARY

A quantitative determination of the amount of osmium found in triglycerides, following a one-half-hour reaction with 1% buffered osmium tetroxide, has shown that the amount of osmium is approximately proportional to the number of double bonds found in the molecule.

REFERENCES

1. Hayes, T. L.; Lindgren, F. T., and Gofman, J. W.; J. Cell Biol. 19:251, 1963.
2. Wigglesworth, V. B.; Proc. Roy. Soc. London Ser. B 147:185, 1957.
3. Bahr, G. F.; in Proceedings of the Stockholm Conference in Electron Microscopy, edited by F. S. Sjöstrand and J. Rhodin, New York, Academic Press Inc., 1956, p. 107.
4. Riemersma, J. C.; J. Histochem. Cytochem. 11:436, 1963.
5. Stoeckenius, W.; Proceedings European Regional Conference on Electron Microscopy, Delft, Nederlandse Vereniging Voor Electronenmicroscopie 2: 716, 1960.
6. Gofman, J. W.; in Advances in Biological and Medical Physics, New York, Academic Press Inc. 8:1, 1962.

Received December 1963.

Lipid Transfer Between Human High-Density and S_f 20-10^5 Lipoproteins

Alex V. Nichols and Lester Smith

In our earlier investigations (1) on the effects of oil ingestion in man, we observed substantial increases in glyceride content of both the very-low-density lipoproteins (S_f 20-10^5) and the high-density lipoproteins (HDL). The observation of glyceride increases in S_f 20-10^5 was in agreement with many reported studies, whereas the increases in HDL glyceride were unexpected. Such increases in HDL glyceride during fat ingestion suggested the possibility of a transfer *in vivo* of S_f 20-10^5 glyceride to HDL species. The existence of such a transfer mechanism would have important implications to any consideration either of glyceride metabolism or basic lipoprotein chemistry. In the present communication, we present our *in vitro* studies of the chemistry of the transfer of S_f 20-10^5 glyceride to HDL species in human serum.

METHODS

The following methods were used in this investigation.

LIPOPROTEIN FRACTIONATION. S_f 20-10^5 lipoproteins that served as sources of glyceride were obtained from freshly separated serum by preparative ultracentrifugation procedures previously reported (2). HDL lipoproteins from control and incubated serum mixtures were isolated also by ultracentrifugal methods (3). Analytic ultracentrifugation and analysis of data were performed according to procedures described by deLalla and Gofman (4). All salt solutions used in the ultracentrifugal procedures contained 10 mg/100 ml of the disodium salt of EDTA.

LIPID ANALYSIS. Lipids were extracted from lipoprotein solutions by a modification of the method of Sperry and Brand (5). Lipid components were fractionated by silicic acid chromatography (6) and quantified by infrared spectrophotometry (7). The infrared spectrophotometric determination of phospholipids used in this investigation included also any lysolecithin associated with the HDL.

RESULTS

IN VITRO TRANSFER OF S_f 20-10^5 GLYCERIDE TO HDL. Serum serving as the source of the HDL was obtained from a normal fasting female with a negligible

Table 1. HDL lipid composition following incubation of serum with varying amounts of S_f 20-10^5 lipoproteins

Incubation mixtures	Lipid composition of HDL (percent of total lipid weight)			
	Cholesterol esters*	Glycerides*	Unesterified cholesterol*	Phospholipids*
Controls				
5 ml serum + 1 ml 0.2 M NaCl Not incubated	42.2 ± 0.6**	3.1 ± 0.0	4.9 ± 0.0	49.7 ± 0.6
5 ml serum + 1 ml 0.2 M NaCl Incubated	47.8 ± 0.2	4.1 ± 0.0	2.7 ± 0.3	45.4 ± 0.1
Experiment (Donor B)				
5 ml serum + 1 ml S_f 20-10^5 stock (3B)***	38.4 ± 0.4	12.3 ± 0.0	3.0 ± 0.1	46.3 ± 0.2
5 ml serum + 1 ml S_f 20-10^5 stock (6B)	34.2 ± 0.0	16.4 ± 0.3	3.1 ± 0.3	46.3 ± 0.6
3 ml serum + 1 ml S_f 20-10^5 stock (6B)	30.7 ± 0.1	18.3 ± 0.1	3.9 ± 0.4	47.1 ± 0.4
Experiment (Donor A)				
5 ml serum + 1 ml S_f 20-10^5 stock (3A)	35.0 ± 0.6	16.6 ± 0.1	3.6 ± 0.0	44.8 ± 0.5
5 ml serum + 1 ml S_f 20-10^5 stock (6A)	30.2 ± 0.0	20.2 ± 0.5	3.9 ± 0.0	45.7 ± 0.4
3 ml serum + 1 ml S_f 20-10^5 stock (6A)	26.7 ± 0.2	24.2 ± 1.0	3.5 ± 0.0	45.6 ± 1.6

*Lipid values expressed as percent of total lipid weight.

**Standard error of the measurement: $\sigma_e = \sqrt{\frac{\Sigma d^2}{2K}}$. d = difference between duplicates; K = number of pairs of duplicates.

***Two stock solutions of S_f 20-10^5 lipoproteins were prepared from each of two donors (Donor A and B). Stock solution (6A) from Donor A was a solution of S_f 20-10^5 lipoproteins at a concentration sixfold that in the serum. Stock solution (3A) had a S_f 20-10^5 concentration threefold that present in the serum of Donor A. Analogous S_f 20-10^5 stock solutions (6B) and 3B) were prepared from Donor B's serum. Dilutions were made with 0.2 M NaCl. The concentrations of lipids present in the two stock solutions (6A) and (6B) were, respectively: cholesterol esters 7.9 and 4.6; glycerides: 24.9 and 13.4; cholesterol: 2.7 and 1.5; and phospholipids: 9.4 and 5.1 mg/ml.

---

serum level of S_f 20-10^5 glyceride (approximately 0.01 mg/ml). S_f 20-10^5 lipoproteins serving as the source of glyceride were obtained from two donors having elevated serum concentrations of these species.

Two sets of experiments were carried out using the S_f 20-10^5 lipoproteins from each of the donors. In the first experiment, duplicate 5-ml aliquots of serum were mixed with 1 ml of each of the S_f 20-10^5 stock solutions described in Table 1. The tubes were tightly sealed and placed into a shaker-water bath at 38°C for 16 hr. In the second experiment, duplicate 3-ml aliquots of serum were mixed with 1 ml of each of the specified S_f 20-10^5 stock solutions. These were sealed and incubated as above. Prior to preparative ultracentrifugation, 2 ml of 0.2 M NaCl were added to these samples to bring the solutions up to a 6-ml volume. HDL were isolated ultracentrifugally from these and from control solutions and then subjected to lipid extraction and analysis.

In Table 1 are presented the lipid-composition data on the isolated HDL from the various incubation mixtures. From these data, it is clear that with increasing concentrations of S_f 20-10^5 glyceride a most significant transfer of

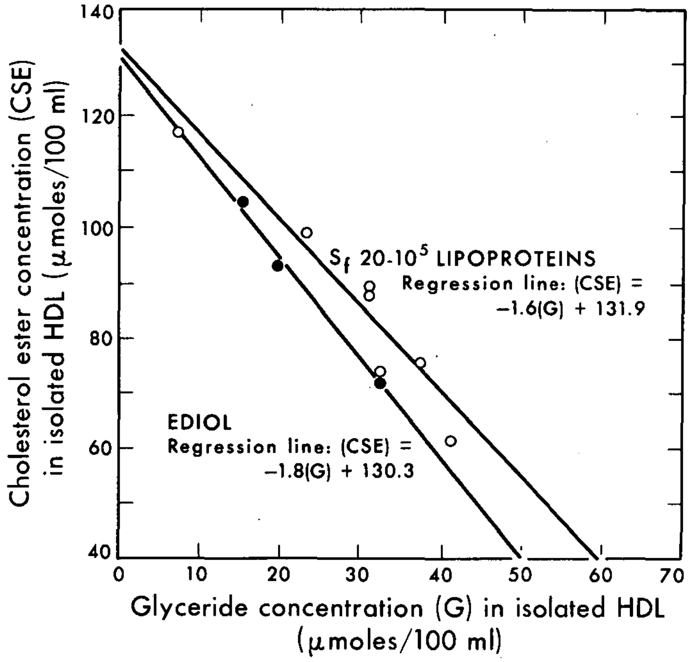

Figure 1. Relationship between glyceride content and cholesterol ester content in HDL isolated after incubation of serum with added S_f 20-10^5 lipoproteins or Ediol. For calculation of micromoles of cholesterol ester and glyceride in isolated HDL, molecular weights of 651 and 885, respectively, were used.

MU-33141

glyceride to the HDL occurs. For the incubation systems employed, the HDL-glyceride content ranged from 3.1% to 24.2% of the total lipid when the S_f 20-10^5 glyceride was increased from negligible amounts to 6 mg/ml in the incubation mixture.

The transfer of S_f 20-10^5 glyceride to HDL is associated with further significant changes in HDL-lipid composition. The content of cholesterol esters markedly decreases with increasing transfer of glyceride. This observation is all the more interesting because persistent observations (8,9) show substantial increases in lipoprotein-cholesterol-ester concentrations following *in vitro* incubation of sera relatively low in S_f 20-10^5 glyceride. In agreement with these observations, a comparison of the HDL-lipid composition from the test serum incubated alone versus the non-incubated serum alone shows an increase in cholesterol ester content in the incubated serum (Table 1). As observed by other workers, reciprocal decreases in unesterified cholesterol and phospholipids with the esterification of the cholesterol also occur. The relationship between the HDL-glyceride and cholesterol-ester content in the incubation systems containing S_f 20-10^5 lipoproteins is shown in Fig. 1. The slope of the regression line for these data indicates a decrease of approximately 1.6 moles of cholesterol ester for an increase of 1 mole of glyceride on the HDL.

IN VITRO TRANSFER OF GLYCERIDE FROM AN ARTIFICIAL EMULSION TO HDL. In order to evaluate the influence of another form of glyceride substrate, we

Figure 2. Percent glyceride in HDL lipid as a function of amount of added glyceride per ml of serum in incubation medium.

MU-33140

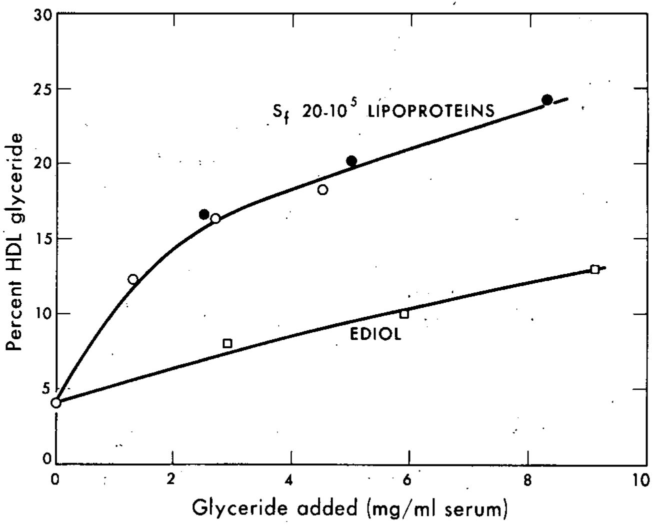

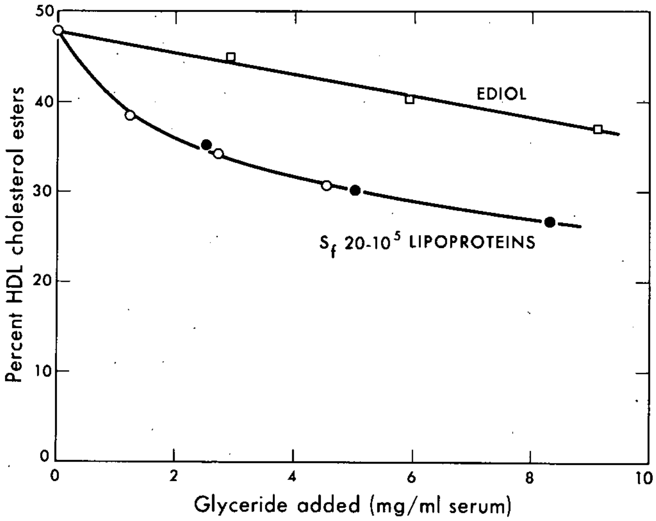

Figure 3. Percent cholesterol ester in HDL lipid as a function of amount of added glyceride per ml of serum in incubation medium.

MU-33139

Table 2. HDL lipid composition following incubation with varying amounts of Ediol

Incubation mixtures	Lipid composition of HDL (percent of total lipid weight)			
	Cholesterol esters*	Glycerides*	Unesterified cholesterol*	Phospholipids*
5 ml serum + 1 ml Ediol stock (1E)**	45.1 ± 0.6***	8.0 ± 0.1	2.6 ± 0.4	44.3 ± 0.8
5 ml serum + 1 ml Ediol stock (2E)	40.3 ± 0.2	10.0 ± 0.1	3.2 ± 0.4	46.5 ± 0.0
3 ml serum + 1 ml Ediol stock (2E)	37.0 ± 1.6	12.9 ± 2.1	3.7 ± 0.9	46.4 ± 1.3

*Lipid values expressed as percent of total lipid weight.

**Two stock solutions of Ediol were prepared by diluting aliquots of Ediol in 0.2 M NaCl. These solutions, (1E) and (2E), had the following glyceride contents: stock (1E) contained 14.6 mg/ml and (2E) contained 29.3 mg/ml.

***Standard error of the measurement: $\sigma_e = \sqrt{\frac{\Sigma d^2}{2K}}$. d = difference between duplicates; K = number of pairs of duplicates.

performed a set of experiments identical to that using the S_f 20-10^5 lipoproteins as the source of glyceride, except that an emulsion of coconut oil, Ediol (oral fat emulsion, SchenLabs Pharmaceuticals, Inc., New York 1, New York) was used. The results of these incubation studies are shown in Table 2. Although the HDL-glyceride content is found to increase, appreciably less glyceride is transferred per unit amount of added glyceride in the Ediol system than in the S_f 20-10^5 incubation system. The decrease in cholesterol esters is again observed to be associated with the glyceride increase. The relationship between the HDL-glyceride and cholesterol-ester content in the Ediol system is presented in Fig. 1. Calculation of the slope of the regression line for these data gives a decrease of approximately 1.8 moles of cholesterol ester for an increase of 1 mole of HDL glyceride derived from Ediol. The complicating feature of the presence of surfactant stabilizers (glyceryl monostearate, polyoxyethylene sorbitan monostearate), preservatives, and antioxidants, in the Ediol emulsion system must, however, be kept in mind when comparing the coconut oil experiment with the S_f 20-10^5 experiment.

Figures 2 and 3 show the changes in HDL-glyceride cholesterol-ester percentages, respectively, as a function of the increase in the amount of S_f 20-10^5 or Ediol glyceride per milliliter of serum in the incubation medium. It would appear from these figures that for the same amount of glyceride added to the incubation system, S_f 20-10^5 lipoproteins appear to transfer more glyceride and displace more cholesterol esters than Ediol. If this difference is not due to the foreign stabilizing components in the Ediol emulsion, then it would be of great interest to determine to what extent particle size and surface area of the glyceride bearer and the degree of saturation and molecular weight of the glyceride play a role in determining the efficiency of glyceride transfer and cholesterol-ester displacement.

Total serum lipoproteins from control and incubation mixtures containing the highest concentrations of added glyceride were isolated and subjected to analytic ultracentrifugation. Briefly, the outstanding difference between the HDL from the control and the S_f 20-10^5 glyceride-enriched systems was a significant increase in flotation rate of the HDL species in the latter. Detailed data on this facet of the investigation will be reported subsequently.

DISCUSSION

The data presented in this report show that in the presence of increased amounts of S_f 20-10^5 lipoproteins an increase in HDL glyceride and a decrease in HDL cholesterol esters occur. These observations establish a determining role for the S_f 20-10^5 lipoproteins in controlling the HDL-glyceride content. The observations of Lindgren et al. (10), of a strong statistical association between the serum S_f 20-10^5 lipoprotein concentration and HDL-glyceride content in humans may be explained in terms of this transfer reaction. This transfer reaction may provide an important pathway in the removal of glycerides from the blood stream.

Prior studies (11) on the influence of in vitro incubation of serum on lipoprotein lipids have been concerned primarily with the esterification of lipoprotein cholesterol. It has been established that upon incubation a serum fatty acid transferase effects the transfer of a C-2 fatty acid from lecithin to unesterified cholesterol and, thus, produces cholesterol esters and lysolecithin. This increase in serum cholesterol esters has been associated (9) with elevations of the cholesterol-ester content of the major lipoprotein classes including the HDL. In the present investigation, however, we observe this increase in HDL-cholesterol-ester content only at the lowest concentration of S_f 20-10^5 glyceride in the incubation medium.

In those experiments where increasing amounts of S_f 20-10^5 lipoproteins were present in the incubation system, no increase in HDL cholesterol esters occurred. As a matter of fact, there were substantial decreases in HDL-cholesterol-ester content to values even below those in the nonincubated system. A reasonable explanation of this would be that as the S_f 20-10^5 glyceride was bound to the HDL, the cholesterol esters were displaced. Furthermore, by its presence on the HDL, the glyceride blocked access to the HDL of any cholesterol esters formed by the transferase activity. The newly formed cholesterol esters would have to seek other sites for binding, such as on the S_f 20-10^5 and S_f 0-20 lipoproteins. In addition, the possibility of some inhibition of the transferase reaction by S_f 20-10^5 lipoproteins is suggested by the lesser magnitude of unesterified cholesterol reductions in incubation systems high in S_f 20-10^5 lipoproteins compared to those low in these species. The observed lipid displacement reaction involves only intact serum lipoproteins. Several investigators (12,13) have reported the uptake of Celite-dispersed lipids by human lipoproteins, but uptake and displacement under the native and mild conditions such as in this study have not been previously observed. The consequences of the cholesterol-ester displacement reaction may be extensive. The deposition of cholesterol esters in tissues may be related to such a displacement reaction. The potential atherogenicity of low-density lipoproteins may possibly be due to a relatively loose binding of displaced cholesterol esters and more ready deposition in tissue sites.

The displacement reaction has considerable implications for the interpretation of lipoprotein composition data. The lipid compositions, especially of the HDL, will depend significantly on the S_f 20-10^5 lipoprotein concentrations present in serum at the time of sampling.

This observation of glyceride uptake by HDL, together with the fact that HDL species are activators of lipoprotein lipase (14), suggest the possibility that the lipase reaction may be taking place also at the HDL-glyceride site besides at the large glyceride particle site. The nature of the removal of HDL glycerides by tissues and the action of lipoprotein lipase on HDL glycerides is currently being investigated.

SUMMARY

Transfer of S_f 20-10^5 glyceride to human serum high-density lipoproteins occurs during incubation of serum with S_f 20-10^5 lipoproteins. Uptake of glyceride by HDL is associated with reciprocal reductions in HDL cholesterol ester content. An artificial lipid emulsion, Ediol, also transfers glyceride to HDL and displaces HDL cholesterol esters. The amount of glyceride transferred per amount Ediol glyceride added to incubation system is significantly less than observed for the S_f 20-10^5 glyceride. The implications of such glyceride transfer and cholesterol ester dislocation to lipoprotein chemistry are discussed.

ACKNOWLEDGEMENTS

This work was supported in part by Research Grant HE 02029-09, National Heart Institute, Public Health Service, Bethesda, Maryland (U.S.A.), and by the U.S. Atomic Energy Commission.

REFERENCES

1. Nichols, A. V.; Rehnborg, C. S.; Lindgren, F. T., and Wills, R. D.; J. Lipid Res. 3:320, 1962.
2. Lindgren, F. T.; Nichols, A. V., and Freeman, N. K.; J. Phys. Chem. 59:930, 1955.
3. Lindgren, F. T., Nichols, A. V., and Wills, R. D.; Am. J. Clin. Nutr. 9:37, 1961.
4. deLalla, O. F., and Gofman, J. W.: Methods of Biochemical Analysis, New York, Interscience Publishers, Inc., 1954, p. 459.

5. Sperry, W. M., and Brand, F. C.; J. Biol. Chem. 213:69, 1955.
6. Borgstrom, B.; Acta Physiol. Scand. 25:101, 111, 1952.
7. Freeman, N. K.; Ann. N.Y. Acad. Sci 69:131, 1957.
8. Glomset, J. A.; Biochim. Biophys. Acta 70:389, 1963.
9. Rehnborg, C. S., and Nichols, A. V.; The Fate of Cholesteryl Esters in Human Serum Incubated _In Vitro_ at 38°, in preparation.
10. Lindgren, F. T.; Freeman, N. K., and Nichols, A. V.: The Metabolism of Lipids as Related to Atherosclerosis, Springfield, Ill., Thomas Publishing Co., 1964, in press.
11. Glomset, J. A.; Biochim. Biophys. Acta 65:128, 1962.
12. Avigan, J.; J. Biol. Chem. 226:957, 1957.
13. Ashworth, L. A. E., and Green, C.; Biochim. Biophys. Acta 70:68, 1963.
14. Korn, E. D.; J. Biol. Chem. 215:15, 1955.

Received December, 1963.

Use of the Bragg Peak for Brain-Tumor Therapy

Alexander Gottschalk, John T. Lyman and Larry W. McDonald

The early work in this laboratory demonstrated that the biological effect of tissue ionization produced by the heavy particles from the first cyclotron was greater than that of X rays. This led to the setting up of safety standards for workers around accelerators and also to the investigation of neutron irradiation in cancer therapy (1,2,3). The interest in the relationship between the density of ionization and biological effect, from the standpoint of both basic radiobiology and radiation therapy, has continued here. Since World War II, when larger cyclotrons and linear accelerators were constructed and higher energy, heavy charged particle beams became available, extensive biological and medical research has been carried out with various heavy particles in this laboratory and elsewhere (4), and the work is now leading to advances in the therapy of several diseases (5).

Accelerated heavy particles from the Berkeley 184-inch synchrocyclotron have been used for patient therapy since 1954. Numerous papers have described clinical studies using heavy particles for radiosurgical suppression or ablation of the hypophysis in the treatment of diseases such as metastatic breast carcinoma, diabetic retinopathy, acromegaly, and Cushing's disease, and also for direct irradiation of a soft-tissue lesion and recently for three brain tumors (6-11).

Experiments started already in 1948 included the successful treatment of animal tumors with the Bragg peak and thus demonstrated the unusual clinical implications of heavy particles in therapy using this portion of the heavy particle beam (12). In these investigations it became evident that heavy-particle beams are of great clinical interest. Unlike X rays or gamma rays, they penetrate tissue with little scatter, and the higher linear energy transfer (LET) as the particles slow down produces the Bragg peak, by which it is possible to deliver a cancerocidal dose to deep-seated tumors. This can be achieved with relatively little skin dose, the depth-dose to skin-dose ratio being opposite to that of X rays or gamma rays. In addition, each unit of energy delivered at the Bragg peak has a greater relative biological effect (RBE) per unit of ionization present (4,13) as compared to 250-kVp X rays. Furthermore, factors such as temperature, fractionation, protective agents and oxygen saturation, which all modify electromagnetic or other low-LET radiations, alter to a lesser degree the effect of higher LET irradiation (14,15,16). This report describes the case histories of three patients suffering from brain neoplasms treated with the Bragg peak, discussing the dosimetry and technical aspects of therapy.

CASE HISTORIES

CASE 1. A four-year-old white male had the onset of neurological symptoms December 6, 1960, consisting of a fall, morning vomiting, diplopia, papilledema, and a palsy of the left abducens nerve. Increased intracranial pressure was also present at this time. Subsequent ventriculography and carotid angiography revealed a right parasagittal mass. A craniotomy was performed and a lemon-sized, grade 2 oligodendroglioma was removed. In the interval, February 13 through March 9, 1961, 3,100 rads were delivered to the tumor site with a 250-kVp apparatus of HVL (half-value layer) 2.28 mm Cu.

In May of 1961 signs of increased intracranial pressure again developed, and at a second craniotomy, recurrent tumor was found. Histologically, this also was a grade 2 oligodendroglioma. In October of 1961, because of a developing left hemiparesis, a third craniotomy was performed with a recurrent neoplastic mass once more excised. At this time, the tumor had become a grade 3 oligodendroglioma.

In December of 1961 the patient first manifested right hemiparesis and had a right-sided Jacksonian seizure. Consequently, he was believed to have tumor spread across the midline. In the interval from December 20, 1961, to January 12, 1962, the patient was treated with Bragg-peak irradiation from the alpha-particle beam of the 184-inch synchrocyclotron. He slowly improved and over a period of the next five months experienced a good palliative result. He then gradually began to show a steady deterioration with obvious regrowth of tumor and expired on October 15, 1962.

The autopsy revealed a recurrent oligodendroglioma extending widely into both cerebral hemispheres and into the thalmus. Hemorrhage and necrosis within the tumor were interpreted as being caused either by the irradiation or by the tumor outgrowing its blood supply. Metastases from the intracranial tumor were found in the lungs.

CASE 2. A 50-year-old white male was initially suspected of having a brain tumor in April 1962 after a two-and-a-half year history of progressive weakness in the right hand, a short history of difficulty with speech and right hemiparesis. A left carotid arteriogram demonstrated a left temporal-parietal tumor. On May 21, 1962, a subtotal resection of a grade 3 astrocytoma was performed. Postoperative irradiation using the Bragg peak was started on June 29, 1962, but following the initial two treatments, the patient became unresponsive and suffered from a progressive right hemiparesis, nausea, and

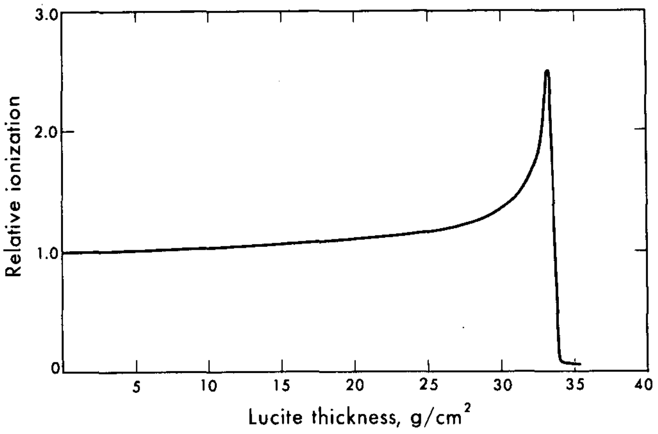

Figure 1. Bragg curve of 910-MeV alpha-particle beam. Mu-31722

vomiting. He was then reoperated, and a lemon-sized tumor was again removed. Bragg-peak therapy was resumed on July 9 and completed on July 13, 1962. In spite of considerable neurologic deficit consisting of aphasia and a persistent hemiparesis, his status improved until October of 1962. He then gradually began a progressive down-hill course and expired in January of 1963. Terminally, the patient appeared to be suffering from bilateral bronchopneumonia for which he was hospitalized. He was treated with antibiotics and seemed to improve when he suddenly became unresponsive and died three days later.

A grade 4 astrocytoma was found extensively involving the left cerebral hemisphere at autopsy. Sections from the more superior portions of the tumor showed some eosinophilic coagulum which was PAS positive; a similar type of coagulum has been noted in radionecrosis of nerve tissue. The greater part of the tumor showed focal necrosis and some vessel thrombosis which are common in grade 4 astrocytomas. Pressure effects produced encephalomalicia of the right occipital lobe and hemorrhage in the brain stem. The hemorrhage in the brain stem and bronchopneumonia were the terminal events.

CASE 3. A 38-year-old white male first noted the onset of left-sided headache and nausea in January, 1962. The symptoms progressed in severity and were associated with rather vague personality change with at least one episode of loss of contact with his surroundings.

Papilledema was evident in June 1962, and on June 9, 1962, a ventriculogram demonstrated a left frontal mass. A left frontal craniotomy was performed the same day with subtotal removal of a grade 2 astrocytoma from the region of the left sylvian fissure. From July 6 to July 13, 1962, the patient was treated with alpha-particle Bragg-peak irradiation. In the immediate post-operative and post-irradiation period a right hemiparesis and pronounced aphasia were evident. The hemiparesis has now (one year later) completely disappeared.

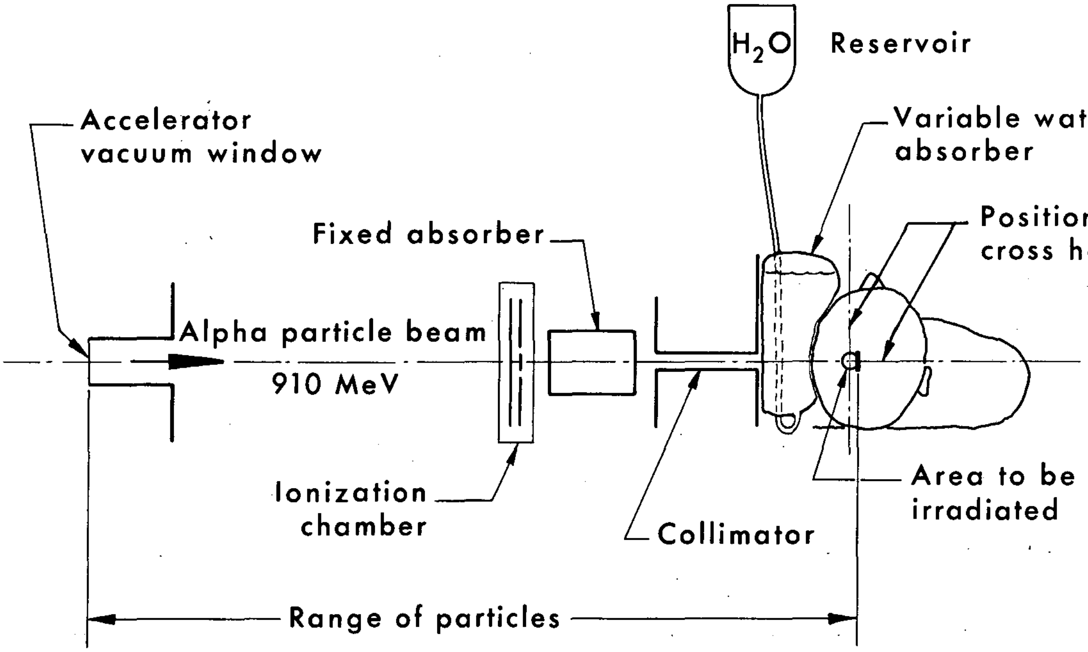

Figure 2. Schematic diagram of treatment setup.

The aphasia has improved, but is still present. The patient is working regularly as a stock clerk and is able to drive his car. At this time there is no evidence of recurrent neoplasm.

METHOD OF THERAPY AND DOSIMETRY

The three patients were all irradiated at the 184-inch synchrocyclotron, utilizing the 910-MeV alpha-particle beam. As this beam of particles is slowed down by interactions with an absorbing medium, an increase in ionization in the medium takes place. This is shown in Fig. 1. This Bragg curve shows the increase in ionization of the nitrogen gas in an ionization chamber as a function of the amount of absorbing medium in front of the ionization chamber, the absorber in this case being lucite.

Relative mass-stopping powers of various materials were calculated or measured (17) so that suitable combinations of absorbers could be used to permit maximum ionization to occur at required depth below the surface of the scalp. A fixed absorber of lucite or copper was used in conjunction with a variable water absorber enclosed in a pliable plastic bag conforming with the patient's head (Fig. 2). The beam was monitored before the first absorber, and from Bragg curves (obtained by using various combinations of absorbing materials) the dose delivered to various depths in the brain was determined.

Isodose curves were obtained by graphically summing the depth-dose curves for the individual treatment fields. In case 3, isodose curves were also obtained by simulating the treatment schedule on the IBM 7090 computer (see Fig. 3).

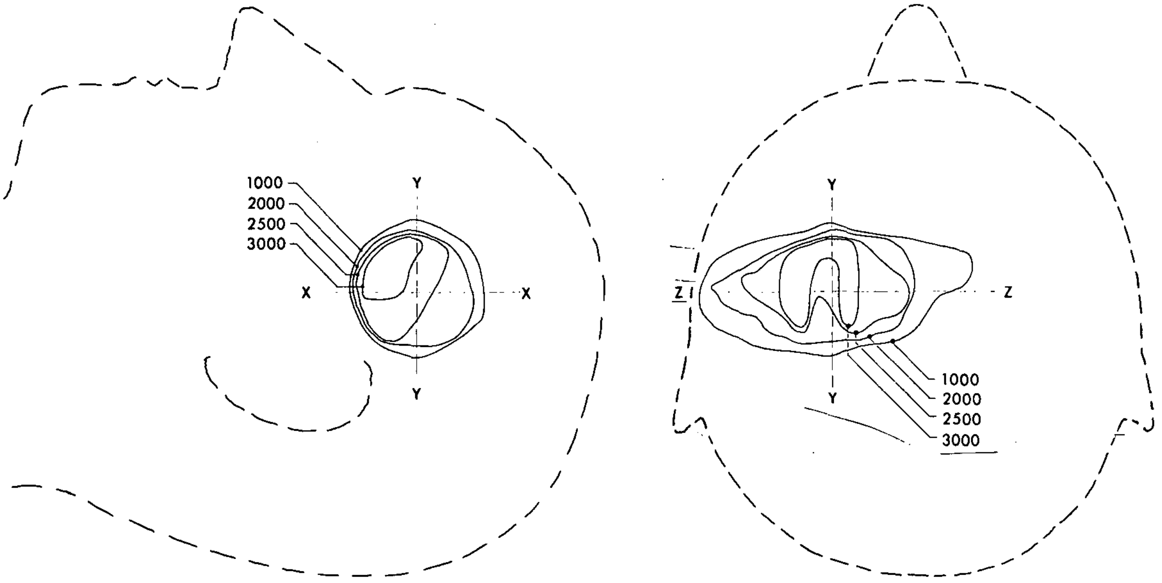

Figure 3. Isodose curves for case 3, calculated by IBM computer.
MU-33279 and 33280

Case 1: Treatment was given on eight separate occasions within a 24-day period. Irradiation was delivered through 13 separate portals. The maximum dose delivered to the tumor was 8,500 rads, with the majority of the treatment field receiving more than 6,000 rads.

Case 2: Treatment was given on five separate occasions during a 15-day period. Irradiation was delivered through nine portals. Maximum dose delivered to the tumor was 5,250 rads, with the majority of the treatment field receiving greater than 4,000 rads.

Case 3: Treatment was given on four separate occasions during an 8-day period. Irradiation was delivered through five different portals. Three of the portals were used more than once, but the beam was allowed to penetrate to a different depth each time. The maximum dose was 4,450 rads. Most of the field received more than 2,500 rads.

DISCUSSION

The largest beam now available for heavy-particle therapy is a circle 6 cm in diameter. Therefore, it is currently possible to treat only a relatively small volume of tissue with a cancerocidal dose. However, modifications that will permit larger treatment fields are presently underway. Nevertheless, effective therapy with the Bragg peak does depend upon precise localization of the residual neoplasm. The surgeon can often help by localizing tumor-containing areas in relation to bony landmarks in the skull; and in most cases, radio opaque clips can be placed around the margins of the operative field to provide a target visible on alignment X rays. Unfortunately, highly malignant gliomas tend to infiltrate widely, often sending out microscopic tumor strands into brain tissue that grossly appears normal. Consequently, the likelihood of a geometric miss with the heavy particle beam (also a problem when X rays are used (18)) is great, although it may be possible to deliver tumorocidal doses to all the tissue obviously invaded by neoplasm.

In both case 1 and 2 this situation almost certainly occurred. It is noteworthy, however, that in case 1 palliation was achieved with the Bragg peak in spite of the fact that a conservative dose of conventional irradiation had no apparent effect. Whether this was due to the higher dose given with the heavy particles, the greater efficacy of the high LET irradiation, or both, is not known. The relative good health enjoyed by case 3 more than one year after treatment is encouraging but as yet permits no ultimate prognosis; because, in a large series of patients with comparable tumors, Kernohan and Sayre (19) found an average survival of almost two years following surgery alone.

SUMMARY AND CONCLUSIONS

Three patients with brain tumors have been treated by the Bragg peak of the 910-MeV alpha-particle beam from the 184-inch synchrocyclotron. All had had subtotal tumor resection prior to therapy. The case histories are presented; the technique of dosimetry, and the method of irradiation are discussed. The series is too small to judge whether or not this form of therapy holds great promise for the future.

ACKNOWLEDGEMENTS

Drs. John H. Lawrence and Cornelius A. Tobias provided both motivation and guidance for this project. Mr. Richard W. Pratt was responsible for constructing the mechanical devices necessary for therapy and was of incalculable aid in helping to position patients. Mrs. Jeannette Cornell provided nursing care. Physicist Jerry Howard and Mr. James Vale and the cyclotron crew were responsible for the proper operation of the therapy beam.

REFERENCES

1. Lawrence, J. H., and Lawrence, E. O.; Proc. Nat. Acad. Sci. U.S. 22:124, 1936.
2. Lawrence, J. H.; Aebersold, P. C., and Lawrence, E. O.; Occas. Publ., Am. Assoc. Adv. Sci. 4:215, 1937.
3. Stone, R. S.; Lawrence, J. H., and Aebersold, P. C.; Radiology 35:322, 1940.
4. D'Angio, G. J., and Lawrence, J. H.; Nucleonics 21:56, 1963.
5. Lawrence, J. H.; Tobias, C. A.; Born, J. L.; Gottschalk, A.; Linfoot, J. A., and Kling, R. P.; J. Am. Med. Assoc. 186:236, 1963.
6. Tobias, C. A.; Lawrence, J. H.; Born, J. L.; McCombs, R. K.; Roberts, J. E.; Anger, H. O.; Low-Beer, B. V. A., and Huggins, C. B.; Cancer Res. 18:121, 1958.

7. Lawrence, J. H.; Tobias, C. A.; Born, J. L.; Wang, C. C., and Linfoot, J. A.; J. Neurosurg. 19:717, 1962.
8. Lawrence, J. H.; Tobias, C. A.; Born, J. L.; Sangalli, F.; Carlson, R. A., and Linfoot, J. A.; Acta Radiol. 58:337, 1962.
9. Linfoot, J. A.; Lawrence, J. H.; Born, J. L., and Tobias, C. A.; New Engl. J. Med. 269:597, 1963.
10. Lawrence, J. H.; Tobias, C. A.; Linfoot, J. A.; Born, J. L.; Gottschalk, A., and Kling, R. P.; Diabetes 12:490, 1963.
11. Lawrence, J. H.; Tobias, C. A.; Born, J. L.; Gottschalk, A.; Linfoot, J. A., and Kling, R. P.; J. Am. Med. Assoc. 186:236, 1963.
12. Tobias, C. A.; Anger, H. O., and Lawrence, J. H.; Am. J. Roentgenol. Radium Therapy Nucl. Med. 67:1, 1952.
13. Lawrence, J. H.; Wang, C. C.; Sillesen, K., and Lyman, J. T.; Semiannual Report, Donner Laboratory, Lawrence Radiation Laboratory, UCRL-11033, Spring 1963.
14. Sayeg, J. A.; Birge, A. C.; Beam, C. A., and Tobias, C. A.; Radiation Res. 15:139, 1961.
15. Barendsen, G. W.; Nature 193:1153, 1962.
16. Brusted, T.; in Advances in Biological and Medical Physics, Vol. 8, New York, Academic Press, 1962, p. 161.
17. Birge, A. C.; Anger, H. O., and Tobias, C. A.; in Radiation Dosimetry, New York, Academic Press, 1956, p. 623.
18. Concannon, J. P.; Kramer, S., and Berry, R.; Am. J. Roent. Rad. Ther. Nucl. Med. 84:99, 1960.
19. Kernohan, J. W., and Sayre, C. P.: Tumors of the Central Nervous System, fascicle 35 of the Atlas of Tumor Pathology, Armed Forces Institute of Pathology, Washington, D. C., 1952, p. 22.

Received October, 1963.

Studies on the Mammalian Radiation Syndrome with High-Energy Particulate Radiation. II.

Some Factors Affecting RBE of 730-MeV Protons

Charles A. Sondhaus, James K. Ashikawa, Cornelius A. Tobias, Vally Paschkes and David Love

The relative biological effectiveness (RBE) of high-energy protons in total-body exposure of the mammal, in addition to its theoretical interest, has also become important in planning for future space exploration (1). Since it is well known that the type and degree of biological effect from a given radiation exposure depends on a number of factors in addition to absorbed dose (2,3), an investigation of some of these has been underway for the past year at this laboratory. These factors may be grouped roughly as follows: a) the intrinsic properties of the radiation; b) the conditions of the exposure; and c) the biological and environmental factors that may modify the effect.

It is now a well-established experimental fact that RBE increases with the average linear energy transfer (LET) of the radiation in many plant- and animal-cell populations, and it may reach a maximum value in mammalian cells and organ systems beyond which further increase in LET produces a decline (4,5). Although general principles resulting from data obtained with microbiological and cytological methods on single cell populations are not easily demonstrated in mammals, it appears to be a valid conclusion that a low LET radiation should exhibit an RBE near unity for any mammalian end point chosen.

It also appears likely that with low LET radiation, a "multi-event" response should be observed in the dose-effect relationship (6), i.e., that the RBE should vary both with the total dose and with the dose rate at which the total dose was delivered. A further condition affecting RBE is the exposure geometry or depth dose distribution (7), which may influence the mode of injury and thus make a particular end point or criterion of effect the significant factor in specifying an RBE value.

In these experiments we deal with short term effects only. In addition, the effects of dose distribution are ruled out as far as possible by producing a uniform whole-body dose with the proton beam of the 184-inch cyclotron. In view of the difference in predominance of the gastrointestinal and hematopoietic syndrome that has been observed by us even in the uniformly irradiated mouse at different total doses and dose rates of proton and X-radiation (8), it was evident that the effect of these latter factors must be included and the mode of injury must be specified in comparing the effectiveness of these radiations.

Because gut and marrow deaths occur at distinct and well-separated times after lethal total-body irradiation in mice, these animals were chosen for the study. The characteristic times of peak death rate for each injury mode suggested that 6-day and 12-day mortality be selected as end points for comparison (9), in addition to the more usual 30-day median lethal dose. These quantities were therefore determined for different total doses of 730-MeV protons, 250-kVp X rays and 100-kVp X rays at constant dose rate. The effect of varying the dose rate was also studied.

METHODS

A series of seven experiments was performed with 730-MeV protons, 100-kVp and 250-kVp X radiation, and the relative lethality and time course of radiation injury was studied in more than 2,000 Swiss Webster white male mice. The experimental conditions under which the animals were maintained and the differences observed in the acute radiation syndrome have been described in part I of this study (8). Exposure factors and methods of dose determination are summarized in this section.

X-ray-exposure dose measurements were made at the centers of lucite mouse cannisters on the mouse exposure wheel, using a 250-r Victoreen thimble ionization chamber. In the high dose-rate exposures, the X-ray beam was partially collimated by use of a modified treatment cone with Pb diaphragm so that the bulk of the intensity was received dorsoventrally by one mouse at a time. Each animal was positioned successively by modifying the rotating mechanism to allow one-step positioning. In order to achieve the high dose rate desired, the animal was placed close to the target of the X-ray tube and left there for the required time, after which the next animal was moved into position. In this process, the neighboring animals also received a small fraction of the dose, so that the total exposure of each animal extended over about five wheel positions and was essentially zero at all other positions.

A series of seven 1-min exposures was therefore made with the chamber occupying each of seven positions successively, and the total dose received was then used to determine the number of minutes needed per position to produce the required total dose. It was found that about 88% of the X-ray dose was received at a dose rate of 100 ± 5 rad/min, 10% at a dose rate of 5.5 rad/min and the remaining 2% at a dose rate of about 0.5 to 1.5 rad/min. To a first approximation this was considered to be equivalent to a total exposure at a dose rate of 100 rad/min. The total dose in passage through all seven positions was read on the ionization chamber and used in each experiment thereafter.

In the low dose rate X-ray exposures, the mouse wheel was rotated continuously and the resulting average dose rate was 20 ± 1 rad/min, midline in air.

The animals exposed to the 730-MeV proton beam were placed in a wheel-positioner that exposed one mouse at a time anteroposteriorly in a ventilated cylindrical holder. The diameter of the holder tube was about one inch. Dosimetry was carried out by the parallel-plate aluminum foil walled ionization chambers, which are routinely used in the medical cave (10). These chambers are placed in the beam following its emergence from the vacuum collimating system into the air. Their effective collecting volumes are accurately known and are defined by guard rings surrounding the central foil discs mounted on mylar film; the discs are somewhat smaller in diameter than the beam. The ion chambers are filled with nitrogen.

The emergent proton beam is nearly parallel and homogeneous and has been found to show an essentially flat intensity-distribution profile across its diameter when traversed by a miniature ionization chamber probe. By magnetically varying beam intensity, dose rates of 100 and 1,000 rad/min were produced and measured within a relative accuracy of 2%. The creation of secondary particles (neutrons, mesons, recoil nuclei) in the body of the animal by passage of the proton beam was not believed to be significant in degree because of the small size of the mouse. Ionization in the mouse body probably remained uniform within 5-10% according to measurements made in a mouse-sized water phantom with a small ionization chamber.

RESULTS

An interesting question in mammalian radiobiology, and an important one in regard to protection against radiation hazards in space, is whether different types of radiation with comparable LET, i.e., high-energy protons and X or gamma radiation, will have a different biological effect on man. Some results of the present experiments pertain to this question and are presented here. The 6-, 12- and 30-day mortality values for Swiss Webster male mice exposed to 100- and 250-kVp X rays and 730-MeV protons are based on a preliminary analysis of our mortality data. In order to compare accurately the different experimental parameters, each LD_{50} value was calculated from the regression of mortality by graphical probit analysis.

For 730-MeV protons, the total-body 30-day LD_{50} was found to be 650 rads, air dose. As shown in Fig. 1, this value was not significantly different at dose rates of 1,000 and 100 rads per minute. The 12-day LD_{50} values, however, were 680 rads at 1,000 rad/min and 700 rads at 100 rad/min, and the 6-day LD_{50} was 730 rads and 810 rads respectively at the two dose rates. Figure 2 shows that for 250-kVp X radiation filtered with 0.5 mm Cu + 1.0 mm Al, the 30-day

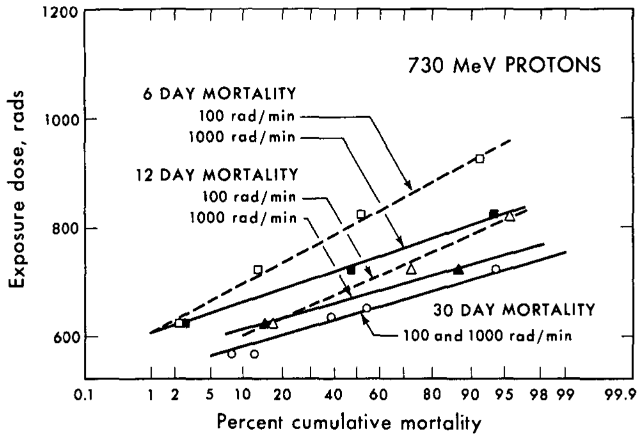

Figure 1. Exposure dose vs. 6-, 12- and 30-day mortality for 730-MeV protons at two dose rates (probit scale).
MU-33235

total-body LD_{50} was 520 rads, air dose, for both 100 rad/min and 20 rad/min dose rates. The 12-day LD_{50} was 610 and 630 rads respectively. The 6-day LD_{50} was approximately 1,000 rads at 100 rad/min; the 6-day LD_{50} at 20 rad/min is being investigated.

For 100-kVp X radiation filtered with 1.0 mm Al, the 30-day total-body LD_{50} was 750 rads, midline air dose, for both 100 rad/min and 20 rad/min dose rates, as seen in Fig. 3. The 12-day LD_{50} was 850 and 900 rads respectively, while the 6-day LD_{50} levels were not reached at the total doses given so far but can be estimated to be approximately 1,100 rads at 100 rad/min and greater than 1,300 rads at 20 rad/min.

Based on these data, tentative estimates of proton RBE may be made for gut death as well as for 30-day LD_{50}. If 30-day LD_{50} is used as end point, a value of 0.8 is found for 730-MeV protons, which agrees well with previous results obtained at this laboratory and elsewhere (11,12). However, if gut death is used as end point, a higher RBE results and dose rate is found to influence it. The 6-day RBE for protons at 1,000 rad/min relative to 250-kVp X rays at 100 rad/min is the highest value observed, a value of 1.4 being found. For protons at 100 rad/min, however, the 6-day RBE was 1.2 if the 250-kVp X irradiation was made at the same dose rate.

The higher but variable RBE at 6-day LD_{50} level appears to be due to two factors. The first is the difference in tissue dose distribution between the two radiations, which favors the production of gut death by high energy proton exposure. The second is the dose rate dependency of the syndrome.

The 100-kVp X radiation is particularly efficient in producing marrow death but causes gut death only at high air doses. Thus, a midline air dose

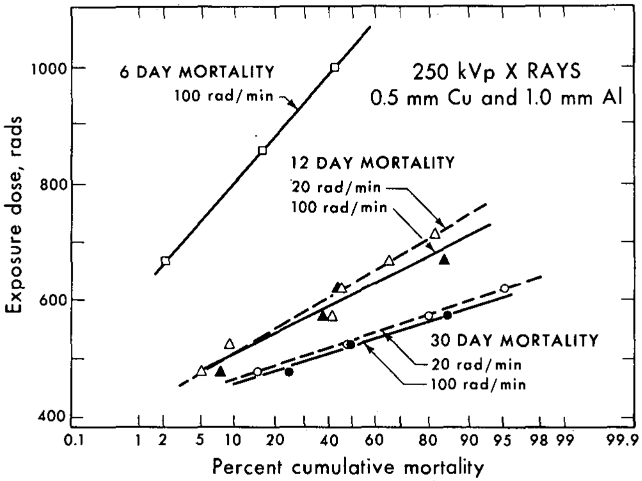

Figure 2. Exposure dose vs. 6-, 12- and 30-day mortality for 250-kVp X rays at two dose rates (probit scale).
MU-33236

more than 1.3 times that for 730-MeV protons was required to produce 50% gut death at 6 days, although 0.9 times the proton air dose produced the same LD_{50} at 30 days. To derive a true ratio of marrow doses, however, the average value of dose in the microscopic marrow cavities for 100-kVp X ray would have to be obtained. This dose has been shown to be several times higher in the smallest cavities than in the soft tissue surrounding the bone (13), but no average value can be assigned to the marrow as a whole at this time.

If the cumulative mortality at 8 days, for example, were subtracted from the cumulative mortality at 30 days, a rough measure of bone-marrow mortality might result for each radiation, since most gut deaths have occurred by this time and marrow injury has not yet manifested itself to any extent. If this is done for the proton exposures, very little mortality remains at later times, in contrast to the X-ray exposures, and much higher marrow RBE values would result for the remaining mortality. The poor statistics that result make this procedure of doubtful significance if present data were to be used. The use of larger numbers of animals together with protection against gut death might, however, make it possible to investigate proton marrow RBE further.

DISCUSSION

It is apparent from the results of these experiments that RBE values can differ between radiations of similar LET even under uniform exposure geometry, when differences in dose-rate dependence and injury mode are present. It is therefore clearly necessary to specify the effect to which a proton exposure RBE applies. In addition, a dose-rate factor must be introduced in calculating RBE for exposures to low-LET radiations. The exposure to high-energy protons in future space operations may be an important practical case of low-LET particulate radiation exposure. Most of the available information on RBE of external radiation for somatic effects on mammals refers to early rather than late

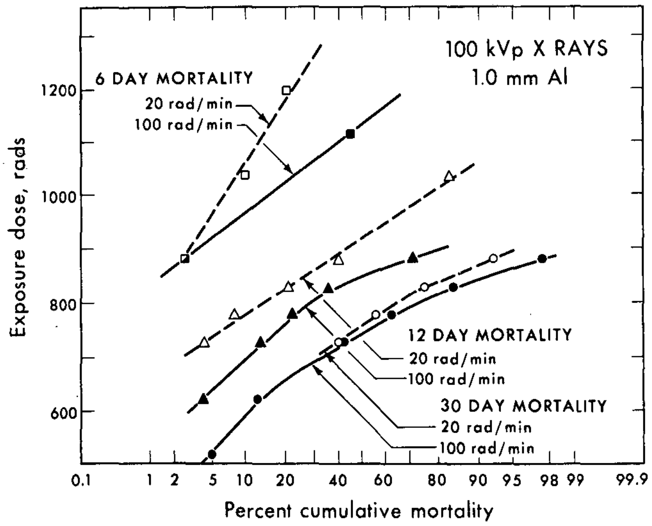

Figure 3. Exposure dose vs. 6-, 12- and 30-day mortality for 100-kVp X rays at two dose rates (probit scale).

MU-33237

effects, and to high rather than low dose rates (14). Direct RBE measurements for late effects at low dose and dose rate present difficulties, and in no experiment thus far has the effectiveness of any radiation been adequately determined over a wide range of dose and dose rates for a given biological end point. In addition, other uncertainties are involved in the extrapolation to man of data from shorter lived species with different response patterns, or of data obtained from tissue cultures or from single-celled organisms. These limitations apply here in seeking to extend this data to the human exposure situation.

It is clear, however, that decreasing the dose rate of a high-energy proton irradiation reduces its effectiveness. Low-LET particulate radiation thus appears to behave similarly to low-LET electromagnetic radiation in this respect (15). The explanation usually proposed for this effect is that damage in the single cell from the first of several events leading to a multi-event effect may be compensated unless followed within a given time by one or more later events. The practical implication of the phenomenon is that RBE values obtained with high dose rates may be underestimates of the RBE at low dose rates or low levels of effect.

Previous work has led to the conclusion that mice exposed to "high-LET" radiations (mainly fast neutrons) show more bowel damage and die earlier than when exposed to "low-LET" radiations (16). The RBE for intestinal death in mice and in dogs irradiated with fast neutrons has been shown to be higher than for bone marrow death, a value of about 2 for gut death and 1 for marrow death having been observed. In the present study, however, greater bowel damage is apparently produced and earlier death has been observed with protons than with X rays. Both the dose-rate dependence of the effect and the known LET spectrum of high-energy protons appear to indicate that this is not a high-LET phenonenon. In addition, the 6-day gut-death RBE of 1.4 for high-energy protons is not much greater than unity although it is almost twice the proton RBE of 0.8 for 30-day mortality.

It appears that the above differences in effect may be ascribed to a difference in distribution of tissue dose, even under conditions of "uniform" depth dose, between the proton and X-ray exposures, the latter favoring the bone-marrow damage caused by higher local dose, the former irradiating gut and bone marrow more equally. Differential radiosensitivity of the two tissues to each radiation may also be involved but cannot be inferred from the present results without additional information as to microdistribution of tissue dose from both primary and secondary particles. The dose-distribution factor and the dose-rate factor appear in any case to be comparable in importance to the LET in assessing the relative hazard of a proton exposure, and further investigation of each would be required to characterize it fully.

ACKNOWLEDGEMENTS

We wish to express our thanks to Dr. John H. Lawrence for his interest and support, to Mr. Jerry Howard for operation and dose measurement in the proton irradiations on the 184-inch cyclotron, and to Miss Glyde Greenfield for her technical assistance.

This work was supported by the National Aeronautics and Space Administration.

REFERENCES AND NOTES

1. Proceedings of the Symposium on the Protection Against Radiation Hazards in Space, Gatlinburg, Tennessee, 1962, Book 1 and 2.
2. Patt, H. M., and Brues, A. M.; in Radiation Biology, Vol 1, edited by A. Hollaender, New York, McGraw-Hill Book Co., Inc., 1954, p. 919.
3. Bateman, J. L.; Bond, V. P., and Robertson, J. S.; Radiology 79:1008, 1962.
4. Zirkle, R. E.; in Radiation Biology, Vol. 1, edited by A. Hollaender, New York, McGraw-Hill Book Co., Inc., 1954, p. 315.
5. Storer, J. B.; Harris, P. S.; Furchner, J. E., and Langham, W. H.; Radiation Res. 6:188, 1951.
6. Lamerton, L. F.; in Radiation Effects in Physics, Chemistry, and Biology, edited by M. Ebert and A. Howard, Amsterdam, North-Holland Publishing Co., 1963, p. 1.
7. Bond, V. P.; Cronkite, E. P.; Sondhaus, C.; Imrie, G. W.; Robertson, J. S., and Borg, D. C.; Radiation Res. 6:554, 1957.
8. Ashikawa, J. K.; Sondhaus, C. A.; Tobias, C. A.; Greenfield, G., and Howard, J.; Semiannual Report, Donner Laboratory, Lawrence Radiation Laboratory, UCRL-11033, 1963.
9. Bond, V. P.; Silverman, M. S., and Cronkite, E. P.; Radiation Res. 1:389, 1954.

10. Birge, A. C.; Anger, H. O., and Tobias, C. A.; in Radiation Dosimetry, Chap. 14 N, edited by G. J. Hine and G. L. Brown, New York, Academic Press, 1956, p. 624.
11. Wang, C. C.; Lyman, J., and Tobias, C. A.; Semiannual Report, Donner Laboratory, Lawrence Radiation Laboratory, UCRL-10211, 1962.
12. Bonet-Maury, P.; Deysine, A.; Frilley, M.; Stefan, C.; Compt. Rend. 251: 3087, 1960.
13. Wingate, C. L.; Gross, W., and Failla, G.; Radiology 79:984, 1962.
14. Bond, V. B.; Carter, R. E.; Robertson, J. S.; Seymour, P. H., and Hechter, H. H.; Radiation Res. 4:139, 1956.
15. Logie, L. C.; Harris, M. D.; Tatsch, R. E., and Van Hooser, E. N.; Radiation Res. 12:349, 1960.
16. Bond, V. B., and Easterday, O. D.; Radiation Res. 10:20, 1959.

James Ashikawa is a consultant to the University of California, Lawrence Radiation Laboratory, from Loma Linda University School of Medicine, Los Angeles County General Hospital, Los Angeles, California.

Received August, 1963.

Characteristics and Intensity Profile of a High-Energy-Proton Beam After Scattering in a Thick Target

Roger Wallace, Kenneth Kase and Charles A. Sondhaus

Total-body irradiation of large animals is presently impractical with the narrow strongly focussed proton beam of the 184-inch cyclotron. Attempts have been made to scan large animals by sweeping the exposure holder uniformly through the beam, but mechanical difficulties and stress to the animal have made the technique impractical. In order to produce a total-body irradiation of a large animal without scanning, the first requirement is to enlarge the beam diameter until it exceeds the dimensions of the animal. If an omnidirectional exposure is required to simultate solar-flare proton-exposure geometry, an additional requirement is to present equal portions of the body surface to the beam for equal times at all possible angles by rotating the animal within the broad beam.

Scattering the beam, rather than using magnetic deflection, has been selected as the method of choice for producing angular divergence. Based on the known properties of the multiple coulomb scattering process, calculations have been made that predict the angular distribution of the emergent primary proton flux after passage through a scattering target (1,2). Substances considered as scatterers include lead, copper, aluminum and graphite, and the energy range 1,000-10 MeV has been investigated.

An angular divergence is predicted in the emergent beam which increases with target thickness and is greatest in the heaviest material for a given fraction of particle range. At the same time, the intensity of the emergent primary beam within a given small solid angle is reduced because of nuclear interactions which result in secondary particles, mostly protons but also neutrons and mesons. The majority of these particles is scattered through somewhat larger angles than are the bulk of the multiply scattered primary protons. The resulting reduction in intensity is found to be greatest for the lightest material.

A second scattering effect that has been investigated is the reduction in energy of the emerging particles. The degree of energy degradation for any material is dependent on the fraction of the proton range traversed in the target; this requires a greater thickness of light material than of heavy material. Because angular dispersion of the beam is also a function of target thickness, it is evident that neither can be produced without the other. Thus a beam of angular divergence sufficient to irradiate a whole large animal will necessarily consist of lower energy protons than did the incident beam before striking the target; similarly, a lower energy beam cannot be used without introducing angular spread and resultant lower intensity. In addition, an energy spread will be produced in the emergent primary beam, with increasing target thickness; this energy straggling, however, remains a small percent of the emergent energy until very low degraded energies are reached, of about 10 to 50 MeV, at which region it becomes comparable.

METHODS

In order to determine the intensity profile of a proton beam degraded by scattering, calculations were made based on the analysis of a variable energy beam for the proposed National Aeronautics and Space Administration synchrocyclotron (1); this has been extended to the broad beam case for biological use (2). The initial beam was assumed to be a thin pencil of monoenergetic 730-MeV protons. This initial beam was then assumed to be degraded in a carbon or copper scatterer to some final energy. The beam profile at some given distance from the scatterer was calculated using circular Gaussian error probabilities (3), and the remanent intensity was then determined.

Circular error probability states that if a set of points is distributed normally in two dimensions with equal standard deviations, the probability that a point will fall within a distance r of the mean (or a distance r from the center of the circle in this case) is $1 - e^{-K_2/2}$ where $K = \frac{r}{\sigma}$ and σ is one standard deviation. In the case under discussion, the scattering was in terms of a root mean square scattering angle ϕ_a; and so K was expressed as $\frac{r}{d}/\phi_a$ where d is the distance from the scatterer to the target.

The beam profile is thus dependent upon both the rms scattering angle ϕ_a and the distance from the scatterer to the target d. The angle ϕ_a is in turn dependent upon the scattering material and the energy to which the beam is degraded.

The first step in the procedure is to choose a scattering material and a degraded energy. From this a ϕ_a is determined. It is then assumed that the beam emerges from the scatterer at a point and diverges with a circular intensity cross section. A scatterer to target distance is chosen and the K's are then calculated as a function of perpendicular distance from the beam axis across the beam cross section. The calculations were usually done in 1-cm increments from the center of the beam to about 20-cm radius.

From the values of K, the probability that a proton will strike within a circle of radius $K\phi_a d$ about the center of the beam is next calculated. The beam

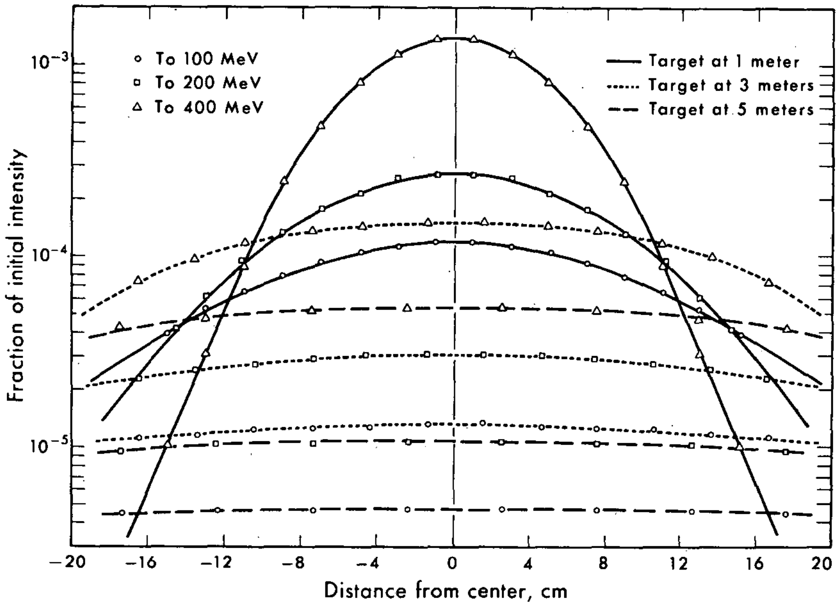

Figure 1. Beam-intensity profiles produced by degradation of 730-MeV protons in graphite to energies of 400, 200 and 100 MeV.
MU-31935

cross section is then divided into circular rings of 1-cm thickness, and the probability of a proton striking within each ring is calculated by: $\Delta P = (1 - e^{-K_2/2}) - (1 - e^{-K_1/2})$, where K_1 and K_2 correspond to two successive radii.

The remanent intensity is found by applying a remanent intensity factor f based on the degree of energy degradation and the scattering material (2). This factor describes the primary beam attenuation in the scatterer. The flux profile of the degraded beam is then found in terms of protons/cm^2-sec by multiplying the initial intensity I by the probability ΔP of a proton striking in a given ring and dividing by the area of the ring A.

$$\Phi = \frac{I\Delta P}{A} .$$

It should be noted that these calculations do not take into consideration the fact that the beam is spread somewhat in the scatterer and is thus subject to a radial as well as an angular divergence. However, the correction required by the radial spreading within the scatterer is small; and moreover, it will serve to flatten the profile and hence improve the picture.

RESULTS AND DISCUSSION

These calculations allow predictions to be made of the energy and intensity profile of the primary beam emerging from a target of Pb, Cu, Al and C. It appears that intensity can be made sensibly uniform over a circular area of diameter greater than 30 cm at a sufficient distance from the scattering target exit port. Some representative results are seen in Fig. 1, which shows profiles produced by degradation in graphite to energies of 400, 200, and 100 MeV. It

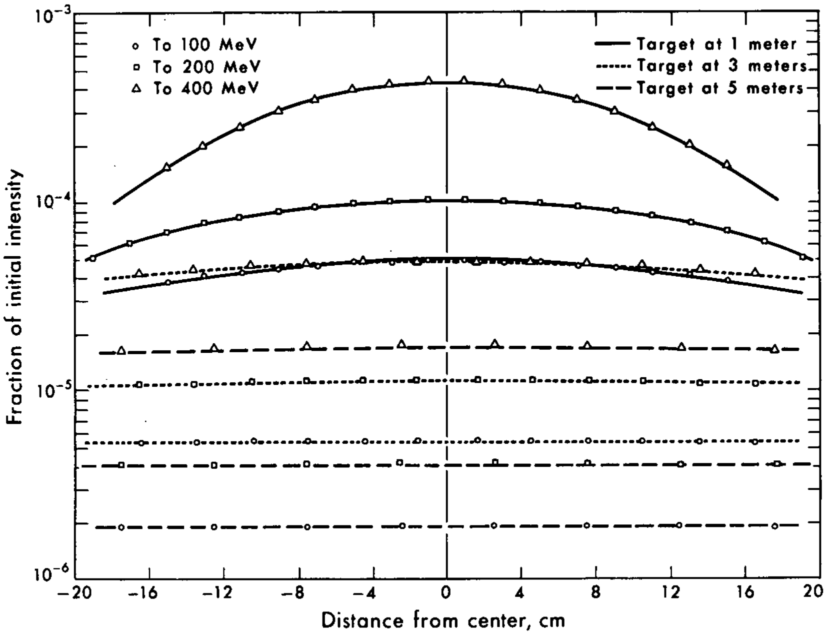

Figure 2. Beam-intensity profiles produced by degradation of 730-MeV protons in copper to energies of 400, 200 and 100 MeV.
MU-31934

is seen that a uniform distribution will result over this diameter at a distance of 3 to 5 m, if a graphite target is used with thickness great enough to degrade the initial energy of 730 MeV to roughly 400 MeV. The resulting primary flux intensity appears to be reduced by a factor of between 100 and 1,000, suggesting that the maximum dose rate attainable in air in the target region may lie in the range of 10 to 100 rad/min. Different profiles and intensities are obtained for other scattering materials and distances from the scatterer to the target at the same degraded beam energy. In general, the more energy is degraded, the more the beam is spread so that a uniform field over a large area can be found at shorter scatterer-to-target distances for larger energy degradations in thicker targets. A copper scatterer spreads the beam more than does a carbon scatterer and so produces a more uniform intensity over a given area at a given scatterer to target distance. However, a copper scatterer will also result in a much smaller remanent flux intensity than will carbon for a given energy degradation.

Figure 2 shows profiles produced by degradation in copper to the same energies. If a 100-MeV beam is desired, it is seen that the same size area of roughly uniform intensity can be found at a distance of 1 m from a copper target, and dose rate due to the primary beam may be kept to about the same value as above.

Since secondary particle production also occurs in the scattering target and some fraction of the secondary particle flux will also reach the animal, calculations are under way to estimate the increase in dose caused by this component. The theory predicts that the secondary particle flux will be smallest in graphite. For this reason, and also because of the higher remanent intensity predicted for graphite, this material has been chosen for the primary-beam scattering target for large-animal whole-body irradiation at high energy with the 184-inch cyclotron. It appears that a second target of copper following the graphite target will be optimal in producing a lower energy broad beam while conserving the most intensity. Thus, a 400-MeV exposure at 5 m from a graphite target should produce uniform dose distribution in a large animal, whereas exposures at 100 MeV and below appear feasible at 1 m from the graphite target when an additional target of copper is added. Alternatively, a copper target alone might be substituted for the graphite.

It appears from these calculations and those for depth dose that the stepwise simulation of a solar-flare proton exposure in the lethal dose range (4) would be possible by using as few as three proton energies, of say 50, 100 and 400 MeV in the intensity ratio 5:2:1 such as to produce a midline dose in the order of 200-400 rad. It appears that this would require very roughly a 10-min exposure to 400-MeV protons, a 20-min exposure to 100-MeV protons and a 2- to 4-hour exposure to 50-MeV protons if the scattering targets discussed here are used. To produce the lowest energy proton dose in the outer 2 cm of tissue appears to be the most time consuming step. Rotating the animal in the 88-inch cyclotron beam may be a logical procedure for this part of the exposure. For the production of a uniform total-body proton dose in a large animal, however, the scattering technique appears to lead to reasonable exposure times at fairly high energies.

ACKNOWLEDGEMENTS

We wish to thank Dr. John H. Lawrence and Dr. Cornelius A. Tobias for their interest and support.

This work was supported by the National Aeronautics and Space Administration through the Atomic Energy Commission.

REFERENCES

1. Moyer, B. J.; Appendix II of National Aeronautics and Space Administration Report No. 200-90-1-R3 (by W. Brobeck and associates).
2. Sondhaus, C. A., and Wallace, R. W.; Solar Proton Exposure Simulation with the 184-Inch Cyclotron, Lawrence Radiation Laboratory UCRL-10447, 1962 (unpublished); also in Proceedings of the Symposium on Protection Against Radiation Hazards in Space, Gatlinburg, Tennessee, TID-7652, Nov. 1962.
3. Harter, H. L.; J. Am. Stat. Assoc. 55:292, 1960.
4. Jackson, K. L.; in Proceedings of the Symposium on Protection Against Radiation Hazards in Space, Gatlinburg, Tennessee, TID-7652, Nov. 1962, p. 375.

Received August, 1963.

Some Metric Properties of the Systems of Compartments

Aldo Rescigno and Giorgio Segre

One of the most important problems correlated to the analysis of the compartment systems is the calculation of the transfer function between any two compartments a and b, i.e., of the function g (t) such that

$$\{x_b(t)\} = \{g(t)\} \cdot \{x_a(t)\} + \{h(t)\}$$

where the brackets represent functions according to Mikusinski (1), $x_a(t)$ and $x_b(t)$ are the amount of material in compartments a and b, at time t, and the functions g(t) and h(t) do not depend on the choice of the function $x_a(t)$, Rescigno (2). To this end, a system of compartments can be represented by a directed graph. A directed graph is formed by a finite set of nodes with certain directed lines or arms connecting the nodes. The nodes represent the compartments, and the arms represent their connections, Rescigno (3). Furthermore, to each node we assign a function equal to the amount of material versus time present in the corresponding compartment; to each arm connecting node i to node j, we assign a function T_{ij} equal to $k_{ij}/(s + K_j)$, where k_{ij} is the fractional flow from compartment i to compartment j, K_j is the fractional outflow from compartment j and s is the operator $1/\{1\}$.

TYPES OF GRAPHS

A node that is not entered by any arms is called an initial node. We shall consider only graphs with at least one but no more than one initial node. This is equivalent to considering only systems of compartments in which the tracer is introduced into one compartment. Because of the superposition principle, a system of compartments with more than one input can be considered as the sum of a number of systems with one input each. The initial node will be called node 0. Node 0 does not represent a real compartment of the system, but the hypothetical compartment from where the material is first introduced into the system (3). We can write $k_{0j} = 1$ for any arm connecting the initial node 0 to a noninitial node j.

The definition of path, elementary path, cycle, elementary cycle, G_0 subgraph, linear subgraph, strong component, given in a previous paper, Rescigno and Segre (4), apply to this kind of graphs too.

VARIABLE ADJACENCY MATRIX

A square matrix A, whose elements are the functions T_{ij}, is called the *variable adjacency matrix* of the system of compartments or of the graph associated with it. The matrix A^2 is formed by the elements

$$T_{ij}^{(2)} = \Sigma_k T_{ik} T_{kj} .$$

Therefore matrix A^2 indicates the paths of length 2 in the associated graph. In an analogous way, we can define matrix A^r, indicating the paths of length r.

DETERMINANT OF THE VARIABLE ADJACENCY MATRIX

The determinant D of the variable adjacency matrix of order n of a G_0 subgraph (i.e., of the subgraph obtained from G by deleting node 0 and the arms leaving it) is called *zero-axial* or *invertebrated* because all the elements of its principal diagonal are null. Its development was obtained by Cayley (5). He used the notation

$$|ij| = T_{ij} T_{ji} ,$$
$$|ijk| = T_{ij} T_{jk} T_{ki} ,$$

and omitted the second bar when two such symbols were written consecutively in a product, for instance

$$|12|345| = |12| \cdot |345| .$$

We now observe that the symbol $|ijk....|$ represents the product of the values of the arms forming an elementary cycle through the nodes i, j, k, ..., and that the symbol, say, $|12|3...|n - 1, n|$ represents the product of the values of the arms forming a strong component of G_0. According to Cayley, D is equal to the sum of the products formed with the values of the arms of the strong components of G_0. Each product has the sign + or −, depending on whether the number of cycles with an even number of arms is even or odd. When there are no strong components, D is equal to 0. For instance, with n = 4, Cayley (6),

$$D = + \Sigma |12|34| - \Sigma |1234| ,$$

where the two sums are extended to the permutations of the numbers 1, 2, 3, 4, giving different values of the products. As $|12| = |21|$, $|34| = |43|$, with our notation this is equivalent to

$$\begin{aligned} D = {} & T_{12}\, T_{21}\, T_{34}\, T_{43} + T_{13}\, T_{31}\, T_{24}\, T_{42} + T_{14}\, T_{41}\, T_{23}\, T_{32} + \\ & - T_{12}\, T_{23}\, T_{34}\, T_{41} - T_{12}\, T_{24}\, T_{43}\, T_{31} - T_{13}\, T_{32}\, T_{24}\, T_{41} - \\ & - T_{13}\, T_{34}\, T_{42}\, T_{21} - T_{14}\, T_{42}\, T_{23}\, T_{31} - T_{14}\, T_{43}\, T_{32}\, T_{21} . \end{aligned}$$

For n = 5, Cayley (5),

$$D = + \Sigma \ |12345| - \Sigma |123|45| ,$$

the first sum being formed by 24 terms and the second by 20 terms. For n = 6, Muir (7) gave a formula which evidently contains a printing error and should read

$$D = - \Sigma |12|34|56| + \Sigma |12|3456| + \Sigma |123|456| - \Sigma |123456| ;$$

the number of terms in each sum is 15, 90, 40, 120. The convenience of the Cayley notation is very apparent.

Calling $\bar{D}$ the determinant formed by the elements $-T_{ij}$, the development of $\bar{D}$ has the same terms as the development of D; the terms corresponding to cycles with an even number of arms have the same sign in $\bar{D}$ as in D; the terms corresponding to cycles with an odd number of arms have the sign changed. Therefore the sign of the terms of $\bar{D}$ is + or - according to whether there is an even or an odd number of cycles in the corresponding strong component.

For instance, with n = 4,

$$\bar{D} = + \Sigma \left|12\left|34\right| - \Sigma \left|1234\right| \;;$$

with n = 5,

$$\bar{D} = - \Sigma \left|12345\right| + \Sigma \left|123\left|45\right| \;.$$

ENUMERATION OF THE STRONG COMPONENTS

The number $\psi(n)$ of terms of an invertebrate determinant of order n was first calculated by Stockwell (8); he expressed it with the recurrent formula

$$\psi(n) = n \cdot \psi(n-1) + (-1)^n \;.$$

Baltzer (9) showed that

$$\psi(n) = n! \{ \frac{1}{2!} - \frac{1}{3!} + \ldots + (-1)^n \frac{1}{n!} \} ,$$

and later (10) he demonstrated that $\psi(n)$ is the nearest integer to $n!e^{-1}$. Because of what was said previously about D, $\psi(n)$ is the number of strong components in a complete graph of order n, i.e., a graph with n nodes and n(n - 1) arms. From Stockwell's formula one obtains

$$\psi(n) = (n-1)\,[\psi(n-1) + \psi(n-2)] ,$$

that shows the law of formation of the strong components of a complete graph of order n from the strong components of the graphs of order n - 1 and n - 2. Given the strong components of a graph of order n - 1, the strong components of a graph of order n, obtained by adding a new node and the corresponding arms, are obtained by 1. including the new node in the cycles of the $\psi(n-1)$ old strong components after each one of the old nodes, i.e., in n - 1 different ways, and 2. connecting the new node in a cycle with each one of the n - 1 old nodes and coupling each one of these new cycles with the $\psi(n-2)$ strong components containing the other nodes. The same reasoning is true for a noncomplete graph. For instance, given the graph of Fig. 1, the determinant of which is

$$\begin{vmatrix} 0 & T_{12} & T_{13} & T_{14} \\ 0 & 0 & T_{23} & T_{24} \\ T_{31} & T_{32} & 0 & 0 \\ 0 & T_{42} & T_{43} & 0 \end{vmatrix}$$

we first construct the subgraph suppressing node 4, then the three subgraphs

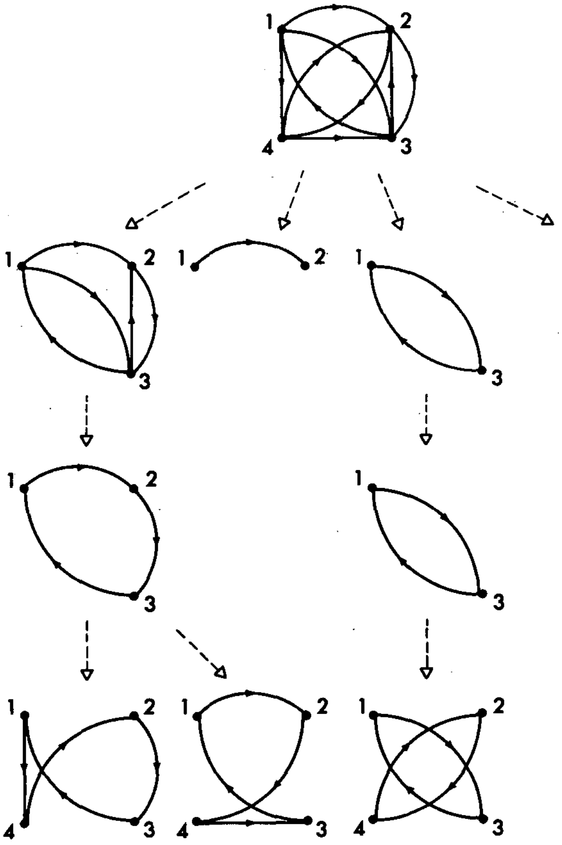

Figure 1. MU-32034

suppressing each one of the nodes 1, 2, 3. Of each one of them, we construct the strong components, if any. In the cycles of the strong components of order 3, we insert node 4 after node 1, node 2, node 3, if possible, (i.e., if there are the corresponding arms); to the strong components of order 2 we add a cycle formed by node 4 and the node missing, if possible. As shown in Fig. 1, there are three strong components symbolized by $|1423|$, $|1243|$, $|13|24|$.

DETERMINANT OF A SYSTEM

The solution of a compartment system corresponds to the solution of a system of first order linear differential equations with constant coefficients. And any system of first order linear differential equations with constant coefficients can be represented by a graph and solved by the method described here. The system of differential equations is

$$\frac{dx_1}{dt} = -K_1x_1 + k_{21}x_2 + \dots + k_{n1}x_n$$

$$\frac{dx_2}{dt} = + k_{12}x_1 - K_2x_2 + \dots + k_{n2}x_n$$

$$\dots\dots\dots\dots\dots\dots\dots\dots\dots\dots\dots$$

$$\frac{dx_n}{dt} = + k_{1n}x_1 + k_{2n}x_2 + \dots - K_n x_n$$

with the initial conditions $x_i = k_{0i}x_0$ for $t = 0$, where $k_{0i} = 1$ or 0, according to whether compartment i is connected or not to the initial compartment. In operational form the system is written

$$\begin{aligned}
&(s + K_1)\{x_1\} - k_{21}\{x_2\} + \dots - k_{n1}\{x_n\} = k_{01}x_0 \\
&-k_{12}\{x_1\} + (s + K_2)\{x_2\} + \dots - k_{n2}\{x_n\} = k_{02}x_0 \\
&\dots\dots\dots\dots\dots\dots\dots\dots\dots\dots\dots\dots\dots \\
&-k_{1n}\{x_1\} - k_{2n}\{x_2\} + \dots + (s + K_n)\{x_n\} = k_{0n}x_0 ,
\end{aligned}$$

or

$$\begin{aligned}
&-T_{01}x_0 + \{x_1\} - T_{21}\{x_2\} - \dots - T_{n1}\{x_n\} = 0 \\
&-T_{02}x_0 - T_{12}\{x_1\} + \{x_2\} - \dots - T_{n2}\{x_n\} = 0 \\
&\dots\dots\dots\dots\dots\dots\dots\dots\dots\dots\dots\dots\dots \\
&-T_{0n}x_0 - T_{1n}\{x_1\} - T_{2n}\{x_2\} - \dots + \{x_n\} = 0 ;
\end{aligned}$$

in matrix form

$$(I_{n+1} - A^T) \cdot \begin{vmatrix} x_0 \\ \{x_1\} \\ \vdots \\ \{x_n\} \end{vmatrix} = \begin{vmatrix} x_0 \\ 0 \\ \vdots \\ 0 \end{vmatrix}$$

where I_{n+1} is the $(n + 1) \times (n + 1)$ identity matrix, and A^T is the transpose of A.

The solution is obtained by the Cramer's rule:

$$\frac{\{x_i\}}{x_0} = (-1)^i \frac{\det (I_{n+1} - A^T)_{0;1}}{\det (I_{n+1} - A^T)}$$

where $\det (I_{n+1} - A^T)_{0;1}$ is the minor of $\det (I_{n+1} - A^T)$ obtained by suppressing its row $\underline{0}$ and its column $\underline{i}$.

The row $\underline{0}$ of $\det (I_{n+1} - A^T)$ is $1, 0, 0, \dots$; furthermore, the value of a determinant does not change if its columns are changed with its rows. Therefore, $\det (I_{n+1} - A^T) = (I_n + \bar{D})$, where $(I_n + \bar{D})$ is the determinant obtained by changing the sign of all elements of D and putting equal to 1 all elements of its principal diagonal. If we put the first column of $\det (I_{n+1} - A^T)_{0;i}$ after the i-th, and then change the columns with the rows, we obtain the determinant $(-1)^{i-1} (I_n + \bar{D})_i$, where $(I_n + \bar{D})_i$ is $(I_n + \bar{D})$ with its i-th row substituted by the elements $-T_{01}$, $-T_{02}$, $\dots$, $-T_{0n}$. Therefore

$$\frac{\{x_i\}}{x_0} = - \frac{(I_n + \bar{D})_i}{(I_n + \bar{D})} .$$

DEVELOPMENT OF THE DETERMINANT OF A SYSTEM

If the rows and the columns of $(I_n + \bar{D})$ are rearranged such that all nodes from where no paths go to node i are represented after i, and all nodes from where a path goes to node i are represented before i, then all the elements belonging jointly to the rows after the i-th and to the columns to the i-th are zero. Therefore $(I_n + \bar{D})$ is equal to its principal minor M corresponding to the node i and to the nodes from where a path goes to node i, times the principal minor N, corresponding to the nodes from where no paths go to node i. If from every node a path goes to node i, then $(I_n + \bar{D}) = M$. In the same way it can be shown that

$$(I_n + \bar{D})_i = M_i \cdot N \, ,$$

where M_i is the determinant M with the i-th row substituted by the elements $-T_{01}, -T_{02}, \ldots, -T_{0i}$. Therefore

$$\frac{\{x_i\}}{x_0} = \frac{-M_i}{M} \, .$$

The determinant

$$M = \begin{vmatrix} 1 & -T_{12} & \ldots -T_{1i} \\ -T_{21} & 1 & \ldots -T_{2i} \\ \cdots & \cdots & \cdots \\ -T_{n1} & -T_{n2} & \ldots \; 1 \end{vmatrix}$$

can be developed in terms of $\bar{D}$ and its principal minors, following a theorem enunciated by Cayley (11) for skew determinants, but evidently valid for any determinant: M is equal to 1, plus the determinant $\bar{D}$ of the subgraph obtained from the original G_0 suppressing the nodes from where no paths go to node i, plus all principal minors of this last determinant.

According to Cayley's rule, each of these determinants is equal to the sum of the products of the values of the arms forming a strong component. Therefore, M is equal to 1 plus the sum of the products formed with the values of the arms forming a linear subgraph of G, the sum being extended to all possible linear subgraphs, including G_0, if the case, and each product has the sign + or -, according to whether in the corresponding subgraph there is an even or odd number of cycles. The expansion of

$$-M_i = \begin{vmatrix} 1 & -T_{12} & \ldots & -T_{1i} \\ -T_{21} & 1 & \ldots & -T_{21} \\ \cdots & \cdots & \cdots & \cdots \\ +T_{01} & +T_{02} & \ldots & +T_{0i} \end{vmatrix}$$

is the same as M, substituting a 0 to the i's appearing as first subscript, multiplying all terms not containing i as first subscript by T_{0i}, and changing the sign to all terms. Therefore, $-M_i$ is equal to the sum of the products of the arms forming an elementary path from node 0 to node i, plus the same

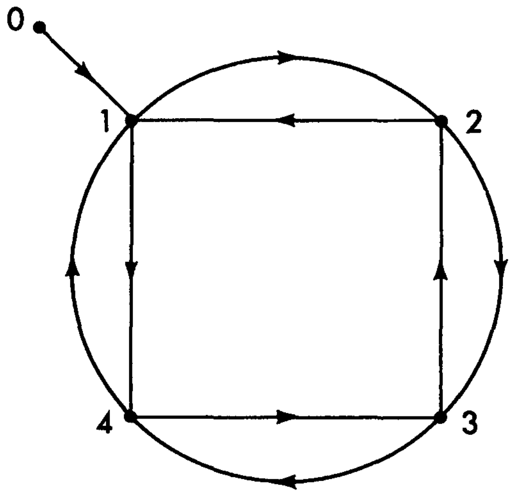

Figure 2.

$$-M_1 = +T_{01} - T_{01}T_{23}T_{32} - T_{01}T_{34}T_{43}.$$
$$-M_2 = +T_{01}T_{12} - T_{01}T_{12}T_{34}T_{43} + T_{01}T_{14}T_{43}T_{32}.$$
$$-M_3 = +T_{01}T_{12}T_{23} + T_{01}T_{14}T_{43}.$$
$$-M_4 = +T_{01}T_{14} - T_{01}T_{14}T_{23}T_{32} + T_{01}T_{12}T_{23}T_{34}.$$
$$M = 1 - T_{12}T_{21} - T_{23}T_{32} - T_{34}T_{43} - T_{14}T_{41} + T_{12}T_{21}T_{34}T_{43} + T_{14}T_{41}T_{23}T_{32} + \\ -T_{12}T_{23}T_{34}T_{41} - T_{14}T_{43}T_{32}T_{21}.$$

MU-32035

products times the products of the arms forming a linear subgraph with the nodes untouched by the said path. Each product has a sign + or - according to whether there is an even or an odd number of cycles. For examples, see Figs. 2 and 3.

TRANSFER FUNCTION

The transfer function $\{g(t)\}$ between any two compartments a and b can be obtained from the ratio of the two functions $\{x_b\}/x_0$ and $\{x_a\}/x_0$, therefore

$$\{g(t)\} = \{x_b\}/\{x_a\}$$
$$\{g(t)\} = M_b/M_a.$$

For instance the transfer function from compartment 1 to compartment 2 in the example of Fig. 3 is

$$\frac{M_2}{M_1} = \frac{T_{12}(1 - T_{34}T_{43})}{1 - T_{23}T_{32} - T_{24}T_{42} - T_{34}T_{43} - T_{23}T_{34}T_{42} - T_{24}T_{43}T_{32}}.$$

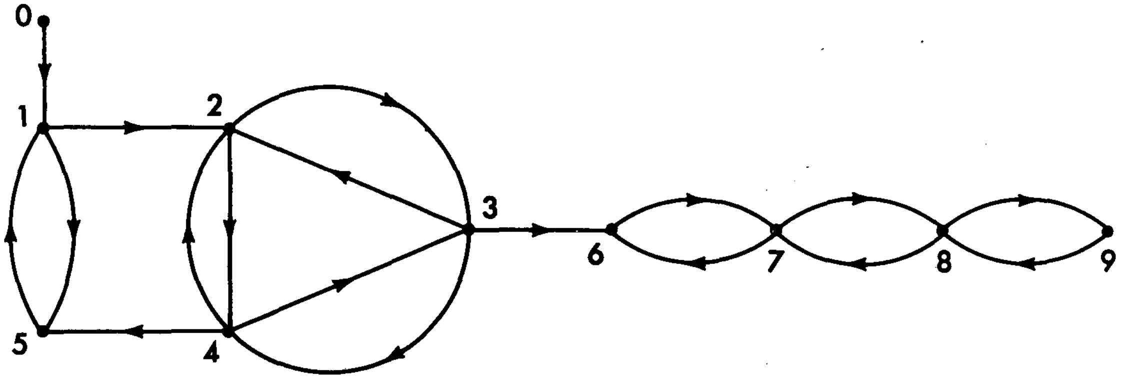

Figure 3.

$$-M_1 = + T_{01}(1 - T_{23}T_{32} - T_{24}T_{42} - T_{34}T_{43} - T_{23}T_{34}T_{42} - T_{24}T_{43}T_{32}).$$

$$-M_2 = + T_{01}T_{12}(1 - T_{34}T_{43}).$$

$$\begin{aligned} M = 1 &- T_{15}T_{51} - T_{23}T_{32} - T_{24}T_{42} - T_{34}T_{43} + T_{15}T_{51}T_{23}T_{32} + T_{15}T_{51}T_{24}T_{42} + \\ &+ T_{15}T_{51}T_{34}T_{43} - T_{12}T_{24}T_{45}T_{51} + T_{15}T_{51}T_{23}T_{34}T_{42} + T_{15}T_{51}T_{24}T_{43}T_{32} + \\ &- T_{12}T_{23}T_{34}T_{45}T_{51}. \end{aligned}$$

MU-32036

SUMMARY

Rules for the enumeration of the strong components of a graph and for the calculation of its variable adjacency matrix are presented. A new method is given, to calculate the transfer function of a graph, by analyzing the strong components of the graph, the elementary paths between two nodes, and the linear subgraphs.

ACKNOWLEDGEMENTS

This work was supported in part by the United States Atomic Energy Commission and the National Aeronautics and Space Administration.

REFERENCES AND NOTES

1. Mikusinski, J.: Operational Calculus, London, Pergamon, 1959.
2. Rescigno, A.; Ann. N. Y. Acad. Sci. 108:204, 1963.
3. Rescigno, A.; Biochim. Biophys. Acta 37:463, 1960.
4. Rescigno, A., and Segre, G.; Bull. Math. Biophys. 1964.
5. Cayley, A.; Phil. Mag. (4) 2:180, 1861.
6. Cayley, A.; Quart. J. Math. 3:275, 1860.
7. Muir, T.; Question 18033 in Mathematical Questions and Solutions from Educational Times (2) 29:100, 1916.
8. Stockwell, J. N.; Astron. J. (Cambridge) 6:145, 1860.

9. Baltzer, R.: Theorie und Anwendung der Determinanten, 3te Auflage, Leipzig, S. Hirzel, 1870, p. 29.
10. Baltzer, R.: Theorie und Anwendung der Determinanten, 4te Auflage; Leipzig, S. Hirzel, 1875, p. 38.
11. Cayley, A.; J. reine ang. Math. 39:93, 1849.

Giorgio Segre is visiting professor of pharmacology at the Division of Mathematical Biology, Department of Medicine of the Harvard Medical School, Boston, Mass. His present address is Instituto di Farmacologia, Universita degli Studi, Torino, Italy.

Received December, 1963

On the Metabolism of Radiobromide in the Thyroid Gland of Rats

Gilles La Roche and R. Richard Brown

The purpose of this study was to detect any evidence of bromine substitution for iodine in the thyroid synthesis of thyroxine under low iodine intake. Bromide uptake in various laboratory animals has been studied and reviewed by Baumann and his co-workers (1,2) and by Perlman, Morton and Chaikoff (3). After 1940, the chemical bromine evaluations were replaced by radioactive bromine (Br^{82}) assays that confirmed most of the prior results. Baumann, et al. (1) for instance, reported agreement between the newer method and their chemical determinations (2) published earlier. In their 1941 paper, (2) Baumann et al. suggested that the high bromine content of the thyroid gland could be explained on the assumption that thyroid tissue could distinguish only imperfectly between iodine and bromine. The 1956 publication reporting thyroid uptake of simultaneously injected I^{131} and Br^{82} indicates that the uptake of bromide increases as iodide uptake decreases.

Perlman, et al. (3), referring to work with rats and guinea pigs, suggested that "The content of radiobromide in the thyroid was too high to be explained by simple diffusion from serum." Yagi, et al. (4), in 1952, mentioned that certain groups of sponges metabolize both bromide and iodide, although in their work with rats they did not observe the organification, or binding to organic products (i.e., amino acids), of bromine. The article states that some rat enzymes can catabolize injected brominated-tyrosines. In view of earlier studies, it was considered of interest to investigate if bromide metabolism, under suitable conditions, might follow a pattern similar to that of iodine in rats. This report outlines the methods and procedures used in a pilot study of this question. The study was undertaken to elucidate bromide concentrating power and metabolism of the thyroid gland in laboratory rats, using radioactive bromide and paper chromatography methods. Variations of age, sex, injection technique and time on low-iodine diet, as well as three different doses of radiobromide, Br^{82}, were used in an attempt to estimate optimal conditions for future work.

MATERIALS AND METHODS

Thirteen rats of the Long-Evans strain, provided by the Department of Anatomy, University of California, Berkeley, were used. Complete data for each animal are included in Table 1. Two experiments were performed to test the effect of iodine diet on the rats for two different time periods. In experiment one, group A, female rats 44 days old were fed the controlled diet for 14 days. In the second experiment, eight male rats 49 days old were divided into groups B and C. In this experiment the controlled diet was fed for 26 days (Table 1).

The fat-supplemented chicken stock diet (CSD) used contained about 0.20-0.27 μg I/g diet as compared to about 1.0 μg I/g diet, considered an adequate supplement of dietary I^{127}. The CSD formula (5) was as follows: corn 30%, wheat 13.5%, barley 10%, alfalfa 4%, bran 15%, fish meal 10%, soybean meal 10%, whey 2.5%, liver meal 2%, limestone 1.5%, bonemeal 1.2%, salt 0.5%, $MnSO_4$ 0.05%, fish oil 0.25%. This mixture was finely ground, with the addition of 10% fat, for use as the rat low-iodine diet.

Radiobromide, Br^{82}, with a half-life of 35.9 hr., decays by beta emission to Kr^{82}, a stable isotope. The beta energy is 0.444 MeV, and gamma radiations are produced with energies ranging from 0.55-1.9 MeV, with an average of 0.77 MeV. This isotope, chosen as most appropriate for the methods employed, was provided by Oak Ridge in the form of high-specific-activity carrier potassium bromide in water. A well-type scintillation detector with a NaI crystal was used to make all counts, from liquid and paper samples. The upper counting limit of the detector was 50,000 counts/min with an efficiency of approximately 30%. Using a 2.0-cc hypodermic syringe with a 1-in. No. 18 needle, the rats of group A received a subcutaneous injection of 275 μC/0.5-cc KBr^{82} in saline solution while under light diethyl ether anesthesia. The rats of group B received 587 μC/0.3-cc KBr^{82} and group C received 963 μC/0.5-cc KBr^{82} by intraperitoneal injection of the radiobromide solution. The dosages were chosen so as to provide a countable quantity of radiobromine that, after chromatographic development and film exposure, might extend to six days after injection. The low level of bromine organification expected, together with the short half-life, made it necessary to use the above doses. Counting standards were prepared at the time of injection. All counted data were expressed as percentage of injected dose.

All animals were sacrificed at 24 hr following the radiobromide injection. Using diethyl ether anesthesia, the thyroid gland was removed, trimmed of fat, weighed, and homogenized in rapid succession. A blood sample was taken from the dorsal aorta, using a 5.0-cc syringe, before the medulla spinalis was severed. After removal and weighing, the thyroid was placed in a small, motor driven, glass homogenizer for one minute, along with 500λ (0.5 ml) NaCl-Tris buffer, pH 8.5. A 20λ (0.02 ml) sample of the final homogenate was taken for counting to determine the percentage uptake of the gland. The remainder of the mechanically homogenized thyroid was transferred to a small test tube where 2.5 mg Pronase (a protease enzyme) was added as well as two drops of toluene, to inhibit bacterial growth. The tube was tightly stoppered, and the enzymatic

Table 1.

	Rat identification	Body weight (g)	Thyroid weight (mg)	Ratio: thyroid wt. (g)/ body wt. (g) $(\times 10^{-4})$	% Injected dose whole thyroid	% Injected dose ml serum	% Injected ml NaI serum	% Injected dose/g thyroid
Group A								
	70-1	130	15.5	1.19	0.030	1.68	0.009	1.94
Age-44 days	66-2	147	13.5	0.92	0.025	1.69	0.008	1.84
Sex-	70-3	154	20.0	1.30	0.031	1.45	0.006	1.55
Dose-275 μC/0.5 cc	48-4	155	17.0	1.10	0.024	1.56	0.007	1.42
Inj-subcutaneous	69-5	135	22.0	1.63	0.043	1.77	0.005	1.96
Low-I^- diet-14 days								
	Ave: A	144.2	17.6	1.23	0.031	1.63	0.007	1.74
Group B								
	53-1	181	24.0	1.33	0.019	0.59	0.006	0.80
Age-49 days	54-2	190	20.5	1.08	0.015	0.63	0.005	0.71
Sex-	55-3	194	21.5	1.11	0.010	0.66	0.004	0.45
Dose-578 μC/0.3 cc	56-4	230	28.5	1.24	0.013	0.47	0.004	0.44
Inj-intraperitoneal								
Low-I^- diet-26 days	Ave: B	198.8	23.6	1.19	0.014	0.59	0.005	0.60
Group C								
	57-5	205	24.5	1.20	0.013	0.61	0.004	0.53
Age-49 days	58-6	180	25.0	1.39	0.013	0.71	0.004	0.52
Sex-	59-7	160	22.0	1.38	0.019	0.87	0.007	0.87
Dose-963 μC/0.5 cc	60-8	187	26.0	1.39	0.015	0.66	0.005	0.59
Inj-intraperitoneal								
Low-I^- diet-26 days	Ave: C	183.0	24.4	1.34	0.015	0.71	0.005	0.63
Ave: Group B and C		190.9	24.0	1.27	0.015	0.65	0.005	0.61

hydrolysis was allowed to proceed in a water bath at 37° C for eight hours. After the digestion was completed, aliquots of the hydrolyzate were taken for chromatographs, counting samples, and microiodine analysis.

Ascending chromatograms, using 3-in. strips of Whatman No. 3 MM paper, in an atmosphere of 74% collidine-26% ammonia for 15 hr were utilized. This procedure was adapted by Rosenberg, et al. (5) to study radioiodine (I^{131}) metabolism in the thyroid gland. Duplicate chromatograms of each digest were made, one of which was authentic markers of labelled monoiodotyrosine (MIT), diiodotyrosine (DIT), thyroxine (Tx) and iodide (I^-). The developed chromatograms were sandwiched between X-ray film for approximately three days. The radioiodine compounds were seen as exposed bands on the developed film. By comparing digest chromatograms and chromatograms with markers, against their respective exposed film, the various bands containing radioactivity were located and cut out for counting. The percentage distribution of each labelled thyroid component can be determined and eventually expressed as percentage of injected dose.

The blood obtained at sacrifice was placed in individual centrifuge tubes and refrigerated for about three hours before centrifugation. After centrifuging at 2,500 rpm the serum was removed by micropipettes. A 100λ (0.1 ml) counting sample was taken to determine the percentage of injected dose/ml blood serum. Several serum samples (10λ, 20λ) were run through the chromatogram procedure, as previously described for thyroid digests. A serum sample for each animal was taken for PBI (protein-bound iodine) estimates and total iodine in the rat sera, according to La Roche, et al. (6,7).

RESULTS

The 49-day-old, male rats of groups B and C averaged 190.9 g total body weight as compared to the average of 144.2 g for the 44-day-old females of group A. The average weight of the thyroid gland was 24.4 mg and 17.6 mg, respectively. The ratios for weight thyroid gland total body weight were: group A, 1.23; group B, 1.19; group C, 1.34 ($x 10^{-4}$). A greater variation was noted between the two male groups than between the combined average of group B and C, which was 1.27, and the female group A. The rats of group A had been on the low-iodine diet for fourteen days before sacrifice, as compared to 26 days for groups B and C. The analysis of these data suggests that no significant differences existed within the total rat population as regards age or thyroid weight relative to body weight, at the time of autopsy. The average radio-bromide thyroidal uptake at 24 hr, expressed as percentage of injected dose was 0.031% for group A; for group B this value was 0.01% and for group C, 0.015%. The value for group A was greater by a factor of 2.5 than the average value for groups B and C combined. A similar difference appears to exist in the percent of the injected dose per ml of serum at 24 hr between group A and groups B or C. The dose of radiobromine used for group A was 275 µC/0.5-cc saline solution. The dose of 578 µC/0.3 cc for group B was greater by a factor of 2.1 than A, and the dose of 963 µC/0.5 cc for group C was 3.5 times greater than the group A dose. There was no detectable effect from the amount of administered radioactivity and the percent of injected radiobromide found in either the thyroid tissue or sera.

Using thyroid hydrolyzate aliquots of 20λ, 50λ, and 100λ, chromatograms with or without radio-bromide carrier were run as previously described. The autoradiographs (X-ray film) indicated that all of the radiobromide was located in a single band about 10.0 cm from the origin. Two sera aliquots, of 10λ and 20λ, and two samples of radiobromide were run on separate chromatograms at the same time. The average distance of the radioactivity from the origin was the same in every trial. It was concluded that all of the injected radiobromide remained as bromide in both the thyroid gland and the serum.

DISCUSSION

It was believed that the bromide uptake of the thyroid would be increased if the rats were placed on a known low-iodine diet. A column in Table 1 expresses the Br^{82} content of the thyroid as percent injected dose/g thyroid tissue for comparison with previously published data. Perlman, et al. (3) reports the percent of the injected dose per gram of thyroid in rats as averaging 2.02% at three hours post-injection and 1.68% after six hours. In the same paper, normal guinea pigs averaged 0.66%/g after two hours and 0.47%/g after 24 hr. The results of the present study, 24 hr post-injection, were: group A, 1.74%; group B, 0.60%; and group C, 0.63% when expressed as percent of the injected dose per gram thyroid (Table 1). Direct comparisons of published data are not possible, because the iodide content of Perlman's diets is not known. However, as already stated by Bauman (1) a lower I^{131} thyroidal uptake would suggest an adequate iodine (I^{127}) intake (sufficient intrathyroidal I^{127}) which would appear to be associated with a higher Br^{82} thyroidal uptake. Conversely, as evidenced by the present work, lower iodine intake should eventually induce a lower thyroidal iodine content. This seems preceded by a lower radioactive bromide uptake and a lower serum Br^{82} at 24 hr. The implications of a correlation between Br^{82} levels and I^{127}-dietary intake (or thyroidal I^{127}) are difficult to discuss in the light of a single uptake measure at 24 hr.

The present study offers further evidence that bromine organification does not occur in the thyroid gland even when the animal is maintained on a low iodine intake for 24 days (Table 1). The chromatographic procedure represents a sensitive procedure for testing this possibility. Artifactual bromine organification induced by the high dosages of radiobromide were considered a reasonable possibility but were not observed upon examination of either the thyroid or sera chromatograms (Table 1). The known variables involved in the present study can be listed as: modes of injection (group A: subcutaneous; groups B

Table 2. Thyroid gland iodine (I^{127}) contents

Groups	Rat number	μgmI/gland	μgmI/mg of gland
A	70-1	0.8	0.052
	66-2	1.3	0.096
	70-3	3.4	0.170
	48-4	2.9	0.171
	Average	2.1	0.122
B	53-1	3.2	0.133
	54-2	2.5	0.122
	55-3	1.3	0.061
	56-4	4.9	0.172
	Average	3.0	0.122
C	57-5	4.8	0.196
	58-6	2.2	0.088
	59-7	2.5	0.114
	60-8	2.8	0.108
	Average	3.1	0.127

and C: intraperitoneal), sex and length of time on a low iodine diet. Of these three factors the first one can be dismissed because a two-fold difference in thyroidal uptake and serum distribution of a highly diffusible electrolyte at 24 hr could not be solely dependent on the route of injection. The differences could be attributed to sex differences. However, a significant drop in 24-hr radiobromide uptake associated with a doubling of the period through which the animal was maintained on low iodine intake indicates the effect of prolonged iodine depletion. Although the doubling of the time period on low-iodine diet did not induce a decrease in the total intrathyroidal iodine (Table 2), it may have altered the bromide metabolism of the gland.

SUMMARY

No evidence was found to support the hypothesis of bromine organification by the thyroid gland or serum of rats maintained on low-iodine diet up to 24 days. Radiobromide dosage was not found to significantly influence the concentrating ability of the thyroid gland or the amount of radiobromide in the sera as observed between groups B and C. The level of radiobromide present in the thyroid gland or serum, 24 hr after administration, may be dependent on sex or on the chronic effects of low iodine intakes.

ACKNOWLEDGEMENTS

We acknowledge the assistance of Dr. Lawson Rosenberg, Dr. Max Goldman, and Mr. Clarence Johnson. The authors are also grateful to Mrs. Dorothy Carpenter and Mrs. Georgia Reichert. Mr. R. Richard Brown's participation in the research project was supported by an N.S.F. stipend for highschool teachers.

REFERENCES AND NOTES

1. Baumann, E. J.; Searle, N. Z.; Yalow, A. A.; Siegel, E. and Seidlin, S. M.; Am. J. Physiol. 185:71, 1956.
2. Baumann, E. J.; Sprinson, D. B., and Marine, D.; Endocrinol. 28:793, 1941.
3. Perlman, I.; Morton, M. E., and Chaikoff, I. L.; Am. J. Physiol. 134:107, 1941.
4. Yagi, Y.; Michel, R., and Roche, J.; Bull. Soc. Chim. Biol. 35:289, 1953.
5. Rosenberg, L. L.; Dimick, M. K., and La Roche, G.; Endocrinol. 72:749, 1963.
6. La Roche, G.; Oakes, C., and Blanquet, P.; Lawrence Radiation Laboratory Report, UCRL-10211, Spring, 1962.
7. La Roche, G.; Carpenter, D., and Coxworth, A.; unpublished.

Present address of R. Richard Brown is The Thacher School, Ojai, California.

Received August, 1963.

STAFF PUBLICATIONS

Anger, Hal O.: Gamma-ray and positron scintillation camera, Nucleonics 21, No. 10:56, 1963.

Anger, Hal O., and Gottschalk, Alexander: Localization of brain tumors with the positron scintillation camera, J. Nucl. Med. 4:326, 1963.

Beck, James S.: Effects of X-irradiation on cell differentiation and morphogenesis in a developing beetle wing, Radiation Res. 19:569, 1963.

D'Angio, Giulo, and Lawrence, John H.: Medical research with high-energy heavy particles, Nucleonics 21, No. 11:56, 1963.

Gofman, John W., and Young, Wei: The filtration concept of atherosclerosis and serum lipids in the diagnosis of atherosclerosis, in Atherosclerosis and Its Origin, chap. 6, edited by Maurice Sandler and Geoffrey H. Bourne, New York, Academic Press, 1963.

Hayes, Thomas L.; Lindgren, Frank T., and Gofman, John W.: A quantitative determination of the osmium tetroxide-lipoprotein interaction, J. Cell Biol. 19:251, 1963.

Jones, Hardin B.: Health hazards from fallout, Federation Proc. 22:1415, 1963.

Lawrence, John H.; Tobias, Cornelius A.; Born, James L.; Gottschalk, Alexander; Linfoot, John A., and Kling, Robert P.: Alpha particle and proton beams in therapy, J. Am. Med. Assoc. 186:236, 1963.

Lawrence, John H.: Hypophysectomy in diabetes (by cyclotron), in Ocular Pharmacology and Therapeutics and Problems of Medical Management, edited by Samuel J. Kimura and Ernest K. Goodner, Philadelphia, F. A. Davis Co., 1963, p. 172.

Lawrence, John H.; Tobias, Cornelius A.; Linfoot, John A.; Born, James L.; Gottschalk, Alexander; Kling, T.: Heavy particles, the Bragg curve, and the suppression of pituitary function in diabetic retinopathy, Diabetes 12:490, 1963.

Linfoot, John A.; Lawrence, John H.; Born, James L., and Tobias, Cornelius A.: The alpha particle or proton beam in radiosurgery of the pituitary gland for Cushing's disease, New Eng. J. Med. 269:597, 1963.

Linfoot, John A.: Cardiovascular and renal status of hypophysectomy patients (by cyclotron), in Ocular Pharmacology and Therapeutics and Problems of Medical Management, edited by Samuel J. Kumura and Ernest K. Goodner, Philadelphia, F. A. Davis Co., 1963, p. 181.

Mel, Howard C.: Sedimentation properties of nucleated and non-nucleated cells in normal rat bone marrow, Nature 200:423, 1963.

Mortimer, R. K., and von Borstel, R. C.: Radiation-induced dominant lethality in haploid and diploid sperm of the wasp Mormoniella, Genetics 48:1545, 1963.

Palmer, M. Winnogene, and McDonald, L. W.: A device for the continuous chilling of microtome knife and paraffin blocks, Am. J. Clin. Pathol. 40:633, 1963.

Van Dyke, Donald; Lawrence, John H.; Pollycove, Myron, and Lowy, Peter: Preliminary results from the use of erythropoietin in human volunteers, Mem. Soc. Endocrinol. 13:221, 1963.